REMARKS

The Applicants thank the Examiner for the examination to date and respectfully request reconsideration of the present application in view of the foregoing amendments and the reasons that follow.

The only remaining issue is obviousness.

I. Status of the Claims

New claims 79 and 80 are added to recite respective embodiments of the carbon nanosheets claims 57 and 62; support therefor can be found in, *inter alia,* ¶[0074] of the Specification as published. No new matter is introduced, and claims 57-60, 62-76, and 79-80 are pending in this application, with claims 65-74 withdrawn.

II. Claim Rejections – 35 U.S.C. § 103

Claims 57-59 and 75 are rejected under 35 U.S.C. § 103(a) as allegedly being unpatentable over US 2003/0224168 ("Mack") in view of US 6,361,861 ("Gao"). Claim 60 is rejected under 35 U.S.C. § 103(a) as allegedly being unpatentable over Mack in view of Gao, and further in view of *Carbon*, (39) 2001 505-514 ("Peigney"). Claims 62 and 76 are rejected under 35 U.S.C. § 103(a) as allegedly being unpatentable over *Chemical Physics Letters* 358 (2002) 187-191 ("Shang") in view of Peigney and Gao. Claims 63 and 64 are rejected under 35 U.S.C. § 103(a) as allegedly being unpatentable over Shang in view of Peigney and Gao, and further in view of Mack. The Applicants respectfully traverse all of these rejections.

(A) Current Obviousness Standard

The U.S. Supreme Court reaffirmed the Graham factors for determining obviousness in *KSR Int'l Co. v. Teleflex Inc.*, 550 U.S. 398 (2007). The Graham factors, as outlined by the Supreme Court in *Graham et al. v. John Deere Co. of Kansas City et al.*, 383 U.S. 1 (1966), are: 1) determining the scope and contents of the prior art; 2) ascertaining the differences between the

claimed invention and the prior art; 3) resolving the level of ordinary skill in the pertinent art; and 4) evaluating evidence of secondary consideration. The Supreme Court recognized that a showing of "teaching, suggestion, or motivation" to combine the prior art to meet the claimed subject matter could provide a helpful insight in determining whether the claimed subject matter is obvious under 35 U.S.C. § 103(a) and held that the proper inquiry for determining obviousness is whether the improvement is more than the predictable use of prior art elements according to their established functions. The Court noted that it is "important to identify a reason that would have prompted a person of ordinary skill in the relevant field to combine the [prior art] elements" in the manner claimed and specifically stated:

> Often, it will be necessary . . . to look to interrelated teachings of multiple patents; the effects of demands known to the design community or present in the marketplace; and the background knowledge possessed by a person having ordinary skill in the art, all in order to determine whether there was ***an apparent reason to combine the known elements in the fashion claimed*** by the patent at issue. To facilitate review, this analysis should be made explicit.

KSR Int'l Co. v. Teleflex Inc., slip op. at 14 (emphasis added). As discussed below, the teachings of the cited art cannot render the claimed invention obvious.

(B) The present claims are non-obvious over the teachings of the cited references

The Applicants maintain the position as set forth in the previous Replies and respectfully traverse the grounds of the Office's rejections. In particular, the Applicants respectfully submit that the Office has misconstrued the present invention and the teachings of the cited references to arrive at an incorrect conclusion.

"Nanosheets" are NOT "nanotubes"

The Office has acknowledged that Gao's teachings were only used for the "benefit of alignment" and not for the "nanotube" itself. Advisory Action, page 2. However, the Applicants respectfully submit that the main issue at hand is not whether or not Gao teaches aligning, but if the "nanosheets" of the present invention and the "nanotubes" of Gao are so distinct that

teachings related to these two very different materials should not have been analogized or compared at all.

The Office has stated several different grounds for using Gao's teachings only with respect to the alignment of the nanotubes. However, for the Office to combine the teachings of the nanotube of Gao with those of the nanosheets of Mack and to "pick and choose" between these teachings, the Office has ignored the fundamental differences between a nanotube and a nanosheet. In fact, the Office has not even established any evidence why carbon nanotubes and carbon nanosheets are similar enough for the teachings related thereto to be compared. Such a leap in logic results only in a conclusory statement without any articulated underpinning reasoning that supports a proper rationale for combining the teachings that are related to separate and distinct materials, regardless of how they are combined.

One of ordinary skill in the art can appreciate that a carbon nanotube is **not** a carbon nanosheet, and thus the teachings associated with these two separate entities should not be compared. The Applicants submit herewith Exhibit A, a review article by Su *et al.*, in which the authors clearly demonstrate the distinctions between a carbon nanotube and carbon nanosheet (graphene layer). At the outset, the Applicants respectfully direct the Office's attention to Figure 1 (reproduced below) in Exhibit A for an illustration of the contrast between the **one-dimensional** graphene nanosheet and the **two-dimensional** carbon nanotube. Section 2.1.1. "Carbon nanotubes" and Section 2.1.3 "Graphene" in Exhibit A further explain the differences between these two entities. In sum, the fact that carbon nanotubes can be vertical on a substrate has little to do with whether carbon nanosheets can be vertically aligned on a substrate – this is further evidenced below.

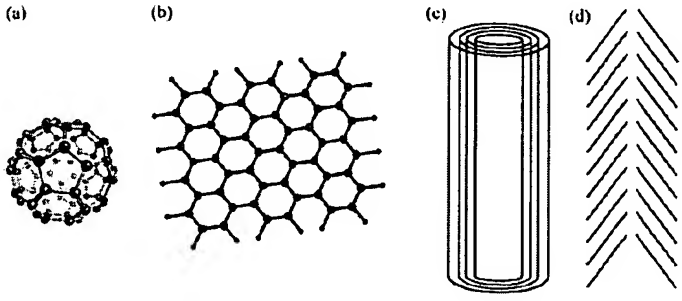

Figure 1. Schematic illustrations of several important carbon nanostructures: a) fullerene, b) graphene, c) carbon nanotube, and d) carbon nanofiber.

A carbon nanotube has its various desirable properties mainly because of its geometry. In particular, the diameter thereof plays an important role in the property of a nanotube, and thus should be controlled. *See e.g.,* Gao, Col. 2, ll. 46-60. By contrast, a nanosheet as recited in the present claims does not have a "diameter." In fact, as explicitly defined in ¶[0052] of the present Specification, a carbon nanosheet herein refers to "a carbon **nanoflake** with a thickness of 2 nanometers or less," wherein carbon nanoflakes are "**sheet**-like forms of graphite..." (bold emphasis added). A "tube" as disclosed in Gao can hardly be characterized as a "flake" or "sheet" as described in the present Specification.

Accordingly, regardless of how they are combined, the combination of the teachings related to a nanotube with the teachings related to a nanosheet is not possible without hindsight. This is particularly true when the Applicants have demonstrated that a combination of the teachings of Gao and Mack would render Mack's teachings unsatisfactory for Mack's intended purpose. *See* July 26, 2010 Reply, pages 6-7. Further, such a combination is in conflict with the guidance of the MPEP and Federal Circuit case law. *See* MPEP § 2145 and *In re Ravi Vaidyanathan* 2010 WL 2000682 at 9 (Fed. Cir. 2010.) (reiterating that "obviousness is determined as a matter of foresight, not hindsight").

An "interlaced" configuration is NOT "vertically aligned"

The Applicants respectfully traverse the Office's construction of independent claim 62 and its corresponding claims. Particularly, the Applicants respectfully traverse the Office's interpretation of the structural description of how the nanoflakes are configured as "intended uses." The embodiment as recited in claim 62 is related to a plurality of nanoflakes and how they are arranged on a substrate. In other words, the claim recites what the nanoflakes **are**, and not what they **do** on the substrate. Accordingly, the Office's characterization of the recitation as "intended use" is improper.

The Applicants maintain the position as set forth in the July 26, 2010 Reply that Shang teaches away from the presently claimed embodiments by disclosing that the carbon nanoflakes of Shang are **interlaced together** to form a layer of carbon nest-like film (*see* Shang, Abstract). This is in stark contrast to the carbon nanoflakes, as recited in present independent claim 62, in which nanoflakes are **aligned** and **freestanding**, and standing on **their edges roughly vertically to a substrate**, as illustrated in, for example, Figures 29A-29B in the present Specification. Also, as the Office has acknowledged on page 6 of the Office Action, Shang is completely silent regarding the specific surface area of the nanoflake.

The Office appears to be of the position that because nanotubes can be vertically aligned, so can carbon nanosheets. This is incorrect. The Applicants submit herewith Exhibit B, an article by Zhu *et al.*, of which the present inventors are co-authors. As can be shown in Exhibit B, as recently as the year 2007, the scientists are still trying to understand the mechanisms of fabricating nanosheets that are vertically aligned on a substrate. In particular, in Figure 5 (reproduced below), the authors proposed a growth model trying to illustrate the unexpected phenomenon of fabricating vertical, freestanding features of carbon nanosheets in terms of the hydrogen etching effect:

> "...that atomically thin graphene sheets result from a balance between deposition through surface diffusion and etching by atomic hydrogen and that the observed

vertical orientation of these sheets results from the interaction of the plasma electric field ..." Abstract.

Further, in the Conclusion section, the authors further distinguish the growth of carbon nanotubes from that of carbon nanosheets:

"...the formation of atomically thin, free-standing carbon nanosheets is strongly favored over the formation of nanotubes ..." Page 2233, Section 3.

Such a **structural** configuration of carbon nanosheets could not have been expected in view of disclosure relating to "interlaced" nest-like structures of Shang and/or any of the disclosures relating to carbon nanotubes.

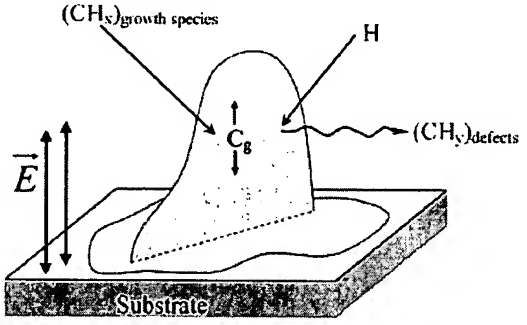

Fig. 5. A schematic explanation of CNS growth model. $\vec{E}$: direction of the electric field near a substrate surface; CH_x: carbon-bearing growth species impinging from gas phase; C_g: growth species diffuse along CNS surface; H: atomic hydrogen impinging from gas phase; CH_y: defects removed from CNS by atomic hydrogen etching effects.

The teachings of Peigney, Gao, and/or Mack do not remedy the deficiencies of Shang's teachings. Peigney is merely a theoretical study of specific surface area of single- and multi-walled carbon **nanotubes** and of carbon nanotube bundles. As explained above, a carbon nanotube, such as that described also in Gao, is **not** a carbon nanoflake. Thus, the specific surface area of a carbon nanotube, as the Office points to in Peigney's teachings, has **nothing** to do with the specific surface area of a carbon nanoflake, as recited in present independent claim 62. Thus, even assuming, *arguendo*, that the teachings of Shang, Peigney, and Gao were

combined, the embodiment as recited in present independent claim 62 would not have resulted, let alone show the unexpected results as described above. Specifically, such a combination would still fail to teach the carbon **nanoflakes** having a specific surface area between 1000 m^2/g and 2600 m^2/g.

At least in view of the foregoing reasons, the Applicants respectfully submit that one of ordinary skill in the art would not have had a reason to combine the teachings of the cited references. Even assuming, *arguendo*, that these teachings were combined, the presently claimed invention would not have resulted.

Therefore, the Applicants respectfully request that the rejections be withdrawn.

CONCLUSION

The Applicants believe that the present application is now in condition for allowance and respectfully request favorable reconsideration of the application.

The Office is invited to contact the undersigned by telephone if a telephone interview would advance the prosecution of the present application.

The Office is hereby authorized to charge any additional fees which may be required regarding this application under 37 C.F.R. §§ 1.16-1.17, or credit any overpayment, to Deposit Account No. 19-0741. If any extensions of time are needed for timely acceptance of papers submitted herewith, the Applicants hereby petition for such extension under 37 C.F.R. § 1.136 and authorize payment be charged to Deposit Account No. 19-0741.

Respectfully submitted,

Date September 23, 2010 By _____

FOLEY & LARDNER LLP
Customer Number: 22428
Telephone: (202) 672-5483
Facsimile: (202) 672-5399

Richard C. Peet
Attorney for the Applicants
Registration No. 35,792

EXHIBIT A

CHEMSUSCHEM

DOI: 10.1002/cssc.200900182

Nanostructured Carbon and Carbon Nanocomposites for Electrochemical Energy Storage Applications

Dang Sheng Su*[a, b] and Robert Schlögl[a]

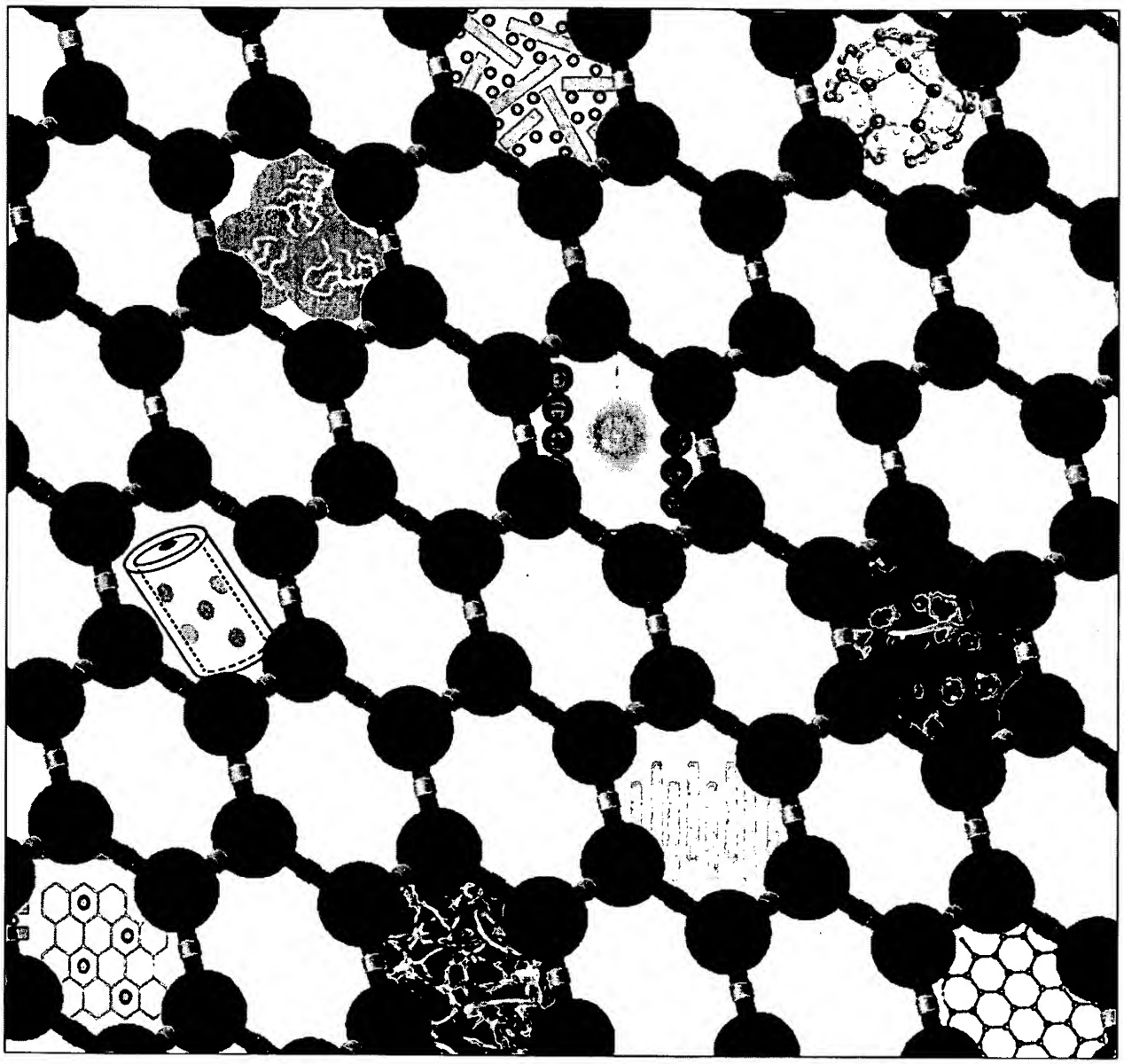

Electrochemical energy storage is one of the important technologies for a sustainable future of our society, in times of energy crisis. Lithium-ion batteries and supercapacitors with their high energy or power densities, portability, and promising cycling life are the cores of future technologies. This Review describes some materials science aspects on nanocarbon-based materials for these applications. Nanostructuring (decreasing dimensions) and nanoarchitecturing (combining or assembling several nanometer-scale building blocks) are landmarks in the development of high-performance electrodes for with long cycle lifes and high safety. Numerous works reviewed herein have shown higher performances for such electrodes, but mostly give diverse values that show no converging tendency towards future development. The lack of knowledge about interface processes and defect dynamics of electrodes, as well as the missing cooperation between material scientists, electrochemists, and battery engineers, are reasons for the currently widespread trial-and-error strategy of experiments. A concerted action between all of these disciplines is a prerequisite for the future development of electrochemical energy storage devices.

1. Introduction

One area of activity in materials science is the development of new materials for energy applications. This includes high-performance materials with specific characteristics, for example employed as electrode materials for lithium-ion batteries and supercapacitors, in fuel cells, and as host materials for hydrogen storage. Carbons (graphite, hard carbon, glassy carbon, carbon black) have previously been utilized in various electrochemical energy storage systems. This was motivated by the good electrical conductance of sp^2-hybridized solid carbon, its high chemical stability, and its enormous adaptability to different interface processes.

In general, sp^2-hybridized carbon materials exhibit a high diversity in crystallinity, morphology, porosity, and texture. These structural parameters play a crucial role in determining and optimizing the electrochemical performance when carbons are used as electrodes. Studying the influence of the characteristics of these diverse materials on the battery/capacitor performance forms the basis of a rational design of improved functional materials. The required disruptive improvement in performance of electrochemical devices for energy applications has motivated the design of the structure and porosity of carbon materials through the choice of proper carbon precursors, through changing the conditions for thermal treatment, and by introducing procedures for activation and functionalization. There are several review articles on state-of-the-art carbons as electrode materials for electrochemical applications.[1-7] Graphite and activated carbon are still the mostly used materials for lithium-ion batteries and for supercapacitors, respectively. The exploration of nanomaterials and nanocomposites is believed to further reveal their great potential for advanced energy storage devices, for example, to increase the high-rate performance of lithium-ion batteries[8-12] and to increase the energy density of supercapacitors (see the reviews listed in Table 1).

Nanomaterials in the broader sense can be classified into two categories: the first is the common "nanostructured material" in which either the size of bulk materials is reduced in one or two dimensions, or a new morphology is formed at low dimension, for example, fullerenes or carbon nanotubes (CNTs). Figure 1 illustrates some zero-, one-, and two-dimensional nanocarbons. There are two kinds of effects that result from

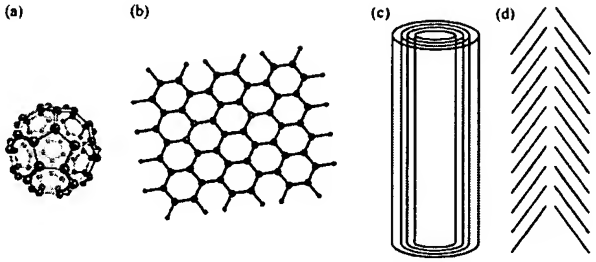

Figure 1. Schematic illustrations of several important carbon nanostructures: a) fullerene, b) graphene, c) carbon nanotube, and d) carbon nanofiber.

nanostructuring: (i) "trivial size effects," which rely solely on the decreased size [diameter of nanoparticles or thickness of (mono)-layers], decreased volumes, or increased surface-to-volume ratios; and (ii) "true size effects," which rely on the change in local properties of materials.[13-15] For nanocarbons, the true size effects play the most important role as fullerenes, graphene, and CNTs exhibit properties that classical carbon materials do not. Nanostructured carbon differs from classical carbon not only in its dimensionality, surface area and porosity, as mentioned above, but more importantly in the distribution of chemical bonding, thus allowing for mixtures of local electronic structures of sp^r carbon, with r being a variable between 2 and 3. This flexibility arises from the possibility to interlink basic structural units of carbon with a variable degree of curvature, ranging from flat graphene (sp^2) to continuous wraps (localized double bonds) with strong covalent linkers (sp^3).[16] The perfect tunability of the local chemical bonding leads to materials with predictable mechanical and chemical properties.

The second type of nanomaterials uses nanostructured materials, such as described above, as building blocks to form a desired morphology.[15,17,18] Nanocomposites mostly combine two or more different nanomaterials with different morpholo-

[a] *Dr. D. S. Su, Prof. R. Schlögl*
Fritz Haber Institute of the Max Planck Society
Faradayweg 4–6, 14195 Berlin (Germany)
Fax: (+49) 30 8413 4401
E-mail: dangsheng@fhi-berlin.mpg.de
[b] *Dr. D. S. Su*
Institute for Metal research, Chinese Academy of Sciences
72 Wenhua Road, 110016 Shenyang (PR China)

Table 1. Several reviews on the state of the art of lithium-ion batteries and of supercapacitors, published since 2000.

Review	Author(s)	Materials	Application(s)	Ref.
Recent development of carbon materials for Li ion batteries	M. Endo et al.	Carbon, graphite	Li-ion battery	[1]
Electrochemical energy storage	F. Béguin et al.	Activated and meso-porous carbon, CNTs	Li-ion battery, supercapacitor	[2]
Carbon anode materials for lithium ion batteries	Y. P. Wu et al.	Graphite composite, polymer coating, CNTs	Li-ion battery	[3]
Carbon properties and their roles in supercapacitors	A. G. Pandolfo et al.	Carbon black, aerogel, fiber, glassy carbon	Supercapacitor	[4]
Advanced battery application of carbons	M. Endo et al.	Classic and nanostructured carbons, alloy composite	Li-ion battery	[5]
Lithium storage in carbon nanostructures	N. Kaskhedikar et al.	Nanocarbons	Li-ion storage	[6]
Recent advances in lithium ion battery materials	B. Scrosati	Anode, cathode	Li-ion battery	[7]
Issues and challenges facing rechargeable lithium batteries	J. M. Tarascon	Li alloy, polymer and electrolyte	Li-ion battery	[8]
Nanomaterials for lithium ion batteries	C. Jiang et al.	Nanostructured metal oxide	Li-ion battery	[11]
Nanomaterials for rechargeable lithium batteries	P. G. Bruce et al.	Nanomaterials as electrode, electrolyte	Li-ion battery	[12]
Nanostructured Materials for electrochemical energy conversion and storage devices[a]	Y. G. Guo et al.	Nanostructured materials	Li-ion battery, DMFCs	[15]
The role of nanostructure in improving the performance of electrodes for energy storage and conversion	G. Centi et al.	Nanostructures	Li-ion battery, fuel cell	[17]
Reversible and high-capacity nanostructured electrode materials for Li-ion batteries[b]	M.G. Kim et al.	Nanostructred anode and cathode materials	Li-ion battery	[18]
Carbon nanotube and conducting polymer composites for supercapacitors	C. Peng et al.	CNTs, conducting polymer	Supercapacitor	[25]
Template-directed materials for rechargeable lithium-ion batteries	F. Cheng et al.	Template-prepared functional materials	Li-ion battery	[19]
Electrochemical storage of energy in carbon nanotubes and nanostructured carbons	E. Frackowiak et al.	CNTs and nano-structured carbon	Li-ion battery, supercapacitor	[20]
Nanostructured materials for advanced energy conversion and storage devices	A.S. Aricó et al.	Nanostructured materials as electrode	Li-ion battery, supercapacitor	[21]
Materials for electrochemical capacitors	P. Simon et al.	Nanoporous carbon, metal oxides	Supercapacitor	[22]
Application of nanotextured carbons for supercapacitors and hydrogen storage	E. Raymoundo-Pinero et al.	Activated and templated carbon, CNTs	Supercapacitor, hydrogen storage	[23]
Application of nanoporous carbon and nanotubes composites for supercapacitors	E. Frackowiak et al.	Nanoporous carbons, CNTs	Supercapacitor	[24]
Carbon-based materials as supercapacitor electrodes	L. L. Zhang et al.	Carbon-based materials, electrolytes	Supercapacitor	[147]
Advanced materials for energy storage	C. Liu et al.	Advanced materials	Energy storage, Li-ion battery, supercapacitator	[255]

[a] Progress Report. [b] Feature Article.

Dang Sheng Su completed his physics studies at Jilin University (PR China) in 1986. He completed his Ph.D. at Technical University of Vienna (Austria) in 1991, and moved to the Fritz-Haber-Institut der Max-Planck-Gesellschaft as a post-doctoral worker in the Department of Electron Microscopy. After a short stay at Hahn-Meitner Institut GmbH and Humboldt Universität zu Berlin (Germany) he joined the Fritz-Haber-Institut in 1999, where he works on nanomaterials in heterogeneous catalysis and energy storage. He is also a Professor at the Institute of Metal Research, Chinese Academy of Sciences, Shenyang (PR China).

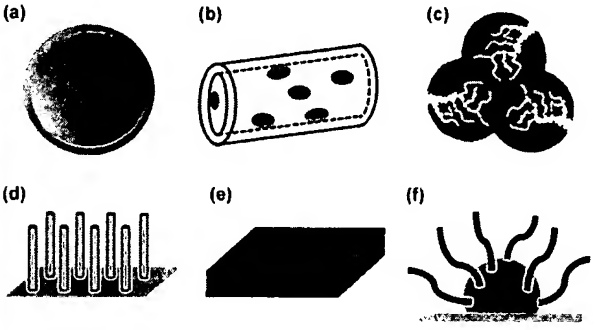

Figure 2. Schematic illustration of some carbon-based nanocomposites (a–c) and nanoarchitectures (e–f). a) Active materials coated with carbon layers. b) Nanoparticles in a CNT. c) Nanoparticles dispersed in a (porous) carbon matrix. Architectures that use nanocomposites to form e) aligned arrays, d) a thin sandwich film, and f) a hierarchical rambutan-like structure with several nanocomponents.

gies and belong to the nanoarchitectured materials. It is possible to assemble the nanometer-scale units in an ordered structure to explore and use their physical and chemical properties in an optimized manner. Examples of nanoarchitectures are illustrated in Figure 2. Carbon layers can encapsulate metal(oxide) nanoparticles; CNTs can be used as holders or containers of active materials, or active materials can be dispersed into a carbon matrix. Nanoarchitecture also includes assembly, for exampel, CNTs, nanowires, or nanobelts in an array, hierarchically arranging several nanocomponents into, for example, rambutan-like structures. Another example of materials design is the sandwich thin film structure with thin layers of alternating physical (electron- or ion-conductive) or mechanical properties (structure buffering).

Some typical textures of relevant conventional and nanostructured carbon materials are given in Figure 3a–d, which shows scanning electron microscopy (SEM) images of graphite, activated carbon, ordered mesoporous carbons, and CNTs, respectively. One can clearly distinguish graphite from nanostructured systems with an obviously discernible substructure (Figure 3c and d). The materials in Figure 3c and d exhibit tubular voids in addition to mesopores. The carbon in Figure 3b displays a combination of all these features plus unresolved micropores, and represents a complex hierarchical pore system. The origin of the high potential of nanostructuring becomes intuittively clear from inspection of Figure 3. Carbons with micro- or nanometer-scale dimensions exhibit different transport properties when in contact with reactants. Storage of energy is directly linked to the mass transport of ionic charge carriers (such as solvated Li ions). The efficiency of this transport is controlled, amongst other factors, by diffusion processes which exhibit typical time constants of seconds at nanometer distances at ambient temperatures.

Nanoarchitecturing allows the creation of materials with very high surface areas accessible to Li, which explains the fact that in such electrodes more Li can be stored than allowed by intercalation. These materials, either as a single component or as an assembly through nanoarchitecturing, in combination with nanostructured metal(oxides), open new perspectives for the development of advanced carbon-based electrodes for high-performance lithium-ion batteries and supercapacitors. This allows the following options:

(1) to introduce new materials for both electrodes that are unsuitable as electric materials themselves because they exhibit insufficient electrical conductivity (e.g., nanocomposite electrodes, hierarchical structures);

(2) to increase the contact surface area between the electrode and the electrolyte and to protect the electrolyte from decomposition by catalytic reactions with the electrodes;

(3) to decrease the transport path length for both electrons and ions by using carbon as structuring agent while maintaining its conductive function (e.g., highly functionalized carbon structures).

There are numerous review papers that cover different topics in the development of electrochemical energy storage with respect to Li-storage[19–21] and to electrical charge storage.[22–25] This Review highlights the most important related works and achievements for electrochemical energy storage published in last few years as well as relevant activities on the same topic within the "EnerChem" network of the Max Planck Society. We focus on the materials science of nanocarbons and carbon nanocomposites used as electrodes in Li-ion batteries and supercapacitors. Current challenges and future strategies will be discussed. Some other important issues on electrochemical energy storage, such as device engineering or electrolytes, are not the topic of this Review.

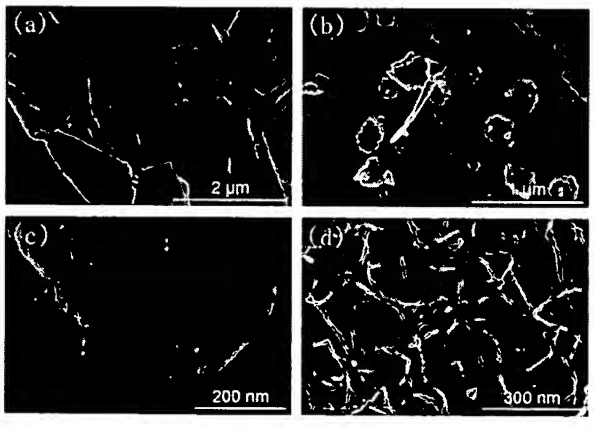

Figure 3. SEM images of several carbon materials used for electrochemical energy storage. a) Graphite. b) Activated carbon. c) Ordered mesoporous carbon. d) CNTs.

2. Lithium-Ion Batteries

Li-ion batteries are one of the great successes of modern materials electrochemistry. Although such batteries are already commercially available and used in portable systems such as notebook computers, cellular phones and digital video cameras, the recent demands for new, low-cost, and environmentally friendly energy conversion and storage systems sets high standards, requiring batteries with high energy and power densities, long cycle life, and good safety.[26,27]

This is reflected in the huge volume of research activity in many laboratories around the world, working on more effective electrode materials and electrolytes as well as studying the ion transport mechanisms and developing more reliable device technologies (see Table 1).

A Li-ion battery consists of two electrodes [an anode (negative) and a cathode (positive)] that are capable of reversibly hosting Li in ionic form (Figure 4). The electrolyte typically contains lithium salts dissolved in an organic carbonate solution, for example a solution of $LiPF_6$ in ethylene carbonate–diethylcarbonate. It should be a good ionic conductor and electronic insulator. The electrodes in a Li-ion battery are separated by a porous polymer membrane. The storage capacity of a battery is given by the amount of Li that can be stored reversibly in the two electrodes. During the charging process, Li ions are extracted from the $Li_{1-y}MO_2$ electrode and simultaneously inserted into the graphitic carbon electrode, coupling with negatively charged electrons to keep overall charge neutrality. During the discharging process, Li ions are reversibly extracted from

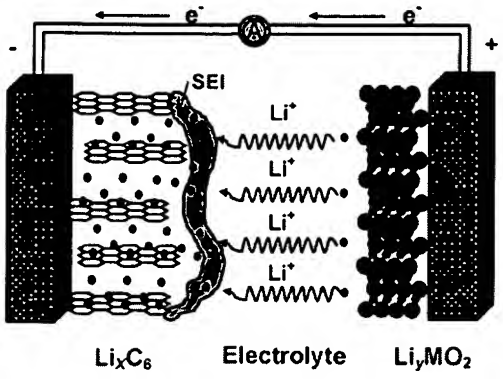

Figure 4. Schematic illustration of an intercalation-type Li-ion battery in a charging process with graphite as the anode and Li_yMO_2 as the cathode (M = metal). SEI is the abbreviation for Solid-Electrolyte-Interphase. Adopted from Ref. [2]. Copyright 2008, Elsevier.

the negative electrode and simultaneously inserted into the positive electrode. The Li ions have to shift back and forth easily between the storage hosts of the cathode and anode (this is the origin of the so called "rocking chair" or "shuttle rock" notation of this kind of Li-ion secondary battery). The electrochemical insertion–extraction process is a solid-state redox reaction involving electrochemical charge transfer coupled with the insertion–extraction of mobile guest ions into/from the structure of the electronic and ionic conductive solid host. Typical discharge chemical equations are:

$$Li_xC \rightarrow C + x\,Li^+ + x\,e^- \quad (1)$$

$$Li_{1-y}MO_z + x\,Li^+ + x\,e^- \rightarrow Li_{x+y}MO_z,\ (x+y=1) \quad (2)$$

The charging process is the reverse of these equations. In the ideal case, the structural features of the host materials should remain unchanged during and after the insertion/extraction of the guests resulting in a long cycling life. In practice initially a large number of additional irreversible reactions occur. They are associated with structural phase transformations of the electrodes and chemical processes related to the Li ion transport. The number of such additional reactions and therefore the capacity fading caused by such reactions decreases with each cycle. By using graphite or nanocarbon as the host, capacities of 250–800 $mA\,h\,g^{-1}$ have been achieved. Alternatives with even higher capacities are Si, Ge, or some metals and alloys.

The operating voltages of Li-ion batteries, typically 3.6–2.5 V, are close to the stability limits of both the electrolyte and the oxide electrodes.[29] The formation of free metallic lithium by destruction of the overcharged electrode materials is possible, as is the formation of polymers from decomposition of the electrolyte. Polymers with or without Li metal deposits at the solid/electrolyte interface modify the ideal electrode–electrolyte contact in a manner that is difficult to predict. This is of critical relevance because it is speculated that this poorly defined interface is the geometric location where Li loses or receives electrons during the discharge–charge operations.[30] Another poorly understood issue is the exact nature and form of the Li ions during transport, as they tend to be solvated and may even form clusters in the electrolyte. Operation of the system is impaired if any of these species associated with naked Li ions are co-intercalated into the electrode materials. The role of such surface-deposited solid electrolyte interface materials and the kinetic management of these processes remains poorly understood.

Intercalation of Li ions is only one of the possible storage mechanisms of Li in its charged form. The storage of one Li atom between every six C atoms is only valid for graphite (Figure 5a). This LiC_6 stoichiometry permits to graphite a storage capacity of 372 $mA\,h\,g^{-1}$; a value lower than other anode materials.[31] However, this low storage capacity results in only a small volumetric change of about 10% and allows for a life of at least 500 cycles, depending on the current rate used. In general, the storage of Li in carbon materials can be described as:

$$6\,C + x\,Li^+ + x\,e^- \rightleftharpoons Li_xC_6 \quad (3)$$

For graphite the capacity index x is almost equal to 1. Even in the most crystalline form of graphite [highly oriented pyrolytic graphite (HOPG)] there is some residual Li left upon deintercalation, associated with the interlayer defects in the material. The intercalation of Li into graphite has been studied extensively and both the mechanism of intercalation, as well as the

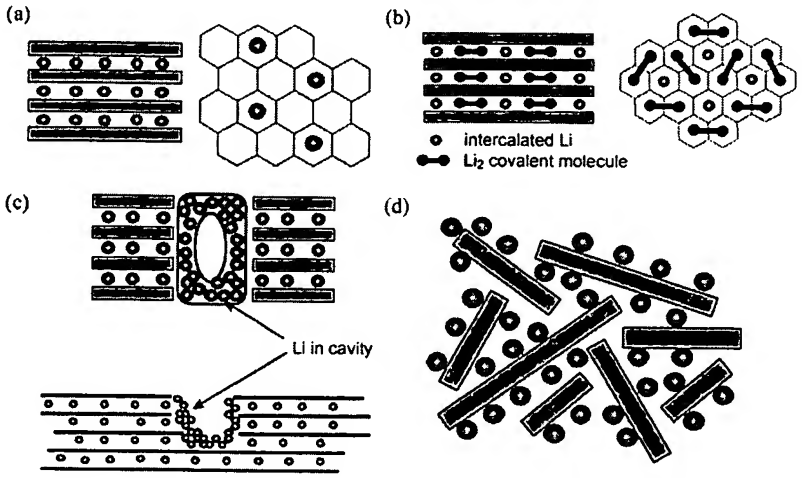

Figure 5. a) Storage mechanisms of Li ions in graphite. b) Li storage in form of Li_2 covalent molecules as proposed by Sato et al.[38] c) Schematic model of Li storage in cavities and nanopores according to Ref. [35]. d) Dahn's model of Li adsorption on the two sides of an isolated graphene sheet.[28] Reproduced with permission from Ref. [35].

electronic host–guest interactions, are well understood.[32,33] For nongraphitic C with a low storage capacity x is in the range 0.5–0.8; whereas for nongraphitic C with an exceedingly high storage capacity $x = 1.2–3.0$.[34,35] This high value makes such carbons very tempting. However, such high values are obtained when the potential is close to 0 V vs. Li/Li^+. This is not beneficial towards safety for high power applications, such as in electric vehicles. An important part of Li is in a pseudo-metallic state.[36,37] For nanostructured carbons with very high specific surface areas, it is suggested that the storage capacity can be increased through the formation of Li_2 molecules between layers (Figure 5b),[38] by the presence of charged Li^+ clusters in the cavities (Figure 5c),[35] in the micropores, or in the inner space of CNTs, through the adsorption of Li ions on the surface and edges of graphite grains. For single-layer carbon Li may adsorb on both sides of graphene (Figure 5d). A more detailed discussion about Li storage in carbon nanostructures can be found in a recent review paper by Kashkedikar and Maier.[6] These authors also propose Li storage in carbon vacancies as a further variant. In many cases the Li storage capacity can be increased due to the presence of hydrogen.[39,40]

High-performance Li-ion cells exhibit a cell voltage of up to 4.5 V and, depending on the type or purity of the electrolyte, may operate beyond the electrochemical stability window of the organic electrolytes used. This causes electrolyte decomposition inhibited only by kinetic reasons and, hence, is difficult to control. During the charging process electrolyte reduction produces solid electrolyte interphase (SEI) films at the negative electrode (see Figure 4). SEIs are porous, electronically insulating structures that hinder further electrolyte reduction while acting as a membrane for the active charge carrier. The formation of SEIs is associated with the irreversible consumption of both Li ions and the electrolyte. The process of their formation is detrimental to the specific capacity of the battery. However, stable SEIs stabilize the cycle life once formed. The formation of SEIs is influenced by the properties of the anode material, including surface area, surface morphology, and surface chemical composition. Much is known, but little is actually understood about the SEI, and many fundamental questions (formation details, chemical and phase composition, dynamic behavior during charging–discharging, electrical and transport properties) remain unanswered.[26] An important challenge related to nanostructured carbons is the fabrication of a surface layer on electrodes prior the use in batteries. This surface layer should exhibit the positive effects of the SEI hindering the decomposition of the electrolyte. Such a material would allow for an electrode that combines a high reversible capacity with a good cycling stability of Li ion batteries.

2.1 Nanostructured carbon materials

2.1.1 Carbon nanotubes

2.1.1.1 Carbon nanotubes as active materials for electrodes

CNTs are the most representative nanocarbons and have been claimed to exhibit outstanding electrical properties, strong mechanical strength, high chemical stability, high aspect ratios, and high activated surface areas. The potential of CNTs as electrodes in Li-ion batteries has been proposed and tested by many research groups as early as the 1990s.[41–46] The reported Li storage capacities exceeded the values for the LiC_6 composition observed for graphite. Li ions can be stored in electrodes comprising CNTs via the following different ways:

(1) intercalation (LiC_6 stoichiometry);
(2) adsorption and accumulation on the outer surface;
(3) adsorption and accumulation in the inner channel when CNTs are open;
(4) storage in the void space between bundles of tubes.

In addition, the Li storage in CNT materials can be increased through:

(5) adsorption on the surface of CNTs via reaction with heteroatoms or functional groups;
(6) storage as in (1), (2), (4) and (5) in/on the graphitic or amorphous co-components in CNT materials (intended or unintentional from impurities).

Figure 6 shows the discharge (Li insertion)/charge (Li extraction) curves of an electrode comprising CNTs with highly ordered graphitic structure, cycled in 1 M $LiPF_6$ ethylene carbonate (EC)/dimethyl carbonate (DMC) (1:1 by volume) at a rate of C/5. Flat plateaus can be observed at low voltages in the discharge and charge curves, and were ascribed to Li intercalation–deintercalation between graphitic layers. Sloped regions in the discharge–charge curves are also observed and were ascribed to Li via other mechanisms mentioned above. X-ray diffraction (XRD) and Raman measurements revealed ordered graphitic and disordered structure features of the used CNTs. A large irreversible capacity was observed in the first discharge and charge process, which is due to the formation of an SEI. The first charge capacity is about 360 $mA\,h\,g^{-1}$ and the reversible capacity stabilizes at 350 $mA\,h\,g^{-1}$ after 20 cycles. It is obvious from Figure 6 that a significant part of capacity is not obtained at a constant potential. At constant voltage, the capacity is only 200 $mA\,h\,g^{-1}$.

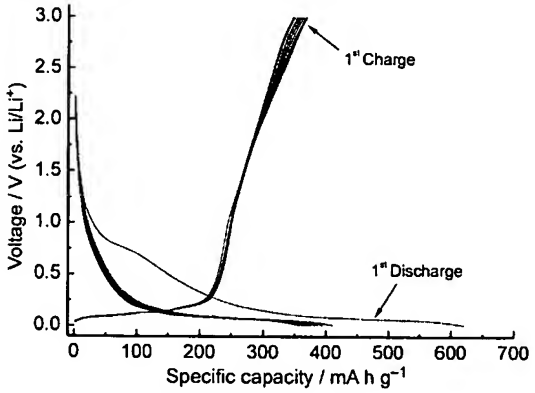

Figure 6. Galvanostatic discharge (Li insertion, voltage decreases)/charge (Li extraction, voltage increases) curves of CNT sample cycled at a rate of C/5 in 1 M $LiPF_6$ in EC/DMC solution (courtesy of Dr. Yongsheng Hu, PR China)

In fact, the performance of CNTs in Li-ion batteries as shown in Figure 6 is only an exception for CNTs with well-graphitized wall structure. The diversity of CNTs in microstructure and tex-

ture as well as surface functionality combined with the multiple storage mechanisms render reported Li storage capacities highly variable, but usually with a huge irreversible capacity and hysteresis. The Li intake can be as high as 1400 mAh g^{-1} or only a few hundred mAh g^{-1}, with rather different irreversible and reversible capacities (see Table 2 for details). This is expected as the above-mentioned storage mechanisms are strongly dependent on textural parameters and the degree of graphitization. There are some major aspects of CNTs that need to be taken into account when used as electrode materials

An essential aspect of CNTs with regard to their application in Li-ion batteries is the texture. Mass-produced commercially available CNTs are defect-rich, both on the surface and in the bulk.[47] Figure 7 compares the microstructure of a defect rich CNT (Figure 7a) with a CNT with well-ordered graphitic wall (Figure 7b). A higher density of defects increases the Li-storage capacity. Treatments (e.g., ball-milling the CNTs) that increase

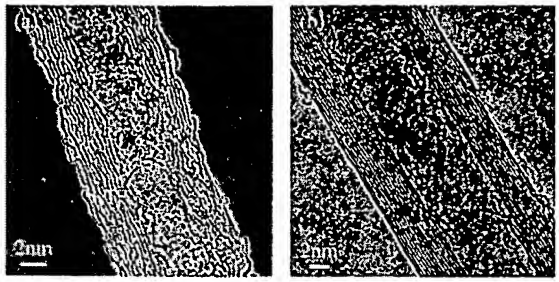

Figure 7. High-resolution TEM images of CNTs with a) defect-rich surface and walls and b) well-ordered graphitic walls.

Table 2. Some results of nanocarbon and carbon-containing composite materials used in Li-ion batteries.[a]

Sample	Capacity [mAh g^{-1}]		Test conditions		Electrolytes	Ref.
	Reversible	Irreversible	Voltage [V]	Scan rate		
MWCNTs	220–390	370–870	0.02–3	30 mA g^{-1}	1 M $LiPF_6$ in EC & DEC (1:1 v/v)	[43]
SWCNTs	ca. 460	ca. 1200	0.01–3	20 mA g^{-1}	1 M $LiPF_6$ in EC & DMC (1:1 v/v)	[44]
CNFs	160–450	80–250	0–2	0.2 mA cm^{-2}	1 M $LiPF_6$ in EC & DMC (1:1 v/v)	[45]
MWCNTs	ca. 250	ca. 250				
SWCNTs	ca. 600	ca. 1400	0–3	50 mA g^{-1}	1 M $LiClO_4$ in EC & DMC (1:1 v/v)	[46]
Ball milling SWCNTs	ca. 1000	ca. 600				
CNTs	300–650	875–900	0.005–2.8	20 mA g^{-1}	1 M $LiClO_4$ in EC & DEC (1:1 v/v)	[50]
CNFs@CNTs	400–430	300–330	0.01–3	C/5	1 M $LiPF_6$ in EC & DMC (1:1 v/v)	[76]
BCNTs	ca. 320	–	0–2		1 M $LiPF_6$ in EMC & DMC (1:1 v/v)	[60]
CMK-3	850–1100	2000–2250	0.01–3	100 mA g^{-1}	1 M $LiClO_4$ in EC & DEC (1:1 v/v)	[81]
HPCM-700	500–900	680–1080	0.01–3	C/5	1 M $LiPF_6$ in EC & DMC (1:1 v/v)	[87]
Si@SiOx/C	100–1600	1050–2550	0.05–1	150 mA g^{-1}	1 M $LiPF_6$ in EC & DMC (1:1 v/v)	[119]
Si@SiOx/C	1100–1200	1000–1100			1 M $LiPF_6$ in EC &DMC (1:1 v/v.) + 2 wt% VC	
Si@C	2750–3150	500–900	0–1.5	C/5	1 M $LiPF_6$ in EC & DMC (1:1 v/v)	[121]
Sn/Mn/C	50–600	100–550	0–1.3	37.2 mA g^{-1}	1 M $LiPF_6$ in EC & DEC (3:7 v/v)	[140]
C/SnPs	520–600	430–350	0.01–3	C/5	1 M $LiPF_6$ in EC & DMC (1:1 v/v)	[104]
Sn/C	100–170	530–600	0.0–2.0	50 mA g^{-1}	1 M $LiClO_4$ in EC & DEC (1:1 v/v)	[108]
Sn/MSPC	350–450	750–850	0–2	C/20	1 M $LiPF_6$ in EC & DMC (1:1 v/v)	[110]
Co_3O_4/C	700–900	–	0.02–3.0	C/30	1 M $LiPF_6$ in EC & DMC (1:1 v/v)	[128]
Co_3O_4/C	ca. 900	ca. 380	0–3	C/5	1 M $LiPF_6$ in EC & DMC (1:1 v/v)	[130]
V_2O_5/CTIT	80–280	–	2–4	C/40-C/2.5	1 M $LiPF_6$ in EC & DMC (1:1 v/v)	[137]
3DOM	150–300	400–550	0–2	1.52–15.2 mA g^{-1}	1 M $LiPF_6$ in EC & DMC (1:1 v/v)	[141]
3DOM/Sn	180–260	20–100				
Fe_3O_4-C	500–800	200–500	0–3	C/2	1 M $LiPF_6$ in EC & DEC & DMC (1:1:1 m/m/m)	[142]
MnO_2/CNT	500–1100	1100–1700	0.02–3.2	50 mA g^{-1}	1 M $LiPF_6$ in EC & DMC (1:1 v/v)	[139]
$Si_{70}Sn_{30}$/C	1300–2050	500–1250	0–1.2	0.2 C	1.1 M $LiPF_6$ in EC & DMC (1:1 v/v)	[143]
Si/C	450–550	650–750	0.05–1.2	300 mA g^{-1}	1 M $LiPF_6$ in EC & DMC (1:1 v/v) + 2 wt% VC	[144]
MWCNT@m-SiO_2	350–450	170–270	0.25–2	33.3 mA g^{-1}	1 M $LiPF_6$ in EC & DEC & DMC (1:1:1 m/m/m)	[145]
SnSb-CNT	500–700	700–900	0.05–1.5	100 mA g^{-1}	1.1 M $LiPF_6$ in EC & DMC (1:1 v/v)	[146]
CNT@SnO_2-Au	620–750	1000–1130	0.01–1.2	0.18 A g^{-1}	1 M $LiPF_6$ in EC & DEC (1:1 m/m	[147]
B-MWNTs	165–175	100–110	0–2.5	50 mA g^{-1}	1m $LiClO_4$ in EC & DEC (1:1 v/v)	[159]
SnO2 film	450–580	–	0.2–0.9	0.32 mA cm^{-2}	1m LiClO4 in EC & DEC (3:7 v/v)	[103]
SnO_2 nanofiber	700–760	–				
Ge film	850–1420	980–1550	0–1.5	375 mA g^{-1}	1.0 M $LiPF_6$ in EC & DMC (1:1 v/v)	[125]
Ge nanocry	1700–1800	650–750				
TiO_2-R15	210–260	110–160				
TiO_2-R30	140	190	1.0–3.5	0.05 A g^{-1}	1 M $LiClO_4$ in EC & DMC (1:1 v/v)	[132]
TiO_2-R300	50–60	50–60				
rutile TiO_2-FGS	170	–	1.0–3.0	1C	1 M $LiPF_6$ in EC & DMC (1:1 v/v)	[135]
GNS	300–500					
GNS+CNT	500–700	–	0.1–3.5	0.05 A g^{-1}	1 M $LiClO_4$ in EC & DEC (1:1 v/v)	[80]
GNS+C60	600–800					

[a] A two-electrode system, in which Li metal was used as the counter and reference electrode simultaneously, was most often used.

defect density and reduce the length of CNTs can change their performance as electrode materials.[48] A complex and open interface of defective CNTs may facilitate the initial insertion of Li, however during discharge the removal of Li proceeds highly retarded and results in an overvoltage higher than 3 V (Figure 8a).[49] This is direct proof that some Li ions are not intercalated between the graphitic layers in CNTs, because intercalation and deintercalation proceed with a low voltage profile. The local turbostatic disorder arising from the highly defective structure plays a significant additional role in both specific capacity and cycle life for Li-ion storage.[50]

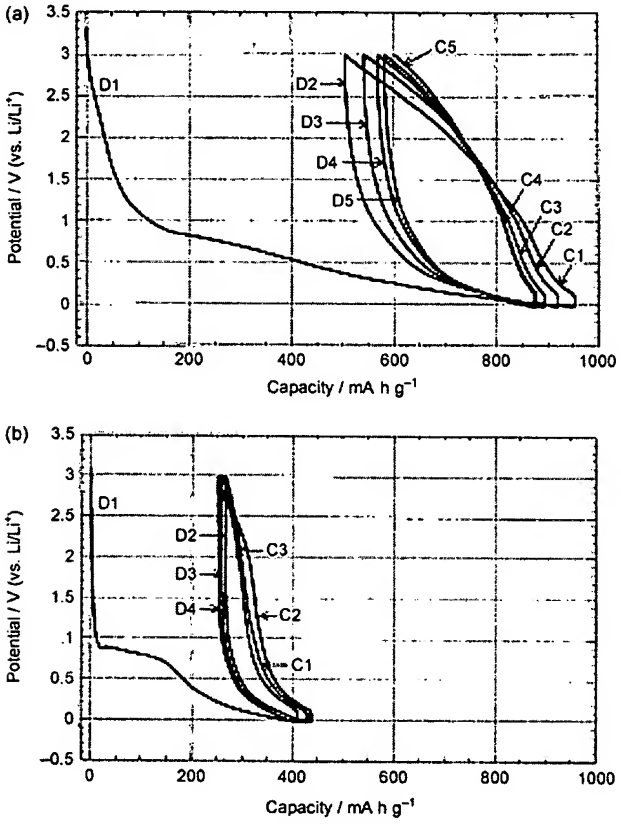

Figure 8. Charge–discharge characteristics of Li insertion into a) multiwalled CNTs treated at 900 °C and b) multi-walled CNT heat treated at 2000 °C at a current of 17 mA g^{-1}. Adopted with permission from Ref. [49]. Copyright 1999, Elsevier.

Carbon materials can contain heteroatom species (e.g., hydrogen). Functionalization of CNTs with other atoms produces various functional groups, changing the surface properties of CNTs.[51–54] The oxidative "purification" of nanocarbons, designed to enhance their CNT content, is unintentionally also a poorly selective functionalization process that affects the whole surface and provides oxygenated species with a wide variety of reactivity on the CNTs.[55] The very popular reagent nitric acid is a strong etchant for CNT surfaces and leaves a high concentration of reactive surface acidic functions on the surface,[56] increasing the specific surface area of commercial carbon materials and therefore resulting in changes in electrochemical performance.[57] The effect of oxygenated species on electrochemical performance can be significant.[58] For example, surface C–O–H groups adsorb Li through formation of C–O^-Li^+, resulting in a large hysteresis (i.e., the divergence between insertion potentials and extraction potential) between electrochemical insertion and deinsertion of Li (Figure 8a). The loss of reversible storage capacity could, through the formation of surface Li-salts, be as high as several hundreds mA h g^{-1}. In this sense, functional groups are considered to be harmful for the performance of Li batteries. It should be mentioned here that the quantity of, in particular, oxygen species is strongly dependent on the texture or defect density of CNTs. Therefore, the roles of oxygen-functional groups and of CNT textures in the electrochemical storage of Li-ions are correlated.

Graphitization at high temperature appears to be the only way to remove defects and oxygen species from CNTs. This decreases the specific charge capacity, but increases the Columbic efficiency and cycle stability. Figure 8 shows that less-graphitized CNTs with 12 at% oxygen on the surface exhibit a high specific charge capacity of 640 mA h g^{-1} during the first cycle. In contrast, the well-graphitized CNTs with nearly no oxygen remaining show a low charge capacity of 282 mA h g^{-1} during the first cycle. After 20 charge–discharge cycles, the charge capacity of the less-graphitized CNTs fades to 65.3% of their original charge capacity, but the well-graphitized CNTs maintain 91.5% of their original charge capacity as a result of their stable structure (Figure 8b).[1,49] Doping CNTs with B atoms can increase the Li-ion uptake, but there was no significant improvement in cycle life and Coulumbic efficiency.[59]

Apart from the microstructure, the morphology of CNTs plays a pivotal role in Li-ion storage. Bamboo-like CNTs as electrode materials show a performance different from common CNTs.[60] Open CNTs exhibit large surface areas; the inner wall and the inner tubular space are available for electrochemical sorption of Li. An increase in the first discharge capacity in the open CNTs was observed.[61] Interestingly, the difference between the reversible capacity of closed and open CNTs is less significant. The main consumption of Li during first cycle could be assigned to the more pronounced SEI layers on electrodes comprising open CNTs. Another factor presently limiting the use of CNTs as electrode materials concerns their physical nature: CNTs are generally supplied as loose particles. As much as 30 wt% polymer binder has to be used to form an electrode using CNTs as main constituent. There are many more creative methods to formulate CNTs in such a way that a percolating electrical path and a sufficient void space for a large electrode-electrolyte interface exists. The strategy towards such useful nanocarbon forms is hierarchical assembly, which can be done by various bottom-up synthetic strategies.[62–64] It is only mentioned here that one major factor that was previously believed to limit the application of CNTs in Li-ion batteries is disappearing: the cost of CNTs as base material is ceasing to be prohibitive for mass application.

2.1.1.2 Carbon nanotubes as additives in electrodes

Because of their one-dimensional structure and large aspect ratio, CNTs easily form a network by entanglement. Together with their excellent electric and thermal conducting properties as well as high mechanical strength, CNTs are used as the fillers or additives of choice for electrode materials, improving their electrical and thermal conductivity and mechanical stability to sustain volume changes during the charge and discharge processes.[65–67] Additionally, penetration of the electrolyte is also favorable. This is currently the only *commercialized* use of CNTs in Li-ion batteries.[4]

The texture of such a composite anode, as shown in Figure 9, exemplifies the value of CNTs but clearly shows the long way that is still to go before arriving at a suitable and

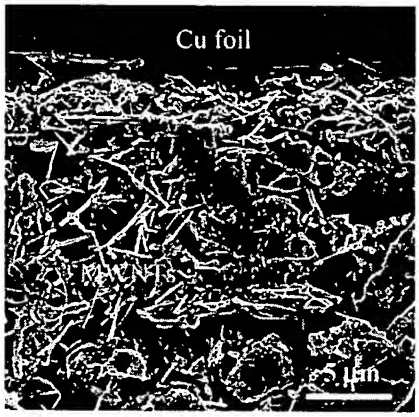

Figure 9. SEM image of a carbon anode in a commercial cell in which multiwalled CNTs were used as additive. Adopted from Ref. [72]. Copyright 2001, Elsevier.

stable electrode. The authors speculate that a complete bottom-up approach, in which the synthesis of a hierarchically structured carbon through combining CNTs with a reactive organic matrix to form the final electrode, is the most appropriate approach. This can, however, only be done in a rational manner if we optimize the structure, texture, and surface chemistry of the CNTs with full knowledge of the other reaction partners. Both an integrated synthesis strategy (requiring close collaboration between polymer and inorganic carbon chemistry) and a controllable reaction process technology will be required.

2.1.2 Carbon nanofibers

Carbon nanofibers (CNFs) are also graphitized 1D carbon nanostructures (Figure 1 d) with or without a tubular channel. The graphitic layers of CNFs can be inclined at any angle with respect to the fiber axis. Their structure arises from the stacking of very small graphene basic structural units to a tower-like morphology, and not from wrapping large graphene units in a tubular structure. This difference is not obvious from any schematic and low-resolution microscopic images. CNFs are mostly fabricated by chemical vapor decomposition of hydrocarbons.[68,69]

2.1.2.1 CNFs as active materials for anodes in Li-ion batteries

The Li storage mechanism in CNFs is similar to that in CNTs. A critical issue is the enormous exposure of prismatic faces (Figure 1 d) to the electrolyte, allowing for very facile intercalation but on the other hand creating a stability problem, as the towers of the graphene unit may lose contact and the CNFs may break easily. CNFs also exhibit a performance as electrode materials similar to CNTs depending on their microstructure/morphology.[70] CNFs of high graphitization degrees showed capacities of 297–431 $mAhg^{-1}$, especially in the low potential region. However, the low first-cycle Coulombic efficiency of ca. 60% is a problem to be solved. Although the product costs for CNFs decrease now, electrodes consisting of CNFs are still not competitive, neither in prices nor performance, with those consisting of graphite. The only commercialized application of CNFs in Li-ion batteries at present is the use as filler or as additive, where the problem of stability is solved through their incorporation in a matrix.[71,72]

Recently, porous CNFs prepared by electrospinning of bicomponent polymer solutions, followed by thermal treatment,[73–75] were explored as Li-ion storage materials. The electrospun nanofibers exhibited thin web morphologies. Porous CNFs could be collected in the form of porous mats and used directly as anodes in a Li-ion battery without adding any polymer binder or other additives. The charge and discharge capacities were as high as 858 and 566 $mAhg^{-1}$, respectively, during the first cycle.[75] A large irreversible capacity of about 292 $mAhg^{-1}$ was obtained, leading to a relatively low Coulombic efficiency of about 66%. High reversible capacities greater than 400 $mAhg^{-1}$ were obtained for long cycling life, higher than those of nonporous CNFs. The main advantage to using electron spun CNTs as electrode materials is that the electrodes are free from binder/conductive additives.

2.1.2.2 CNF–CNT composites

Nanocarbons with poor graphitic structures exhibit a high initial storage capacity, but have a large irreversible loss of Li ions and suffer from volumetric changes during charging–discharging. This can cause exfoliation and disintegration of electrodes and, thus, break-down of the SEI during cycling. As a consequence, the irreversible loss of capacity is not only limited to the first few cycles but occurs continuously, reducing the cycle life of the battery. On the other hand, carbon materials with a highly graphitized structure show only small volume changes during charge–discharge cycling, are mechanically stable, and robust when used as anodes. A combination of these two carbon materials would ideally increase the storage capacity and improve the cycle life, as evidenced by a recent work by Zhang et al. using well-graphitized CNTs (50 nm in diameter) as nanocontainers to confine CNFs with increased storage capaci-

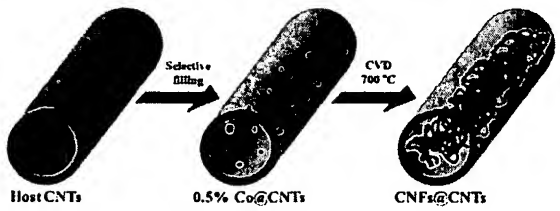

Figure 10. Sectional drawing of the synthesis route to CNFs@CNTs. Reprinted with permission from Ref. [76].

ty (5–6 nm in diameter).[76] The nanoarchitecture concept is shown schematically in Figure 10.

For this purpose, CNTs with a highly graphitized wall structure were used. CNFs encapsulated in a CNT composite (denoted as CNFs@CNTs in the following) were synthesized by (1) selective deposition of the active metal (Co) in the channel of the CNTs, and (2) growth of CNFs via catalytic chemical vapor deposition (CCVD; Figure 10). Such a synthesis protocol is one example of the hierarchical ordering of nanocarbons allowing the combination of otherwise conflicting properties, such as high storage capacity, high mechanical stability, and good electrical contact. The electrochemical performance of CNFs@CNTs in 1 M $LiPF_6$ EC/DMC (1:1 by volume) electrolyte at a rate of C/5 is given in Figure 11 a. In both discharge and charge curves extended flat plateaus can be observed. Clear reduction and oxidation peaks, corresponding to Li intercalation–deintercalation into graphene layers, can be identified in the cyclic voltammogram curve (Figure 11 b). Highly noteworthy is the excellent cycling performance of this composite in a propylene carbonate (PC)-based electrolyte (Figure 11 c). PC is considered as a safe and low-temperature electrolyte,[35,77] but tends to co-intercalate into graphite. This results in severe exfoliation of graphite layers and thus destruction of the graphite structure. The CNFs@CNTs composites also exhibit a superior stability towards high Li storage capacity. During 120 cycles, the reversible capacity of CNFs@CNTs remained approximately constant at around 410 mAh g^{-1} for a potential region 0–3 V. Considering only the plateau region in Figure 11 a, the reversible capacity was 200 mAh g^{-1} and would still need to be improved for realistic applications. Enhancing the discharge–charge rate from C/5 to 1C, the reversible capacity remained higher than

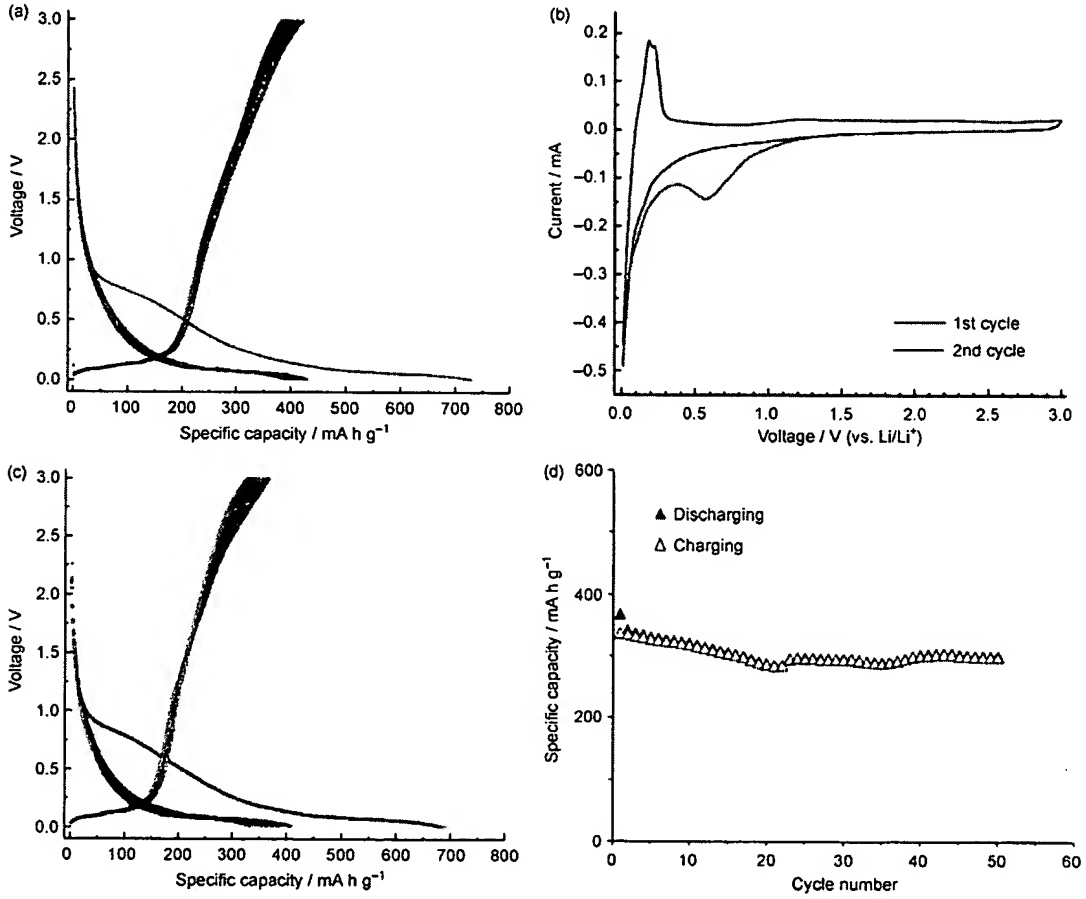

Figure 11. a) Galvanostatic discharge–charge curves of CNFs@CNTs that were cycled at a rate of C/5, and b) cyclic voltammogram at a scan rate of 0.1 mV/s in 1 M $LiPF_6$ in EC/DMC solution. c) Galvanosatic discharge/charge curve cycled at a rate of C/5 in 1 M $LiPF_6$ in PC solution. d) Stability test of CNFs@CNTs at a rate of 1 C in 1 M $LiPF_6$ in EC/DMC solution. Reprinted with permission from Ref. [76].

300 mA h g^{-1} over 50 cycles (Figure 11 d). The obtained stability of CNFs@CNTs over less-graphitized carbon materials mainly arose from steric hindrance effects. The compact structure was able to suppress the diffusion of large electrolyte molecules over the defective walls.

The CNFs@CNTs composites give an example of carbon materials with a hierarchical nanoarchitecture, combining two or more building blocks in a desired fashion, in which the advantages of each unit are explored while the disadvantages are suppressed. In contrast to the frequently promised very high storage capacities of nanocarbons, one observes here a storage behavior comparable to that of good graphite. Graphite is however less sensitive to cycling kinetics. This sensitivity is reduced in CNFs@CNTs due to the nanostructuring and the highly accessible nature of the system. There is room for substantial improvement of the capacity and the storage kinetics through dimensional optimization and through improvement of the structural ordering of the storage medium by optimizing the deposition kinetics and by changing the catalyst system.

2.1.3 Graphene

Graphene, the new star in nanoscience and nanomaterials, is a two-dimensional carbon sheet of one atom thickness representing the basic structural unit of graphite. It is easy to understand that a free standing graphene sheet can afford two surfaces (front and back) for hosting Li ions (via adsorption rather than intercalation; Figure 5 d). Graphene materials obtained by exfoliation of graphite exhibit a large surface area and more prismatic edge sites anchoring functional groups through the preparation procedure. The aggregation of graphite structural units or graphenes in an irregular fashion creates more void spaces. Some works have been dedicated to graphene and graphene-based materials as electrode for Li ion batteries, as highlighted in a recent paper of Liang and Zhi.[78] Anodes prepared from chemically synthesized graphene nanosheets delivered a specific capacity of 945 mA h g^{-1} in the initial discharging and a reversible capacity of 650 mA h g^{-1} in the first charging.[79] A specific capacity of 540 mA h g^{-1} was also reported using graphene nanosheets (thickness 3–7 nm) obtained by the chemical reduction of exfoliated graphite oxide as anode materials.[80] The incorporation of reduced graphene oxide with CNTs or C_{60} further improved the capacity to 730 and 784 mA h g^{-1}, respectively. The presence of functional groups on the perimeter of the graphene sheets can also enhance the Li storage capacity.[81]

All of the reported values are significantly higher than that of graphite. However, the graphene electrode exhibits some major disadvantages that hinders its application in Li-ion batteries: (1) the irreversible capacity is very high at the first cycle (Figure 12); (2) the discharge capacity continuously decreases with the increasing cycle number (although the loss is not as large as in the first cycle, and the specific capacity, e.g., 460 mA h g^{-1} after 100 cycles,[79] is still larger than that of graphite); (3) the galvanostatic charge curve does not exhibit a plateau, as is shown in Figure 12. The chemical interaction of Li with graphene, leading to a finite charge transfer that is strongly dependent on the concentration of the Li with respect to the carbon mesh, is another unresolved issue.

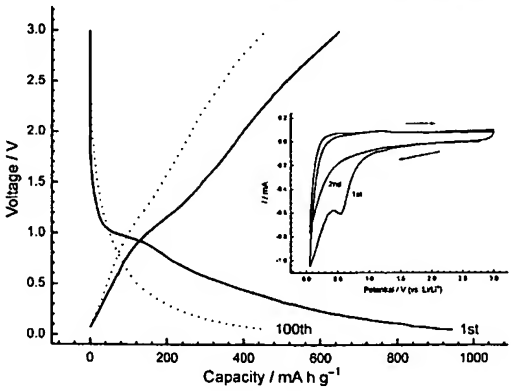

Figure 12. Charge and discharge curves of graphene nanosheets as anodes in Li-ion cells. The inset is the cyclic voltammograms of graphene nanosheet electrode. Adopted with permission from Ref. [79]. Copyright 1999, Elsevier.

Whether or not graphene can be really used as electrode material is highly questionable. Graphene is defined as a two-dimensional carbon sheet of one atomic thickness. The above mentioned "graphene" does not adhere to that definition, but is rather a nanographite with a thickness of up to several nanometers. These are well-known in the carbon community, describing the structure of carbon black or soot.[82] Such materials are not graphene but represent a class of carbon–carbon composites with a complex hierarchical structure, providing nanometer-scale dimensions well-suited for transport processes occurring during battery operation. The intrinsic electronic properties of graphene play no role in this application and should not be considered in relation to such materials. Finally, one has to consider the possibility of the macroscopic connectivity and the current collection limiting the electro-kinetic properties of such a system.

2.1.4 Ordered mesoporous carbon

An essential issue to improve the rate performance is the optimization of the ion transport pathways, without sacrificing electron transport, as the chemical diffusion of Li ions within the bulk electrode materials may be a rate-limiting step.[83,84] A design of a hierarchy of transport routes within the storage medium is desirable. Ordered mesoporous carbon (OMC) materials can be synthesized by the carbonization of suitable carbon precursors inside silica or aluminosilicate mesopores followed by the removal of the template.[85,86] Zhou et al. reported an electrode of OMC [average pore size: 3.9 nm, Brunauer–Emmett–Teller (BET) surface area: 1030 m^{2}g^{-1}] with enormous capacity for Li storage.[81] It displayed a Li extraction potential in the range of 0.1–0.5 V, and delivered an initial Li storage capacity of 3100 mA h g^{-1}, corresponding to a lithiated composition of $Li_{8.4}C_6$. A reversible capacity of 850–1100 mA h g^{-1}, corresponding to Li_3C_6 chemistry, was observed at a constant current density of 100 mA g^{-1}. The enhanced electrode performance was believed to arise from the 3D or-

dered porous structure.[81] The exceedingly high reversible capacity (Li_xC_6: $x = 2.3–3.0$) is most probably a combination of several Li storage mechanisms discussed above.

Mesoporous materials usually exhibit a very large irreversible capacity and hysteresis in the charge–discharge curves. This is characteristic of this kind of material, where a too large surface area with too much active sites leads to an uncontrollable interaction at the electrode/electrolyte interface. These intrinsic, when used in electrochemistry, properties hinder their application in lithium-ion batteries. In addition, SBA-15 templates, which are expensive, are usually employed for the preparation of OMCs. The obtained OMCs are powders of a small size and have a very low density. This could be a second major drawback of this type of materials for industrial applications in portable devices due to the low volumetric capacity. Currently it seems that nanomaterials, especially porous materials with nanostructure, mainly provide a platform to study some fundamental aspects in electrochemical energy storage, for example, the transport limitation, the role of pores, and the electrode/electrolyte interface interaction.

2.1.5 Carbon monoliths with hierarchical structure

Recently, large porous carbon monoliths were fabricated by nanocasting using a preformed silica monolith of macroscopic size as a hard template and mesophase pitch as a precursor.[87] The obtained carbon monolith mimicked the structure of the silica monolith template and had a macroscopic form.[88] The mixed conducting 3D network contained large pores with sizes up to 4 μm (Figure 13a) and mesopores of around 7.3 nm, facilitating the diffusion of electrolyte into the bulk of the electrode materials. The well-interconnected carbon wall structure also provided a continuous electronic pathway, resulting in an overall electronic conductivity of approximately 0.1 $S\,cm^{-1}$ for Li insertion. At a rate of C/5, the first charge density was as high as 900 $mA\,h\,g^{-1}$ for a sample carbonized at 700 °C. The surface contribution to the capacity was estimated to be around 291 $mA\,h\,g^{-1}$ (for a BET surface area of 330 $m^2\,g^{-1}$), explaining the excess capacity in the hierarchically porous carbon.[6]

The stationary capacity of around 500 $mA\,h\,g^{-1}$ at C/5 is substantially larger than that of pure graphite and also higher than the above-mentioned CNFs@CNTs composite. The real benefit of the hierarchical monolithic pore structures is the high rate performance: at 60 C, the material exhibits a capacity of about 70 $mA\,h\,g^{-1}$ with good cycling properties (Figure 13b). These examples illustrate the benefits for materials performance when both the chemical and the pore structure of an active mesoporous material are optimized.[89]

The advantage of carbon monoliths compared to other OMCs is their macroscopic, instead of powder, form, which is easier for handling.[85] But the presence of macropores together with mesopores renders it a very low volumetric density. So the volumetric capacity could be too low for any portable applications where volumetric capacity is much more essential than the gravimetric capacity. Similar to anodes using graphene nanosheets, the charge curve of the electrode using hierarchically porous carbon does not have a plateau but rather extends steeply from nearly 0 V to almost 3 V, while the discharge curve shows storage at low voltages.[81] To which degree this is compatible with the storage modes discussed above remains to be explained.[6]

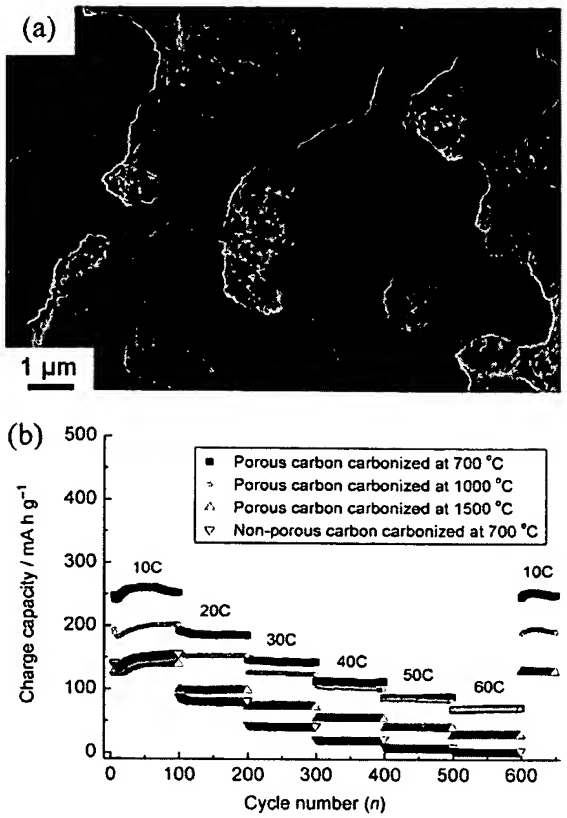

Figure 13. a) SEM image of a carbon monolith. b) Rate performance of carbon samples carbonized at different temperatures and nonporous carbon carbonized from mesophase pitch without template at 700 °C. Reprinted with permission from Ref. [87].

2.1.6 Summary of nanostructured carbon materials for Li-ion batteries

All of the reviewed data of CNTs, CNFs, graphenes, and ordered mesoporous carbons are a good example that some caution is needed when very high storage capacities are reported for nanocarbons. The adsorptive and irreversible parts may be superimposed on a much lower reversible storage capacity, which is the only relevant property of such an electrode. The data further shows that strong limitations exist for overenhancing the storage capacity compared to the intercalation value by increasing the outer surface of an electrode. It is felt that well-ordered carbon structures are a prerequisite for good electrode materials and that great care is needed with post-synthetic modifications to enhance the initial Li storage capacity.

In the literature one often finds a long list of factors that affect Li-ion storage, such as porosity, defect density, preparation history, chemical purity, and "chemical bonding in CNTs." These global parameters are all derivatives of the local chemical composition and the distribution of the hybridization exponent r (between 2 and 3). Only few studies that have controlled and analyzed this single property exist, and thus no clear structure–function correlation yet exists. In addition, the role of carbon as a catalyst for electrolyte decomposition in the presence of metallic Li has not been studied systematically and therefore the results of many studies, including the examples shown here, are obscured by the large irreversible effects which preclude a solid statement regarding the importance of intercalation versus adsorption of metallic Li on nanocarbon electrodes.

It should be pointed out that there is still no standard uniform structure and homogenous morphology available for CNT materials. A comparison between electrodes consisting of various kinds of CNTs is nearly impossible, because CNTs produced by different manufacturers exhibit different structures and properties.[47] In general, as a result of the numerous Li storage mechanisms electrodes that use CNTs do not have a voltage plateau, exhibit a large hysteresis, and have irreversible capacities.[3,41,50,90] This not only precludes practical applications but also prevents a rigorous assessment of their potential in this field. The published speculations and projections of the value of CNTs in battery technology are by far more advanced than the documented performance. This is not due to the inadequacy of the expectations but merely due to a lack of collaboration between CNT experts and electrochemists. Here a great potential exists for improving the performance of CNTs made and formulated suitably for battery applications.

A major drawback of mesoporous materials (also of CNTs or graphene) is the low density. Gravimetric capacities of such materials are given in the literature, while the volumetric capacity could be more of interest for manufacturers when those materials are studied with the aim of applications. The poor packing density of electrodes comprising mesoporous carbons limits the volumetric energy density because a large proportion of "inert" components, such as binder or carbon black, has to be used.[15]

2.2 Carbon-based nanocomposites with other elements or oxides

Some metals and semiconductors can react with Li-forming alloys, Li_xM_y, through electrochemical processes.[35,91] The reaction is partially reversible and involves a large number of atoms per formula unit. The specific gravimetric and volumetric capacities exceed those of graphite. For example, $Li_{4.4}Sn$ has a gravimetric and volumetric capacity of 993 $mAh\,g^{-1}$ and 1000 $mAh\,cm^{-3}$, respectively, versus 372 $mAh\,g^{-1}$ and 855 $mAh\,cm^{-3}$, respectively, for graphite. The corresponding values for $Li_{4.4}Si$ are 4200 $mAh\,g^{-1}$ and 1750 $mAh\,cm^{-1}$, respectively. Because of their high theoretical capacity many efforts have been made to apply these materials in the design of anodes for Li-ion batteries.[18] The rate capability of the battery, defined as its ability to deliver a large capacity when discharged at high C rates, needs to be improved due to the low diffusion rate of Li ions in the solid state. In addition, the accommodation of such a large amount of Li through electrochemical alloy formation also results in a large volume expansion–contraction of the host materials. Sometimes multiphase transitions occur during Li insertion–extraction processes. The volumetric change with large mechanical strain rapidly leads to deterioration of the electrode (cracking, crumbling, or eventually pulverization) and causes a substantial loss of capacity in addition to a shortened lifetime of only a few charge–discharge cycles.[92]

Many research efforts have been devoted to overcoming this problem. One approach is to replace bulk with nanostructured materials.[93,94] The major advantage of nanostructuring such materials is the improvement in rate performance (while the safety and cycle life may suffer from this due to the increased reactivity). Nanostructured materials mitigate the problem of slow diffusion because the distance that Li ions must diffuse in the solid state is reduced to the size of, say, nanoparticles. On the other hand, reducing the bulk to nanodimensions can render the phase transitions that accompany alloy formation more facile,[11] but it cannot reduce the extent of the volume change. Carbon-based nanocomposite concepts have been successfully developed to limit or reduce these adverse effects and at the same time enhance the electron or ion transport. Carbon permits rapid Li permeation as well as high electronic conductivity. Nanocarbon was chosen as one building block in the composite due to its manifold morphology and mechanical and physical properties, as mentioned above. Thin carbon layers can encapsulate metal(oxide) nanoparticles;[95] CNTs can be used as support or container for the active materials;[76] or the highly electroactive materials can be dispersed into a matrix (see Figure 2).[96] In all of these nanocomposites, carbon acts as a confining buffer to ensure the stability of the structures and to enhance the electrical conductivity during cycling. One of the challenges is to disperse active particles with as small volumes as possible into the carbon structure buffer to ensure that the volume change of the composite is small, thereby preventing delamination between binder and filler.

2.2.1 Sn/C nanocomposites

Sn-based materials were tested as negative-electrode materials due to their high theoretical capacity, but they also exhibit inherently poor cycling stability.[97–99] Nanosizing Sn powders by laser-induced vapor deposition yielded a first charge capacity as high as 904.4 $mAh\,g^{-1}$. However, a capacity loss occured in the initial cycles due to the reduction of SnO_2 and Ostwald ripening as well as coagulation of nanoparticles into larger structures, which are sensitive to disintegration via cracking arising from the large absolute volume changes.[100,101] High-rate and stable performances over 1400 cycles were obtained on an anode of SnO_2 nanofibers (100 nm in diameter) array template on Pt current collector.[102,103] Because of the brush-like configurations of SnO_2 nanofibers, there is room to accommodate the volume expansion around each nanofiber. However, the im-

proved rate capabilities come at the expense of volumetric energy density for the electrode.[11]

Encapsulation of Sn nanoparticles with carbon was proposed by different protocols.[104–106] A carbon layer coated onto the Sn particles provided sufficient mechanical strength to act as structural buffer, preventing disintegration and aggregation of Sn. One method is a one-step approach of solid-state pyrolysis of allyl triphenyltin (ATP-Sn).[104] ATP-Sn is a Sn-containing complex with active allyl groups that can be polymerized at relatively low temperature.[107] The grain size of the Sn particles is below 20 nm and the majority of them are hollow (Figure 14a and b). A highly stable and reversible capacity of about 550 mA h g^{-1} was achieved for the prepared composite (Figure 14c). This is in contrast to other nanometer-sized Sn/C composite materials for which a lower specific capacity of the first cycle of 452 mA h g^{-1} was reported.[108]

Besides the strategy of coating hollow Sn nanoparticles with a carbon layer, another strategy putting nanometer-sized Sn particles into a hollow inactive container. Sn nanoparticles encapsulated with elastic hollow carbon spheres (TNHCs) with uniform size (ca. 500 nm) was reported,[109] in which 5–10 Sn nanoparticles (<100 nm) were encapsulated in one thin hollow carbon sphere (thickness ca. 20 nm). The content of Sn was up to 74 wt%, which resulted in a high theoretical specific capacity (831 mA h g^{-1}). The volume ratio of the Sn nanoparticles and the encapsulated void space was about 1:3, which could accommodate the volume expansion during Li insertion. For a maximal 4.4 Li uptake, the formed $Li_{4.4}Sn$ alloy occupied about 83% of the total inner space of the hollow carbon spheres.[15] As a result, this type of Sn-based nanocomposites had a very high specific capacity, larger than 800 mA h g^{-1}, in the initial 10 cycles, and ca. 550 mA h g^{-1} even after 100 cycles, as well as good cycling performance.

A sonochemical process has also been developed for the insertion of Sn nanoparticles into mesoporous carbon, yielding a product which was used as a building block for the anode of a rechargeable Li-ion battery. This electrode could deliver a reversible capacity of 400 mA h g^{-1} at 100% cycling efficiency.[110] OMC[111] and CNTs[112,113] were also reported to be suitable as structural buffers for volume changes of Sn nanoparticles during repeated lithiation–delithiation. A more complicated hierarchical Sn/C composite nanostructure was tested for Li storage.[114] Although this composite nanostructure was built up from several basic nanoscale blocks, the improvement for Li storage was less pronounced than observed for the other Sn/C composites described above.

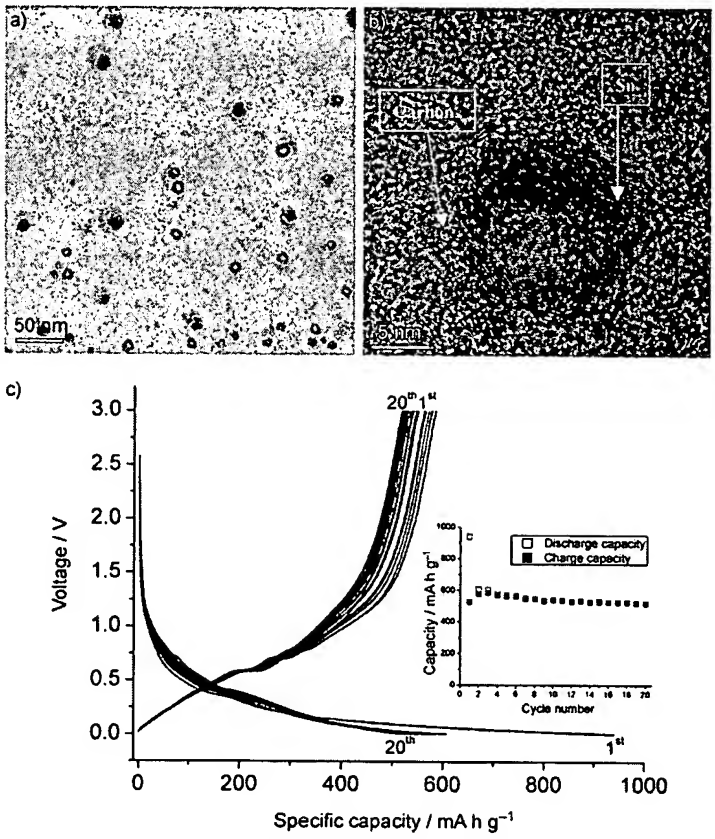

Figure 14. a) Typical TEM image of a Sn/C composite. b) HRTEM of a hollow Sn particle encapsulated in carbon. c) Galvanostatic discharge–charge curves of a Sn/C nanocomposite cycled at a rate of C/5 between voltage limits of 0.01 and 3 V. The inset shows the cycling performance of the Sn/C nanocomposite. Reprinted with permission from Ref. [104].

An important issue in forming such Sn/C nanocomposites is to find an appropriate compromise between a high packing density of Sn particles and sufficient space to buffer the volume variation.[115] Recently, Sn@C (Sn coated with C layers) nanoparticles were encapsulated in porous multichannel carbon microtubes[112] and in bamboo-like hollow CNFs.[116] The carbon fibers or microtubes containing Sn precursors were prepared by electrospinning techniques, followed by carbonization at high temperature. The Sn content was as high as 70 wt%. A novel feature of the obtained composites was the in-situ formation of Sn@C encapsulated in the CNFs/microtubes. The thin carbon layer coated on the surface of Sn nanoparticles increased the conductivity and additionally buffered the large volume change during cycling, as described above. The Sn@C structure was further encapsulated in hollow carbon fibers/microstubes that offered adequate void space to digest the large volume change, preventing the electrical isolation after

prolonged cycle time. In addition the dual carbon protection prevented the encapsulated metallic Sn from oxidation, also improved the electronic conductivity. For example, when a composite of Sn@C encapsulated in CNFs was used as anode, a high reversible capacity of 737 mA h g^{-1} after 200 cycles at 0.5 C was obtained. It even exhibited a reversible discharge capacity as high as 480 mA h g^{-1} when cycled at 5 C. All of these performances are superior to the reported Sn@C composites used for Li-ion batteries, although the synthetic method is still far away from a practical application.

2.2.2 Si/C and Ge/C nanocomposites

Si has the ability to store large amounts of Li by alloy formation of $Li_{4.4}Si$ with a theoretical capacity of 4200 mA h g^{-1}. Galvanostatic discharge–charge measurements (Figure 15c) show that pure Si nanoparticles can deliver very high discharge and charge capacities of around 3200 and 1800 mA h g^{-1}, respectively, in the first cycle. However, after several cycles, the capacity rapidly decays to 20 mA h g^{-1}. When vinylene carbonate (VC) was added to the electrolyte, the Si nanoparticles showed a slightly better cycling performance. Anodes of Si/C composites should combine the advantageous properties of carbon (long cycle life) and Si (high Li storage capacity). A reversible capacity of about 500 mA h g^{-1} was obtained when Si was dispersed in carbon by chemical vapor deposition.[95] A better cycling characteristic than for a conventional silicon anode was observed on carbon-coated silicon synthesized by a thermal vapor deposition method,[117] while carbon-coated Si nanocomposites with high capacities and high Coulumbic efficiencies were prepared by a spray-pyrolysis technique.[118]

In a joint collaboration between three Max Planck Institutes in Stuttgart, Golm, and Berlin, an anode using Si@SiO_x/C nanocomposite was prepared by simultaneous coating of preformed Si nanoparticles in a one-step procedure with a thin layer of SiO_x and with carbon from the hydrothermal carbonization of glucose at 200 °C.[119] Compared to the methods mentioned above, this is a simple and low-temperature process to prepare a Si/C hybrid nanocomposite. Biomass (glucose) was used as the carbon source. The obtained Si@SiO_x/C nanocomposite (Figure 15a and b) exhibited the desired core/shell structure and showed a better cycling performance than pure Si nanoparticles (Figure 15c). However, it still exhibited a rapid capacity decay in the VC-free electrolyte. An excellent cycling performance was achieved in a VC-containing electrolyte. The reversible capacity was as high as 1100 mA h g^{-1} at a current density of 150 mA g^{-1}, with no further decay of capacity even after 60 cycles. The reaction of the C surface layer with VC in the first cycle formed a SEI film that resisted the harsh deformation processes when Si nanoparticles were loaded with Li.

Future work will focus on how the Coulombic efficiency of the first cycle can be improved. The Si/C ratio in such composite materials could play a role in increasing both the specific capacity and the cycle life of the battery. There is still no report on the

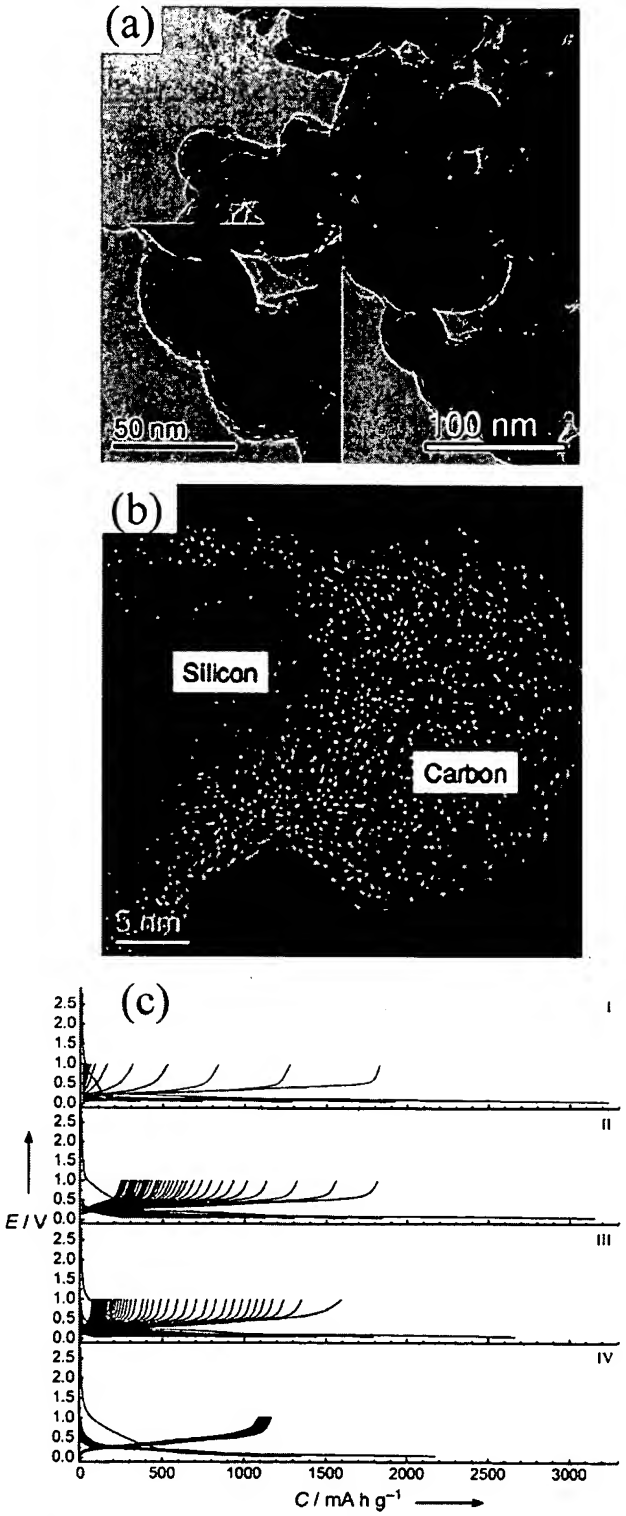

Figure 15. a) Overview of the Si@SiO_x/C nanocomposites. Inset: TEM image at a higher magnification, showing uniform spherelike particles. (b) High-resolution TEM image of the Si nanoparticles coated with SiO_x and C. c) Galvanostatic discharge–charge curves of pure Si nanoparticles (I, II) and Si@SiO_x/C nanocomposite (III, IV) electrodes cycled at a current density of 150 mA g^{-1} between voltage limits of 0.05–1 V in VC-free (I, III) and VC-containing (II, IV) 1 M $LiPF_6$ in EC/DMC solutions. Reprinted with permission from Ref. [119].

optimal Si loading in a carbon matrix, rendering a hight capacity and a long cycle life. Works on the optimization of these materials in order to achieve the optimal electrochemical performance are still needed. The irreversible capacity loss of the reported work is too large.

A porous Si/C nanocomposite was synthesized by adding Si nanoparticles to a process for fabricating a hierarchical carbon monolith.[120] Elsewhere, mesoporous Si/C nanowires were prepared by using a SBA-15 silicate as a hard template.[121] These not only showed excellent Li uptake with a reversible capacity of 3163 $mAhg^{-1}$ at a rate of 0.2 C, but also an excellent rate capability at 2 C. This study provided a further example to validate the concept of using C-containing composites in the design of electrode materials with high Li-ion storage capacity and satisfactory performance. However, the complexity in the synthesis of electrode materials and the high cost of the SBA-15 template do not support a direct rapid technical application in near future.

All of the reported works focus on synthetic strategies and Li uptake tests of carbon-based compounds. Only a few works have tried to reach a fundamental understanding of the improvement in electrochemical performance. The interface interaction of carbon layers with Si, and the C–Si bonds could be essential in the improvement of the electrochemical performance of carbon–Si nanocomposite. For example, it is found by means of electrochemical measurements in conjunction with Raman spectroscopy data that a huge stress is exerted on the Si domains by the in situ-formed carbon layer.[122] When this stress is released, for example by mechanical treatment of the composite, the electrochemical properties change fundamentally. It is suggested that not only the improved electrical conductivity of the Si–C composite, but also the carbon-induced pressure on Si particles, are key parameters for the improved cycling behavior of Si versus Li.

Ge shows a high theoretical capacity of 1600 $mAhg^{-1}$. Compared with Si-based materials, Ge exhibits a higher diffusivity of Li and a lower specific volume change during the Li insertion–extraction process. Even so, an electrode based on Ge still suffers from poor cyclability. Nanometer-sized Ge materials reported in literature still show unsatisfactory cycling performance.[123] Ge/C nanocomposite materials for Li-ion batteries ware prepared by solid-state pyrolysis of an intermediate (PTA-Ge), thermally polymerized from tetraallylgermane.[124] The obtained composite consists of nanospheres with diameters ranging from 50 to 70 nm. Very small Ge nanoparticles with diameters between 5 and 20 nm were observed inside those spheres. The obtained composite shows high discharge and charge capacities of 1190 and 923 $mAhg^{-1}$, respectively, in the first cycle. A highly stable and reversible capacity of about 900 $mAhg^{-1}$ was achieved. The Coulumbic efficiency was rather high. The Ge/C composite also exhibited an excellent rate performance: highly stable reversible capacities around 774, 650, and 613 $mAhg^{-1}$ were obtained at current densities of 300, 600, and 900 mAg^{-1}, respectively. The carbon layer on Ge nanoparticles is mechanically strong enough to prevent Ge particles from disintegration and agglomeration of those nanoparticles. It remains a challenge to achieve a high dispersion of nanoparticles embedded in a carbon matrix. The statement about prohibitive cost of synthesizing large quantities also applies to these options.

2.2.3 Carbon-transition metal oxide nanocomposites

Transition metal oxides are also potential anode materials for Li-ion batteries as they can react with Li reversibly providing a relatively high theoretical capacity.[125,126] The mechanisms are mainly related to reversible formation and decomposition of Li_yO upon Li uptake and release (conversion reaction), which can be described by the following equation:

$$MO + y\,Li^+ + y\,e^- \rightleftharpoons Li_yO + M \quad (4)$$

where M = Fe, Co, Ni, Cr, Mn, Cu and others. These metals do not react with Li. Usually, the reversible capacities are in the range of 200–1100 $mAhg^{-1}$. Details about all possible Li-stor-

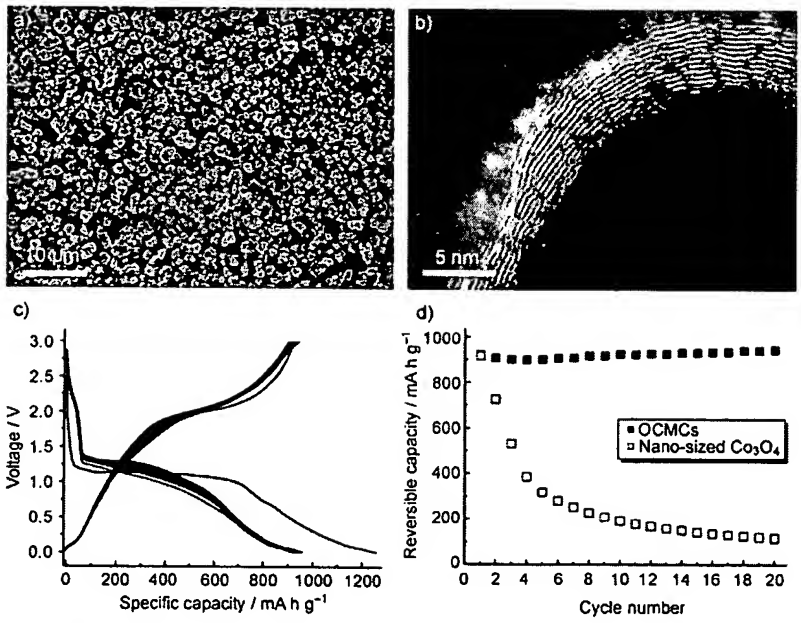

Figure 16. a) SEM image and b) high-resolution TEM image of the carbon/cobalt oxide nanocomposite. c) Galvanostatic discharge/charge curves of carbon/cobalt oxide nanocomposite, and d) comparison of the cycling performance of the nanocomposite (OCMCs) and nanometer-sized Co_3O_4 electrodes. Reprinted with permission from Ref. [130].

age mechanisms in transition metal oxide can be found in literature.[35,91] They have an electrode potential that eliminates Li plating (e.g., Figure 16c). Other compounds such as fluorides, sulfides, nitrides have been also tested as potential anode materials.[12,15] A major drawback of the conversion reaction is their poor kinetics.

2.2.3.1 Co_3O_4/C nanocomposites

Co_3O_4 can store more than eight lithium atoms per formula unit when it is discharged to 0.0 V vs. Li/Li^+, corresponding to a reversible capacity of 890 $mAhg^{-1}$,[127] but it suffers from a large volume change and has an unstable SEI on the surface when used as an anode material.[128] This causes partial pulverization of the electrodes with a decrease in the electrical conductivity and in the reversible capacity.

The cycling stability of nanometer-sized Co_3O_4 can be improved by uniformly embedding the nanoparticles in the pores of hard carbon spherules (HCS).[129] A specific capacity as high as 403 $mAhg^{-1}$ was preserved after 35 galvanostatic cycles. The improvement was attributed to the small size of the embedded Co_3O_4 particles, ensuring negligible volume variation and a good contact with the carbon matrix during repeated cycling, and to the high structural stability of the HCS, preventing possible aggregation of the Co_3O_4 nanoparticles.[129]

Fabrication of Co_3O_4/carbon composites was also achieved recently through solid-state pyrolysis of structurally defined organic cobalt precursors under an inert atmosphere, followed by mild thermal oxidation.[130] The obtained Co_3O_4/C nanocomposites consisted of Co_3O_4 nanoparticles of approximately 20 nm diameter (Figure 16a) and thin carbon layers covering the surface (Figure 16b). The initial reversible capacity reached was ca. 940 $mAhg^{-1}$ at a rate of C/5, with an initial Coulombic efficiency of about 73% (Figure 16c). This is significantly higher than that of pure Co_3O_4 nanoparticles of similar particle size (64%). After 20 cycles, the reversible capacity of C-covered Co_3O_4 was observed to be maintained at about 940 $mAhg^{-1}$ with a Coulombic efficiency of above 99%, whereas the reversible capacity of the pure Co_3O_4 nanoparticles rapidly decayed to around 120 $mAhg^{-1}$ after 20 cycles (Figure 16d). The good cycling performance arose from the action of the carbon layers as structure buffer.

Very recently, cobalt and cobalt oxide–graphene composites were prepared by using planar metallo-organic molecules such as cobalt phthalocyanine (CoPc).[131] This enabled a homogenous dispersion of cobalt and cobalt oxide into/onto the graphene sheets via a simple pyrolysis and oxidation process. The obtained Co_3O_4–graphene composites exhibited remarkable Li storage performances with highly reversible capacity (754 $mAhg^{-1}$), good cycle performance, and good rate capability. However, most of the charge capacity of the Co_3O_4-based composite was observed at ca. 2 V vs. Li/Li+ (see also Figure 16c), a too high potential for practical applications.

Additional effects such as suppressing electrode–electrolyte reactions and anchoring the SEI material to the oxide have also been reported. It is, however, very obvious that much analytical work is still required in order to tailor such chemically highly complex electrode materials.

2.2.3.2 TiO_2–graphene hybrid nanostructure

TiO_2 is an abundant, low cost, and environmentally benign material. It is structurally stable during Li insertion–extraction and has an electrode potential that eliminates Li plating.[15] The storage capacity of TiO_2 is significant lower than other metal oxides.[132] Li-ion batteries with TiO_2 as electrode, however, also have a reduced energy density due the increased potential of the negative electrode. Nanostructured TiO_2 has been extensively investigated as electrode material.[132] Nanometer-sized TiO_2 with rutile structure showed a much higher electroactivity towards Li insertion than micrometer-sized rutile. Up to 0.8 mol of Li could be inserted into nanometer-sized rutile at room temperature, while only 0.1–0.25 mol of Li could be inserted into micrometer-sized rutile.[133] In terms of rate performance, nanometer-sized rutile is also advantageous over other TiO_2 structures, especially at higher rates.

Maier and co-workers fabricated a hierarchically nanostructured electrode by using TiO_2 as electroactive material in a mixed conducting 3D network that exhibited both high power and high energy performance.[134] The conducting networks were built up on both the nano- and microscale levels. The key to its realization were, besides the preparation of nanometer-sized active TiO_2 particles, conductive coating agents (RuO_2, C-RuO_2), which served as mixed conducting 3D nanonetworks. This enabled both Li and electrons to migrate facilely and reach each active particle efficiently, hence realizing the full potential of nanoactive materials. This result is an example of the advantages of using nanoarchitecture materials for energy storage applications. Single-walled CNTs were also used as conductive additives interconnecting nanostructured anatase TiO_2, demonstrating an increased Li-ion insertion–extraction capacity in the hybrid electrodes at high charge–discharge rates.[135]

By using anionic sulphate surfactants to assist the stabilization of graphene in aqueous solutions and facilitate the self-assembly of in situ-grown nanocrystalline TiO_2 with graphene, Wang et al. prepared nanostructured TiO_2–graphene hybrid materials that showed a slightly enhanced Li-ion insertion–extraction in TiO_2 at low charge rate:[136] the specific capacity was more than doubled at very high charge rates of 20–30 C, as compared with the pure TiO_2. (For an anatase TiO_2–graphene composite, the capacity at a rate of 30 C was 96 $mAhg^{-1}$, compared with 25 mAg^{-1} for control anatase TiO_2). This work showed the possibility to increase the electrode conductivity in the presence of a percolated graphene network embedded into the TiO_2 electrode. The lithium uptake capacity of this system was too low to be comparable with other metal oxide–carbon composites. A large irreversible capacity was also observed at the first cycle. In addition, it is still not fully understood why the increase was so significant at high rate.

2.2.3.3. CNT–V_2O_5 nanocomposites

Recently, another nanoarchitectured electrode using V_2O_5 nanoparticles was proposed (Figure 17),[137] consisting of an efficient mixed conducting network using a carbon tube-in-tube (CTIT) as an "electronic wire," providing electrons to the active

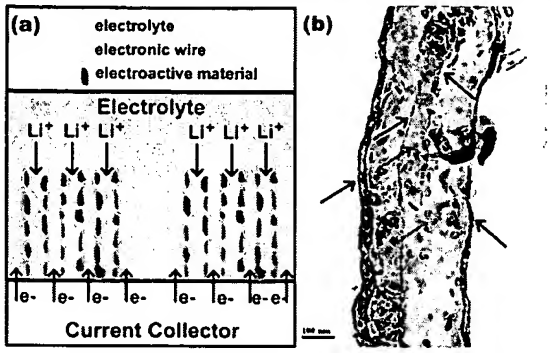

Figure 17. (a) Conceptual representation of the desired design comprising an efficient mixed conducting network. (b) Typical TEM image of the V2O5/CTIT nanocomposites showing that most of the V_2O_5 nanoparticles areen-capsulated within CTIT. Reprinted with permission from Ref. [137].

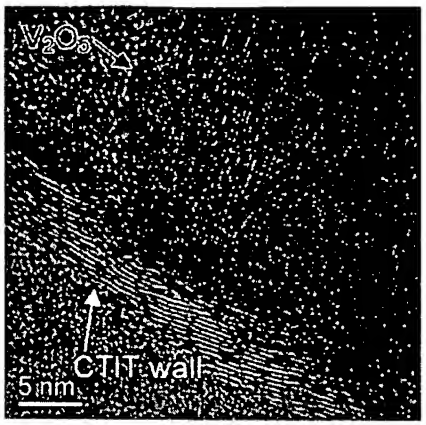

Figure 18. HRTEM image of V_2O_5/CTIT nanocomposites, showing the intimate contact between V_2O_5 nanoparticles and CTIT. Reprinted with permission from Ref. [137].

materials.[138] The specifically designed tube diameter of the CTIT allowed for easy electrolyte access. Such a nanostructure provides the electronic pathway and the Li-ion transport properties that are essential for a Li-ion battery that is rechargeable at high rates. Both the kinetics of Li insertion–extraction and Li storage performance were improved as a result of the intimate electrical contact between the two phases at the nanoscale level and at multiple points along the wall of the CTIT (Figures 17 and 18).

Figure 19a shows the redox kinetics, with peaks at around 3.4–3.2 V, observed for both electrodes. The V_2O_5–CTIT nanocomposite exhibits small polarization differences between the cathodic and anodic peaks for the redox reaction at around 3.4 and 3.2 V with 50 and 60 mV, respectively. The reference microstructured bulk oxide V_2O_5 electrode exhibits unfavourable values of 190 and 300 mV under the same experimental conditions (Figure 19b). A total reversible capacity of about 280 mA h g^{-1} in the voltage range of 2.0–4.0 V was obtained for the V_2O_5–CTIT nanocomposite at a rate of C/2.5 (Figure 19c) (note that the theoretical capacity for two Li per formula unit is 294 mA h g^{-1}). In the discharge process nearly the same amount of Li can be removed, corresponding to a Coulombic efficiency of above 99%. Another excellent property of this V_2O_5–CTIT nanocomposite was its high rate capability. A specific charge capacity of around 265 mA h g^{-1} with a Coulombic efficiency of nearly 100% was obtained at a rate of C/2.5 after 20 cycles; 140 mA h g^{-1} at 20 C, and 90 mA h g^{-1} at 40 C (Figure 19d). This rate capability is higher than that of C-coated V_2O_5 and other V_2O_5-based electrodes. The experimental results obtained here demonstrated that the proposed effectively mixed conducting nanostructure is favourably reducing the diffusion length for Li and thereby enabling the high rate performance of Li-based batteries.

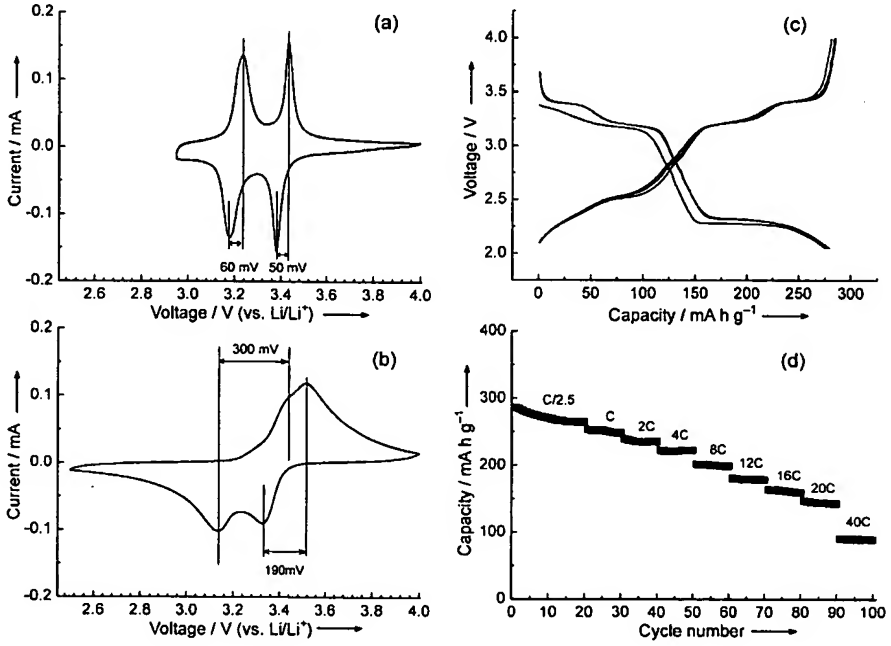

Figure 19. Cyclic voltammograms of a) the V_2O_5/CTIT nanocomposite, and b) V_2O_5 microparticles at a scan rate of 0.1 mV s^{-1}. c) The first three cycles of galvanostatic discharge–charge curve of the V_2O_5/CTIT nanocomposite electrode cycled at a current density of C/2.5 between voltage limits of 2.0–4.0 V in 1 M $LiPF_6$ in ethylene carbonate/dimethyl carbonate solution. d) Cycling and discharging–charging rate performance of the V_2O_5/CTIT nanocomposite electrode. Reprinted with permission from Ref. [137].

The use of CTIT materials provides a more effective nanoenvironment compared to CNTs, increasing the effectiveness of the dispersion and amount per volume of the oxide and thus the storage capacity of the battery. The CTIT also acts as a nanoreactor for the synthesis of nanomaterials, by exploiting its multiple channels and the possibility of confining reagents within them.[17,137] The issue of scaling up the production of CTIT materials, to make them cost-effective for battery applications, remains a challenge for materials scientists.

2.2.3.4 MnO_2–CNT hybrid arrays

Another example of innovative electrodes derived from nanoarchitecturing is a coaxial MnO_2–CNTs array with a thin layer of gold, acting as current collector (Figure 20).[139] A template was required to fabricate MnO_2 nanotubes. This was followed by the growth of CNTs inside the MnO_2 tubes using CVD. The nanosized and porous nature of MnO_2 shells on CNTs allowed fast ion diffusion; the highly electrical conductive CNT core facilitated electron transport to the MnO_2 shell. The presence of CNTs in the core of hybrid nanotubes provided additional Li storage sites, leading to a dual mechanism of Li storage and therefore resulting in an improved reversible capacity when compared with CNTs or MnO_2 under the same test conditions. However, the MnO_2–CNT hybrid materials still showed a large irreversible capacity loss (ca. 1000 mA h g^{-1} at the first cycle) and a steady loss of the capacity even after the second cycle. This could be due to the standing SEI formation because of its cracking and crumbling as a result of volumetric changes of MnO_2. A carbon overlayer may be needed as structural buffer as discussed above. Manganese oxide is, in addition, one of the most potent heterogeneous redox catalysts, so that great care must be taken to prevent the formation of metallic Li on its surface. This would provide a highly active redox catalyst for electrolyte decomposition and irreversible oxide salt formation.

2.2.4 Summary for carbon-based nanocomposites with other elements or oxides

A core challenge in Li-ion battery design is the identification of suitable materials for anode or cathode. Oxides, alloys, and semiconductors are promising because of their high storage capacities. Their strong bonding makes them sensitive to cyclic volume changes, and in many cases electronic conductivities are also problematic. An elegant way around these shortcomings would be the synthesis of nanostructured storage phases interconnected and electronically wired by nanocarbons, for example CNTs. The core benefit would be the adaptation of the diffusion length and of the volume expansion tolerances to the specific material properties of the noncarbon parts. This concept has been described in an elegant manner in the literature many times. The described synthesis strategies seem to fail, however, at improving the system performance, as certain aspects of the concept are well-covered whereas other important factors are not taken care of. No systemic approach has been found so far.

Such an approach would optimize all structural and chemical details of the complex synthesis path to the desired performance. This *rational approach* requires that the important factors that influence the performance of a composite under reversible cyclic chemical stress are known. An example of a conceptual shortcoming is the attempt to minimize the size of electro-active materials for minimizing the diffusion length. However, the choice of material simultaneously has to take into account a minimum sensitivity against reversible volume change, which is not optimized per se when a material is nanostructured. In addition, dividing materials into nanometer-sized objects increases their reactivity, which may decrease the cycle life and lower the safety. An orthogonal approach, to fill the inner volume of a nanotube or mesopores carbon with electro-active materials that upon cycling fragmentation would not fall out of the composite material, is fine but ignores the boundary condition that the fragmented material, to remain electro-active, still requires an electrical contact to the inner walls of a CNT whose morphological and electronic structure are largely unknown.

In the absence of a deep insight into the chemically complex interface processes required to synthesize an optimized composite electrode, it is not surprising that little systematic work is found on optimizing the ratios of chemical constituents and the synthetic protocols for their assembly. Few works on a suitable volume-to-space ratio between electro-active materials in a hollow carbon structure (CNTs, meso-, or macroporous carbons) as structure buffer are known. It is obvious that the required high performance of a composite electrode is strongly influenced by these factors. In addition, the carbon materials used in many studies are not well characterized with respect to their structure, reactivity, and dynamics under operation and under the synthesis conditions of the composite. In summary, the attractive composite concept is not yet put into operation in a convincing

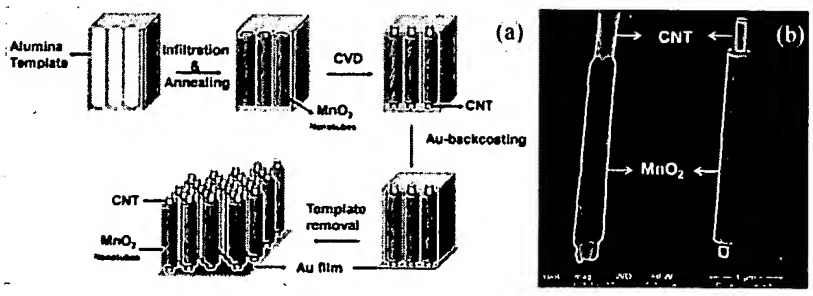

Figure 20. a) Schematic diagram showing the fabrication of MnO_2–CNT hybrid coaxial nanotube arrays inside an AAO template using a combination of simple vacuum infiltration and cCVD techniques. b) SEM image and a schematic representation of a single coaxial nanotube. The MnO_2 shell and CNT core can be clearly seen. Adopted from Ref. [139]. Copyright 2009, American Chemical Society.

manner. Thus, it is premature to draw conclusions about its potential merits, in spite of the reports in the literature.

In the successful reports on the improved performances of composite electrodes achieved phenomenologically, no solid evidence for the cause of the beneficial effect is given; one states rather speculative attributions to hypothetically improved transport kinetics. In the absence of knowing what species are transported through which interfaces, it is challenging to support such speculations by experiments. The mesoscopic mechanical properties associated with material fragmentation are also not well understood. Besides purely mechanical effects also elctromigration, electrocorrosion, and the complex chemistry of the electrolyte acting as reductant, site blocker, or source for bulk impurities of the electro-active material are not well studied.

It seems highly desirable to support the concept of composite electrodes with nanostructured materials by a massive in situ analytical research effort. This effort should clarify the relevant bulk and interface properties of the constituents of a composite. The study needs to focus on the electro-active properties and at the same level of detail also on the conventional chemical properties, as cycling the potential frequently crosses the surface stability boundaries of bulk phases. From this knowledge the boundary conditions for synthesis strategies can be derived. The kinetics of synthesis must be controllable to minimize scale-up and fabrication problems. Such problems can easily spoil the performance of a composite material, as its highly metastable nature will lead to uncontrolled modifications of their critical interfaces. This was frequently experienced in the synthesis of heterogeneous catalysts exhibiting the same basic sensitivity to multiple interfacial properties; the experience collected there may be also useful in the evolution of electrode systems of complex chemical nature.

2.3 Summary for Li-ion batteries

Table 2 summarizes some results of Li-ion storage using nanocarbons and carbon composites from the reviewed works and the literature. In general, the reversible Li storage capacity of nanocarbons is higher than that of graphite, at the expense of higher capacity losses. The use of nanocarbons as electrodes can provide (1) a high electrode–electrolyte contact area, (2) new storage mechanisms that are not possible in bulk materials, and (3) a shorter pathway both for electron and Li ion transport. A shorter transport pathway enables a high charge–discharge rate and, thus, a high power. However, Table 2 reveals that on its own simple nanocarbons in various morphologies can not provide a solution to increase the storage capacity with long-time stability and satisfying safety. "Nanosizing" brings other parameters into operation. For example, the very high surface area and, consequently, the large solid–electrolyte interface enhance the irreversible capacity. Table 2 shows the diverse performances when various nanocarbons are used.

Table 2 also reveals that carbon nanocomposites with metal(oxides) as electrochemically active materials provide increased storage capacities. As discussed above, a better accommodation of the strain of Li insertion–extraction could be achieved by using carbon as structural buffer improving the cycle life. However, in those cases it has not been possible to satisfactorily couple the benefit of the improved cycle life with the operation at higher power. It seems that nanostructuring the electrode materials should remain a general strategy in Li-ion battery research and development.

During the discussion of the examples it was stated several times that high surface areas and large solid–electrolyte interfaces provide challenges for the reversibility of the host–guest interaction. In addition, the question to what extent chemical bonding interferes with purely dispersive host–guest interaction is still unanswered. The lack of analytical data[148] is to be compared with the question about the thermodynamic driving force. The applied potential (how large at the location of reaction?) is opposed by cohesive energies, compound formation, and phase transition energies (irreversible losses), by strain and its structural relaxation, and by entropy. A thorough balance of static energetics, structural dynamics, and transport kinetics through the electrode is still a challenging task. This is not explicitly considered in the more phenomenological approaches reported so far. Starting from a general understanding of carbon bonding mechanisms and their consequences for the structural and chemical disposition, it is possible to construct hierarchical host structures that allow for an optimized ionic and electronic transport. The involvement of additional phases, be they oxides or alloys, should be minimized or avoided in anode structures to minimize the chemical complexity which will in turn minimize the irreversible chemical reactivity.

Another field of nanocarbon synthesis will address the prefabrication of the SEI structure with the dual targets of protecting the electrode material from intimate contact with the electrolyte and of optimizing the ion penetration from the electrolyte into the bulk electrode. Here many fundamental studies are needed before a meaningful design of an optimized structure in which both chemistry and texture are defined can be made. In situ observations of the process of Li transport through the solid–electrolyte interface at realistic conditions will be needed in the first instance. The methodologies of polymerization-carbonization, reactive sputter deposition, and of chemical vapor deposition are at hand to realize the desired protective SEI structures once a clear picture of the functional requirements has been developed.

The Li-ion battery system in its present form is not only limited by the performance of the anode. Although the element carbon is largely associated with the battery anode for storing Li metal species, it must be understood that the bottleneck is not in this part of the system. While developing anodes with larger capacities and slightly higher potentials than carbon is very demanding, developing cathode materials having to store Li and to exhibit the same electrical transport property as the anode is a much greater challenge. Whether nanocarbon can also be used to improve the performance of the electrolyte by structuring the fluid without having to live with the mobility constraints of a polymer remains to be seen.

The techniques used for making carbon–oxide composites for anodes may be adapted to the cathode problem. Here different chemical stability issues are to be met and more elabo-

rate synthesis protocols for the functional oxide nanostructures will be required. Such protocols are available from the synthesis portfolio of heterogeneous oxidation catalysts. These have been only infrequently applied to battery cathodes requiring nanocarbons of modified structure and stability. In contrast to the rich portfolio of anode materials as reviewed here, only few carbon composites, for example, nanocarbon-coated $LiFePO_4$, have been developed for cathodes.

3. Supercapacitors

A supercapacitor, or electrical double layer capacitor (EDLC), is a device that stores charge electrostatically through the reversible adsorption of ions of the electrolyte onto active materials that are electrochemically stable and expose a high surface area. A schematic illustration of an EDLC is shown in Figure 21.

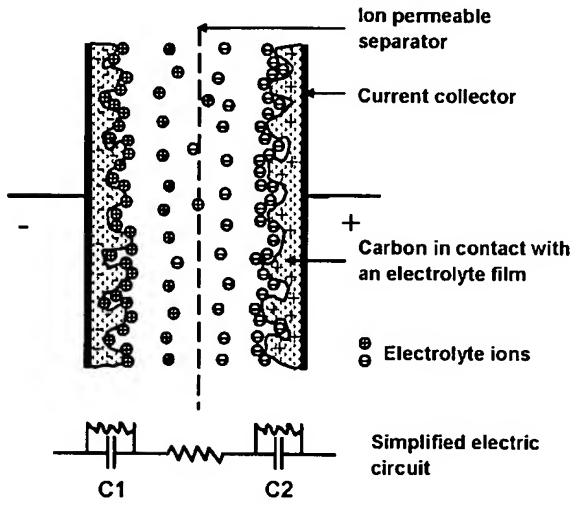

Figure 21. Schematic illustration of an electric double layer capacitor. Adopted from Ref. [4]. Copyright 2006, Elsevier.

It consists of a pair of ideally polarizable electrodes which are immersed in an electrolyte and physically separated by a porous membrane through which ions can diffuse.[149] The capacitance of an EDL-type supercapacitor is assumed to follow that of a parallel-plate capacitor:

$$C = \frac{\varepsilon_r \varepsilon_0}{d} A \quad (5)$$

where ε_r is the electrolyte dielectric constant, ε_0 is the permittivity of a vacuum, A is the specific surface area of the electrode accessible to the electrolyte ions, and d is the effective thickness of the EDL (the Debye length). In a supercapacitor, the charges are stored across a very small distance in the electric double-layer that constitutes the interface between an electrode and the adjacent electrolyte on a highly extended electrode surface area (1000–2000 $m^2 g^{-1}$). The very small d and very big A value renders to EDLC a storage of hundreds or thousands of times more charges (tens to hundreds of Farads per gram) than solid-state and electrolytic capacitors. The maximum energy stored (E) and power delivered (P) for a single cell supercapacitor are given in Equations (6) and (7):

$$E = \frac{1}{2} C_T V^2 \quad (6)$$

$$P = \frac{V^2}{4R_s} \quad (7)$$

where V is the cell voltage (in Volts), C_T is the total capacitance of the cell (in Farads), and R_s is the equivalent series resistance (ESR) of the cell (in Ohms). The cell voltage is limited by the thermodynamic stability of the electrolyte solution. ESR comes from various types of resistance associated with the intrinsic electronic properties of the electrode matrix and electrolyte solution, mass transfer, resistance of the ions in the matrix, and contact resistance between the current collector and the electrode. For a supercapacitor to have a good performance, it must simultaneously satisfy the requirements of having a large capacitance value, high operating cell voltage and minimum ESR.[150] Despite their high power density, the current EDLCs offer a lower energy density than batteries.[21–26,151]

When the charge storage in a supercapacitor is not electrostatic, but occurs instead through a charge transfer that produces a redox reaction (Faradaic reaction) or electrosorption in the electroactive material, the capacitor is called a pseudocapacitor.[21–26] Metal oxides or hydroxides such as Ru, Co, Ni, and Mn oxides/hydroxides are materials with pseudocapacitive properties. Functional groups or heteroatoms in carbon materials can contribute to the pseudocapacitance. The supercapacitor based on pseudocapacitance has a higher specific capacitance (10–100 times) than carbon-based double-layer systems. However, the redox reaction gives rise to a high internal resistance in supercapacitor, resulting in a decrease in the power density. Both of the two different storage mechanisms of EDLS and pseudocapacitance existed for many supercapacitor systems, with one or the other storage mechanism dominating.

EDLCs have a long cycling life and can be easily charged–discharged at a power density exceeding 1 $kW kg^{-1}$. Carbon black or activated carbons are currently the most widely used materials for supercapacitors because of their high specific surface areas and moderate costs.[22] Supercapacitors, using active carbon materials as electrodes, have a much higher theoretical capacitance (100–300 $F g^{-1}$) compared to common capacitors (on the order of micro- or picofarads). However, the energy density of supercapacitors is only a few $Wh kg^{-1}$ or $W h L^{-1}$, much lower than that batteries.[25,147] A lead-acid battery has typically 30–40 $Wh kg^{-1}$ and modern lithium-ion batteries have ca. 120 $Wh kg^{-1}$. Other limitations such as low cell voltage (< 1 V for aqueous and ca. 3 V for organic electrolytes) and sensitivity to impurities prevented the more widespread applications for EDLCs. Their performance needs therefore to be substantially improved with the aim of increasing the energy density while keeping the long cycling life to meet the tough requirements of applications in areas such as in portable elec-

tronics or in hybrid electric vehicles and large industrial equipment.

3.1 Nanostructured carbon materials

The synthesis of electrode materials with highly electroactive regions through the control of the microstructure (e.g., grain size, thickness, specific surface area, and pore character) is a way to develop supercapacitors with high electroactivity. Among these parameters, specific surface area and pore character appear to be the most important factors and have thus far been the most widely studied.[22,25,152] Nanometer-sized electroactive materials with high porosities in contact with liquid electrolytes should also exhibit enhanced electrode–electrolyte interface areas and thus provide highly electroactive regions with decreased diffusion lengths.[153,154] Some of these requirements are the same as for battery electrodes and therefore the same general concepts of dual transport and of hierarchical structuring can be applied.

3.1.1 Carbon with tubular structure

CNTs were evaluated as electrodes to increase the energy density.[155–158] As is shown in Figure 1c, CNTs are highly entangled, forming a well-developed network of open mesopores that is almost impossible to obtain with activated carbon materials.[159] These mesopores allow the rapid transport of ions from the electrolyte to the entire surface of the electrodes and make them quickly available for electric charge exchange. As a consequence the response time to an external potential change is fast, resulting in the capability for energy extraction at high frequencies (about 1 Hz)[23]. Frackowiak et al.[160,161] have investigated the EDLC performance of nanotubes prepared by various methods and have found that the studied CNTs present voltammograms with a regular box-like shape characteristic of an entirely electrostatic attraction (Figure 22). For multiwalled CNTs capacitances of about 120 $F g^{-1}$ and 49 $F g^{-1}$ were reported at 1 and 100 Hz, respectively.[161] A major disadvantage of multiwalled CNT materials for supercapacitor applications is their low specific surface area compared to, for example, activated carbon.

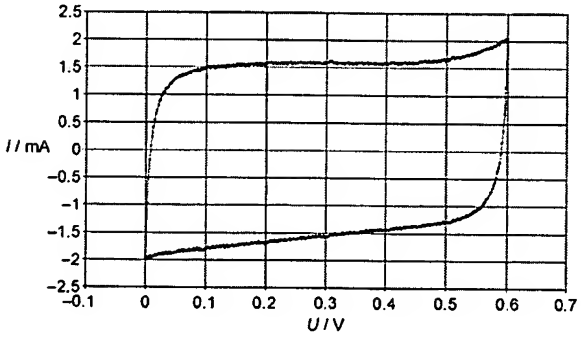

Figure 22. Voltammetry characteristics (2 $mV s^{-1}$) of a capacitor built from CNTs modified by electrodeposited PPy. Electrolyte, 1 M H_2SO_4. Adopted from Ref. [23]. Copyright 2006, Elsevier.

Single-walled CNTs offer particular potential as new carbon electrodes for EDLCs because of their theoretically high surface area. The reported values for the gravimetric EDLC of the SWCNT electrode span a wide range, between 20 and 300 $F g^{-1}$.[162–165] For example, single-walled CNTs with a specific surface area of 500 $m^2 g^{-1}$ were found to exhibit a specific capacitance of 40 $F g^{-1}$.[166] For purified nanotubes (without residual catalyst or amorphous carbon), the specific capacitance varied between 15 and 80 $F g^{-1}$ with surface areas that ranged from ca. 120 to 400 $m^2 g^{-1}$.[161,167] Here again, CNTs provided by different producers exhibited different physical and chemical properties, preventing a generalized conclusion regarding their applications in EDLCs.

The powdered form of CNTs hinders their application for electrochemical energy storage. The macroscopic shaping of CNTs (e.g., to CNT pellets) can result in the deterioration of the intrinsic properties of individual CNTs. One possibility is to form composite materials using CNTs as one component and carbon from an organic precursor as the matrix. Single-walled CNTs have been prepared as composite with polyvinylidene chloride (PVDC). After carbonization the composite electrodes exhibited a maximum specific capacitance of 180 $F g^{-1}$ and a measured power density of 20 $kW kg^{-1}$ in potassium hydroxide.[168,169] This high specific capacitance was attributed to a surface area of 357 $m^2 g^{-1}$ and a redistribution of the CNT pore size to lower values near 3–5 nm. Recently, a high-density packed and aligned single-walled CNT material were fabricated by using the zipping effect of liquids to draw tubes together.[170] To use the zipping effect of a liquid, the single-walled CNTs must be grown in an array on a support. The capacitance of the prepared solid supercapacitor was estimated as 20 $F g^{-1}$ from the discharge curves of cells charged at 2.5 V for a two-electrode cell corresponding to 80 $F g^{-1}$ for a three-electrode cell.[170] This value falls within the range of values reported for single-walled CNTs for EDLCs as mentioned above, but the method allows the macroscopic shaping of aligned CNTs for practical use.

The above-mentioned CNFs@CNTs composites have also been tested for supercapacitive performance.[76] Galvanostatic discharge–charge measurements at two different current densities and the relationship between specific capacity and current density are shown in Figure 23a and b, respectively. The specific capacitance was approximately 70 $F g^{-1}$ at a current density of 148 $mA g^{-1}$ in 1 M H_2SO_4. At higher current densities of 370 and 740 $mA g^{-1}$, capacitance values of approximate 48 and 40 $F g^{-1}$ were obtained. These values are not higher than that of activated carbon in H_2SO_4 solution, mainly due to the relatively low specific surface area of 347 $m^2 g^{-1}$, which is already increased from 82 $m^2 g^{-1}$ after the nanostructuring as shown in Figure 10.

3.1.2 Two-dimensional carbon structures

The theoretical surface area of a single graphene sheet is 2630 $m^2 g^{-1}$, comparable to values derived from Brunauer–Emmett–Teller (BET) surface area measurements of activated carbons used in current electrochemical double layer capaci-

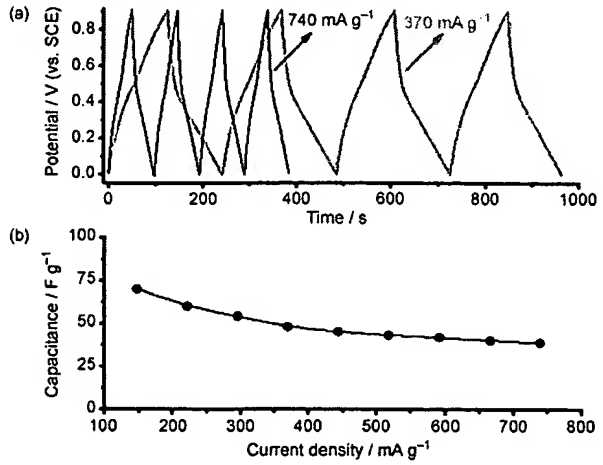

Figure 23. Performance of CNFs@CNTs composite in supercapacitor tests. a) Galvanostatic discharge–charge curves cycled at current densities of 370 and 740 mA g^{-1}. b) Relationship between specific capacity and current density.

tors. This has stimulated some works to use graphene or graphene-related materials in supercapacitors.[171–173] Graphene materials prepared through exfoliation of graphitic oxide can have a BET surface area as high as 925 m^2g^{-1}. The number of graphene sheets is between 3 and 16. This graphene material was reported to show a electrochemical redox behavior similar to that of the basal plane of graphite and to have a specific capacitance of 117 Fg^{-1} at a scan rate of 20 mVs^{-1} in aqueous H_2SO_4 electrolyte with an operation window of 1 V.[171] A significantly higher operating voltage of 3.5 V was achieved when $PYR_{14}TFSI$ was used. The maximum energy density stored in these capacitors was 31.9 $Whkg^{-1}$. Agglomerates of chemically modified graphenes, synthesized by means of suspending graphene oxide sheets in water and then reducing them by using hydrazine hydrate, exhibited specific capacitances of 135 and 99 Fg^{-1} determined at a galvanostatic discharge–charge current of 10 mA in aqueous and organic electrolytes (KOH and $TEABF_4$/AN, respectively).[172] The agglomerate contained particles of 15–25 μm and had a BET surface area of 705 m^2g^{-1}. A good performance over a wide range of voltage scan rates was observed, and assigned to the high electrical conductivity of preformed agglomerate particles prior to the electrode preparation.

The BET values of graphene materials in the reported works are far below the theoretical surface area of a single graphene sheet (2630 m^2g^{-1}), and also lower than or similar to the BET surface area of some activated carbons or carbon blacks that are industrialized products with moderate costs. It should be mentioned that graphene samples need additional stabilization treatment for the practical use in electrochemistry.[171] While in the case of Li-ion batteries the electrode of graphene-like materials shows higher Li storage capacities than that of graphite, the performance of graphene-like materials in supercapacitors is not superior to activated carbon or carbon black. In addition, materials with 3–16 sheets of graphene are not graphene materials, but rather nanographites. Again, also here, the intrinsic electronic properties of graphene play no role in the application and should not be considered in relation to such materials.

3.1.3 Three-dimensional hierarchical carbons

Ordered mesoporous carbons (OMCs) with extremely high surface areas and controllable pore sizes as well as large pore volumes are testing candidates for electrode materials for EDLCs.[174–178] Experiments have demonstrated that an interconnected network of mesopores with the microporosity from the constituent parts lowers the resistance to electrolyte migration and allows for rapid charge propagation to the surface of micropores.[23] An OMC with an interconnected channel (OMC-IC) structure exhibits a much lower impedance to ion transport and thus has better electric double layer performance as compared to conventional OMCs with an unconnected channel structure.[179]

Recently, 3D aperiodic hierarchical porous *graphitic* carbon materials have been developed for high-rate electrochemical capacitive energy storage.[180] This kind of 3D hierarchical carbon is characterized by four typical features at different dimensions (Figure 24): macroporous cores (between 1–2 μm),

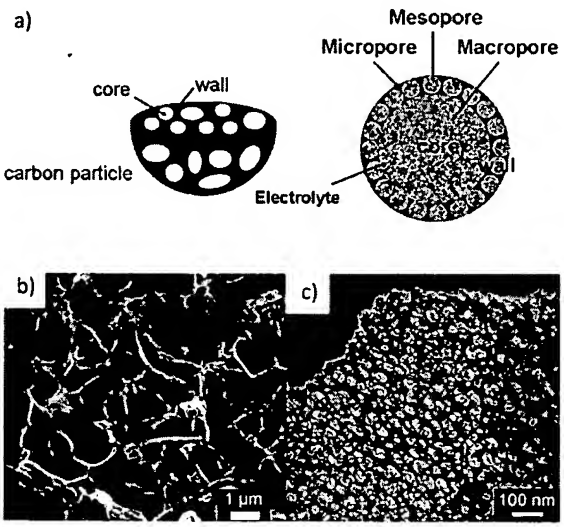

Figure 24. a) Schematic representation of the 3D hierarchical porous texture. b) Macroporous cores of the HPGC material. c) TEM image showing the micropores. Reprinted with permission from ref. [180].

mesoporous walls (with thickness between 100–200 nm), micropores (with sizes about 0.7–1 nm), and a localized graphitic structure. In fact, some OMC activated carbons have a similar pore structure, however this 3D hierarchical carbon features a local graphitic structure. The macroporous cores can serve as ion-buffering reservoirs, the mesoporous walls guarantee a smaller ion-transport resistance while the micropores accommodate charges and the localized graphitic structure enhances the electrical conductivity. A close comparison of this 3D hier-

archical porous carbon with typical microporous carbon (activated carbon) and mesoporous carbon (SBA-15 templated carbon) highlighted its high rate capability. The multihierarchical material demonstrated a superior capacitive performance (180 $F g^{-1}$ at high frequency of 1 Hz) when compared to hard-templated OMCs. This is attributed to the generated pore surfaces.[181]

This work showed that OMC is a platform for investigation of transport limitation, roles of pores, and the electrode–electrolyte interface interactions, and highlights the role of graphitic wall interconnections. The volumetric capacitance could be too small for industrial applications because of the large portion of pores.

The concept of 3D aperiodic hierarchical porosity has previously been realized in porous carbons such as carbon aerogels. Their pore structure can be designed and controlled by changing the conditions under which the microemulsion templated sol–gel polymerization and the subsequent activation are carried out.[182] A 3D aperiodic carbon materials with four types of pores can be obtained: (1) micropores, with diameters below 2 nm; (2) small mesopores, with diameters from 2 to 5 nm; (3) large, mesopores with diameters from 5 to 40 nm; and (4) large pores and channels, with diameters over 40 nm. Appropriate activation with KOH increased both the number of type 1 pores and the BET surface areas, which in turn increased their capacitance.[183] For example, with a specific BET surface area of 1468 $m^2 g^{-1}$, as well as large pores and channels, a high-speed charge–discharge performance of 201 $F g^{-1}$ at 100 $mV s^{-1}$ was observed on such 3D aperiodic hierarchical carbon, which was 82% of the value at 10 $mV s^{-1}$. This high-rate charge-discharge performance is attributed to the abundant type 4 pores, which play an important role in the transfer of the electrolyte. Activating the samples with a high concentration of KOH resulted in an even higher surface area of 1468 $m^2 g^{-1}$ but caused the collapse of the large pores, significantly decreasing their capacitances under high charge–discharge currents. These results confirm the importance of meso- and macropores for charge–discharge propagation.

3.1.4 The role of micropores in charge storage

As discussed above, the role of meso- and macropores of carbon materials in EDLCs are more or less clearly assigned,[4] the role of micropores, which contribute mostly to the specific surface area, is under study. An increase in the specific surface area cannot increase proportionally the capacitance of an EDLC [Equation (5)]. Non-linearity of the double layer capacitance with surface area of carbon has been reported.[184–189] The model calculation for BET surface area, based on nitrogen adsorption–desorption at 77 K, overestimates the value of surface area of activated carbon available for ions.[190] Earlier investigations suggested that pores smaller than 0.5 nm were not accessible to hydrated ions,[184,191] and that even pores under 1 nm might be too small, especially in the case of organic electrolytes where the size of the solvated ions is larger than 1 nm.[192] Sub-nanometer pores were believed not to participate in the formation of an EDL due to the inaccessibility of their surfaces to solvated large ions. However, Raymoundo-Pinero et al. reported the contributions of micropores to the overall capacitance and concluded that partial desolvation of hydrated ions occurred.[193]

The critical effect of the micropore size on the capacitance of an EDLC was re-investigated recently by using carbon materials with controllable micropore size. Activated carbon[193] and carbide-derived carbons[195] (CDCs) have been used for this purpose. CDCs can have a narrow pore-size distribution with a mean value that is tunable in the range of 0.5–3 nm[196] and a specific surface area up to 2000 $m^2 g^{-1}$.[197] In an acetonitrile-based organic electrolyte CDC exhibits very high capacitance. An anomalously large capacitance increase in CDC materials was reported when the pore size decreased below 1 nm (Figure 25),[198,199] while only a marginal increase in the normalized capacitance was obtained when increasing the pore size above 1 nm. A similar dependence of normalized capacitance with average pore size has been previously reported by Raymoundo-Pinero et al. using activated carbons.[193] It was concluded that the pore size giving the maximum double-layer capacitance is very close to the ion size—both larger and smaller pores lead to a significant drop in capacitance.[193,197] In addition, desolvation of ions in nanometer pores takes place. There

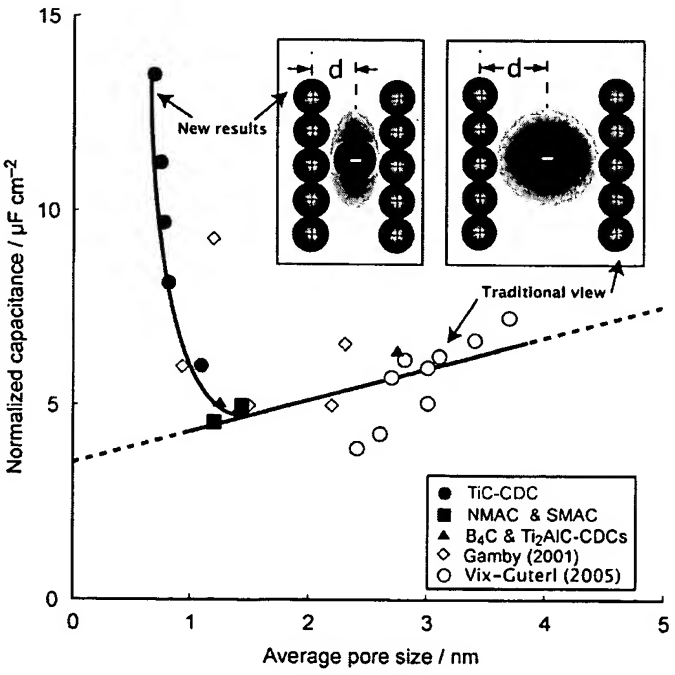

Figure 25. Dependence of material capacitance normalized by surface area on pore size. The results show that increasing the pore size above ca. 1 nm marginally increases the normalized capacitance. Decreasing the pore size below ca. 1 nm sharply increases the normalized capacitance due to constriction of the ion solvation shell (inset). Adopted from Ref. [194]. Copyright 2007, Nanotechnology Law & Business.

must be at least a partial removal of the solvent shell. A decrease in the pore size causes an increase in the number of solvent molecule removed, along with a similar increase in the capacitance.[200] A better understanding of the behavior of ions in confined environments is needed, where Helmholtz double layers cannot form.

The pore-size distribution of porous carbons influences to a large degree the fundamental performance criteria of carbon-based supercapacitors, for example, the relationship between power and energy density, and the dependence of performance on frequency.[1] Having pores that are too small may affect the power capacity of the supercapacitor. In a model study using zeolite-templated carbon (ZTC) with uniformly ordered micropores as the electrode material for an EDLC, it was found that when the pore diameter became smaller than 1.2 nm, the capacitance per surface area increased, but the power density decreased due to the difficulty of smooth ion-transfer in such small micropores.[201] ZTC is a carbon material with tunable and homogenous pore sizes providing a model structural material to study the pore size and ion-size effects in the charge storage mechanism of a supercapacitor providing new aspects in understanding the interaction of pores with electrolyte. For CDC, elimination of macro- and mesopores and matching the pore size with the size of the ions increases the capacitance significantly. However, the numerous above mentioned experiments have shown that macro- and mesopores are a prerequisite for the transport of electrolyte to the micropores or nanopores in many other carbon materials.

The authors note that a simple measure around the somewhat irregular debate regarding the textural properties of supercapacitors would be their classification by fluid-phase adsorption. The convention of using gas phase surface area measurements and then drawing conclusions regarding the fluid phase adsorption properties is erroneous for many reasons related to the experiment and the data analysis of BET isotherms in terms of pore size distributions.[202] It is plausible that not any recipe recommending maximizing one of the textural scales (porosity or electrical conductivity) will be successful; ELDC electrodes are multiscale systems and only a combined and iterated optimization of textural, structural, and chemical properties will lead to success. The authors note that the surface chemistry and the stability issues of solvated ions are rarely taken into account explicitly and that no in situ data exists on the chemical nature of the active surface and its coverage with ions.

3.2 Carbon-based composites

Typical electrode materials for supercapacitors based on pseudocapacitance are metal oxides (e.g., RuO_2, IrO_2, Co_2O_3, MnO_2) and conducting polymers.[203–205] Other nanostructured metal oxides such as NiO have also been tested for this purpose.[206] Because redox reactions can be irreversible as compound formation between electroactive species and the electrode material may occur, pseudo-capacitors often suffer from a lack of stability during long-time cycling.

3.2.1 Metal oxide–carbon composites

Some metal oxides exhibit poor electrical conductivity, which can cause a low power density. Many efforts have been made to develop composite materials consisting of metal oxide nanoparticles and carbon as electrode materials.[207–210] One additional benefit of nanostructuring this electroactive oxide on carbon, besides improving the electrical conductance, is the increase in the specific surface area of metal oxides–composite exposed to electrolyte.

Ruthenium oxide (RuO_2) is a widely studied material in acidic solutions for pseudocapacitors.[211] It is conductive and has three distinct oxidation states accessible within 1.2 V. Its superior performance in sulfuric acid has been attributed to the surface-driven, reversible redox processes involving electron transfer, together with an electro-adsorption of protons on the surface of RuO_2 particles.[212,213] Hydrous RuO_2 possesses high capacitance in aqueous electrolytes. The electrical conductivity of ruthenium-based materials results in a lower power density. Composite electrodes combining hydrous RuO_2 and porous carbon can increase effectively the specific capacitance and improve the rate performance compared to pure porous carbon.[214,215] A Ru/C electrode with mesoporosity has been prepared by a simple one-step pyrolysis procedure with dichlorobis(μ-chloro)bis[(1-3-η:6-8-)-2,7-dimethyloctadienediyl] diruthenium(IV) (DDRu) as precursor.[216] After electro-oxidization of the Ru nanoparticles to hydrous RuO_2 in sulfuric acid, a capacitance of 132 $F g^{-1}$ was obtained. This value is higher than that (27 $F g^{-1}$) of Vulcan XC-72 carbon (surface area 248 $m^2 g^{-1}$), but still lower than that of some reported $RuO_2 \cdot xH_2O$. This could be due to the low water content of the $RuO_2 \cdot xH_2O$ in the composite and some of the embedded Ru particles being inaccessible to the electrolyte.[182]

Another way to increase the electronic conducting pathways for hydrous RuO_2 is the preparation of vapor-grown carbon fiber (VGCF)/$RuO_2 \cdot xH_2O$ nanocomposites by thermal decomposition of ruthenium ethoxide solution containing a weighted quantity of VGCF casted on a Pt electrode.[217] The specific capacitance of VGCF/$RuO_2 \cdot xH_2O$ nanocomposite electrodes at a scan rate of 10 $mV s^{-1}$ is 1017 $F g^{-1}$, and at 1000 $mV s^{-1}$ is 824 $F g^{-1}$, much higher than that when only $RuO_2 \cdot xH_2O$ is used as electrode. Because VGCF has a specific capacitance as low as 1.9 $F g^{-1}$, the benefit of $RuO_2 \cdot xH_2O$ loading over its surface is unambiguous. VGCF is a substantially more conductive (specific resistance: 0.012 Ω cm) carbon material than conventional activated carbons (0.04–1.0 Ω cm) providing an explanation for the high-rate performance of the nanocomposite. VGCF is a cheap industrial product, thus the use of VGCF as support in pseudocapacitor is very attractive.

Less expensive oxides such as iron, vanadium, nickel, cobalt, and manganese oxide have been tested in aqueous electrolytes. Recently, it is reported that by loading 10% Bi_2O_3 onto the mesoporous carbon, the specific capacitance of the composite can be as high as 232 $F g^{-1}$ at a sweep rate of 5 $mV s^{-1}$.[218] However, the mass transfer in the framework of the crystalline metal oxide remains difficult when it is not truly

nanostructured, as evidenced by the decline of the specific capacitance with the increase of the sweep rate.

Thin MnO_2 deposits of ten to hundreds of nanometers have been produced on various substrates such as metal collectors, or activated carbon. Because reaction kinetics are no longer limited by the electrical conductivity of MnO_2, specific capacitance as high as 1300 $F g^{-1}$ have been reported.[219] These kind of experiments proof the concept of nanostructuring electrodes to facilitate the electron transport, however, a system of extremely thin active film on platinum is far away from applications, both from a point of view of scale-up and of cost-saving. This also applies to reported works using composites of CNTs combined with RuO_2[220] or NiO[221] for supercapacitor applications.

3.2.2 Composites of carbon and electroactive polymers

Electroactive polymers (polyaniline, polypyrrole, polythiophene, and their derivatives) offer high electrical conductivities and high doping–dedoping rates during charge–discharge processes.[170–172] These polymers have a high gravimetric and volumetric pseudocapacitance in various nonaqueous electrolytes at operating voltages of about 3 V. However, electroactive polymers commonly have poor mechanical stability owing to repeated intercalation and depletion of ions during charging and discharging. The electrode suffers from swelling and shrinkage, leading to a mechanical degradation of the cell and deterioration of the electrochemical performance. When low-cost electroactive polymers are used as bulk materials for an electrode, they usually have a short cycle life.[24] Electrodes made from carbon materials with polymers as main component show improved mechanical properties.[222,223]

An interesting breakthrough for developing a new generation of supercapacitors is the successful synthesis of composites incorporating a nanotubular backbone coated by an active phase with pseudocapacitive properties.[23] Such a composite combines the large pseudocapacitance of the conducting polymers with the fast charging–discharging double-layer capacitance and excellent mechanical properties of the CNTs. The open mesoporous network formed by the entanglement of CNTs allows the ions to diffuse easily to the conducting polymer. This lowers the equivalent series resistance and consequently increases the power density of the device. These composites exhibit excellent electrochemical charge storage properties and fast charge–discharge switching, making them interesting electrode materials for high power supercapacitors.[28]

The above-mentioned hierarchically porous carbon monolith (HPCM) has been used to support electro-deposited polyaniline (PANI),[224] a promising polymer as an electroactive material. HPCM (surface area: 277 $m^2 g^{-1}$, pore volume: 0.47 $cm^3 g^{-1}$) was used as both a current collector and a high surface support for conducting polymers. Figure 13a shows the network structure of HPCM with fully interconnected macro- and mesoporosity, which offered a very good compromise between infiltration rate and surface area. The connecting carbon bridges are nanoporous in themselves. In a three-electrode cell experiment in 1 M H_2SO_4, a specific capacitance of ca. 2200 $F g^{-1}$ (i.e., per gram of PANI) with a power density of 0.5 $kW kg^{-1}$ at an energy density of 300 $Wh kg^{-1}$ was obtained at a current density of 0.67 $A g^{-1}$ in the potential range 0–0.7 V. Even at a very high current density of 66.7 $A g^{-1}$, the specific capacitance was still as high as 1270 $F g^{-1}$ (Figure 26a). All these values seem surprisingly high. It is reported that determining the capacitance of a PANI composite electrode by means of three-electrode cell can give extremely high values.[225] Such high values cannot be achieved in a practical symmetric capacitor due to the pseudocapacitative behavior of electrically conducting polymer during the doping–dedoping process. For composite materials containing conducting polymers it is more reasonable to determine the capacitance in two-electrode cells.

The advantages of the HPCM as a support for the deposition of active materials are displayed by Ragone plots, as shown in Figure 26b. At the same specific power, PANI deposited on HPCM exhibits a much higher specific energy density than PANI electrodeposited onto a nonporous carbon monolith (abbreviated as NPCM). At a specific power of 0.47 $kW kg^{-1}$, the specific energies were 300 $Wh kg^{-1}$ and 92 $Wh kg^{-1}$ for PANI on HPCM and on NPCM, respectively. At a much higher specific power of 47 $kW kg^{-1}$, specific energies are still as high as 173 $Wh kg^{-1}$ for PANI on HPCM while only 53 $Wh kg^{-1}$ for PANI grown on NPCM. The synergistic effort of PANI with HPCM renders this performance.[224] The network of comparatively large pores in HPCM can facilitate the fast penetration of the electrolyte to the surface of active materials. The electrodeposited PANI not only has a smaller particle size but is also more uniformly dispersed, thus ensuring better utilization of electrode materials. This material is binderfree and conductive-agent-free, and can be quickly and straightforwardly synthesized.

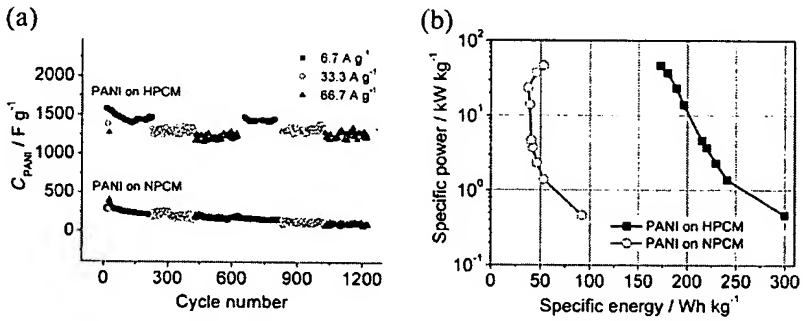

Figure 26. a) Relationship of the specific capacitance for PANI (C_{PANI}) with respect to the charge-discharge specific current for PANI on HPCM, and PANI on NPCM respectively. b) Ragone plots for PANI on HPCM and PANI on NPCM. Reprinted with permission from Ref. [224].

This is again an example of using a strategy of nanoarchitecturing carbons to get electrodes with optimal performance. Furthermore, it has been reported that pellet electrodes obtained by simply pressing the nanocomposite materials can be employed for supercapacitors, especially when an asymmetric configuration is realized.[225] For example, the specific capacitance of an asymmetric capacitor with PANI/CNTs composite materials as positive and polypyrrole/CNTs as negative electrode can achieve a value up to 320 $F g^{-1}$.

Conducting polymers and their derivatives also can be prepared on different materials such as glass, polymer, silica, metal oxide, fiber, and others by means of chemical deposition.[226] It seems that composites of nanocarbons with conducting polymers could be more interesting because they combine two relatively cheap materials to gain the large pseudocapacitance of the conducting polymers coupled with the good conductivity and transport properties of carbon and mechanical strength of nanocarbons. However, the volumetric energy or power density of such porous systems can be expected to be small due to the presence of the large pore volumes. This is the main drawback of such materials for devices for portable applications.

The methodology for determining the specific capacitance of electrodes based on conducting polymers is very critical.[225] It has been shown that experiment using three-electrode cell construction is only useful for the investigation of the electrochemical behavior of a single electrode. The capacitance of conducting polymer depends on the range of the potential window where it is investigated. The obtained value of specific capacitance cannot be simply compared with the value for a two-electrode cell. For example, high values as high as 1100 $F g^{-1}$ have been measured for PANI/CNTs composite electrode in a three-electrode cell. In the two-electrode cell measurement, a much smaller specific capacitance value of 360 $F g^{-1}$ was obtained.[225]

3.2.3 Functional groups and heteroatoms

Functional groups are always present on the surface of carbon. Nanostructured carbons with high surface areas and complex surface structures are especially rich in functional groups that play important roles in an supercapacitor.[227,228] It has been reported that the specific capacitance of carbon materials can be improved in aqueous media by the introduction of hydrophilic functional groups (e.g., oxygenated functionalities) that improve wettability and introduce redox processes that contribute pseudocapacitance to the overall capacitance.[227,228] For organic electrolytes it may be advantageous to apply hydrophobic functional groups to improve the wetability of the electrode.[229,230] Carbonyl groups can take part in the following reaction:[160]

$$> C{=}O + H^+ + e^- \rightleftharpoons > C{-}OH \quad (8)$$

$$> C{=}O + e^- \rightleftharpoons > C{-}O^- \quad (9)$$

Because the reactions are only quasireversible and become irreversible for frequent cycling, they may not provide a long-standing contribution to the pseudocapacitance of supercapacitors. In addition to this instability, oxygenated groups can enhance the inner resistance of the electrode and the leakage current.[231] This can offset the increased capacitance from the surface oxygenated functional groups.

Nitrogen-containing surface functional groups on carbon have attracted much interest due to their enhancing effect on capacitance in both aqueous and,[232,233] not always unambiguously, organic electrolytes.[234,235] Using melamine-based carbons from fluorinated mica as template, it was found that pyridinic nitrogen species affected the electron donor–acceptor characteristics of carbon materials and that there was a pseudocapacitative attraction between the protons of the electrolyte and the carbon electrode materials. This was stated to be the reason for good capacitive behavior of melamine-based carbon in sulfuric acid. A maximum gravimetric specific capacitance of about 200 $F g^{-1}$, especially a capacitance per surface area of 1.5 $F m^{-2}$, can be obtained in aqueous electrolyte of sulfuric acid and sodium chloride in a three-electrode-cell arrangement.[232] It was reported later that nitrogen-enriched carbons prepared from melamine resins also showed good capacitive behavior in KOH despite the absence of protons that were initially thought to be responsible for the high capacitance in an acidic electrolyte.[233] In nonaqueous media, however, the performance was less promising than in an aqueous electrolyte.

A specific capacitance as high as 159 $F g^{-1}$ at 0.5 $A g^{-1}$ in an organic electrolytes was obtained when adding nitrogen into the framework of mesoporous carbon spheres of high specific surface area (1460 $m^2 g^{-1}$).[236] This remained 130 $F g^{-1}$ at a high current density of 20 $A g^{-1}$. This improvement in pseudocapacitance was assigned to the enhanced surface wettablility and the reduced resistance due to the moderate nitrogen content in the mesoporous carbon. The negative impact of nitrogen heteroatoms was also reported for porous carbon materials prepared using chemical vapor deposition of acetonitrile on zeolite Y templates.[242] Clarifying the exact mechanism of pseudocapacitive interactions between the ions and nitrogen atoms is highly desirable.

The chemical modification of surface of carbon materials, for example, by phosphoric acid activation, can reduce the number of functional groups on C through the blockage of active sites by phosphate groups. This has been exploited in many applications.[243–245] Recently, it was reported that carbons enriched with phosphorus groups and optimized porous structures showed a uniquely high and stable performance.[246] Using P-rich carbon as electrodes, the supercapacitors are capable of stable operation at voltages greater than 1.3 V in H_2SO_4. Surface modification by a sodium oleate surfactant was reported to have improved the wettability of carbonaceous materials in organic electrolytes.[247] After the modification, the internal resistance of the capacitor decreased, and the specific capacitance and energy density increased.

3.3 Summary for Supercapacitors

Many efforts have been made to achieve a significant increase in the energy density of supercapacitors while retaining their characteristic advantages of high power and extraordinary cycleability. Table 3 summarizes recent achievement in this area. The highest capacitance is achieved with pseudocapacitors when RuO_2 is used as active material.

The development of new materials is characterized by phenomenological studies. As a result, sets of conflicting "rules" can be elucidated as to how optimal performance is achieved. An example is the ongoing discussion about the best texture of carbon electrodes described above. It is obvious that electrodes for supercapacitors are multifunctional materials with a strong component of interfacial molecular transport combined with requirements for electrical conductivity and excellent chemical stability in large potential gradients and at high absolute current flows. It is unlikely that any single property, such as microporosity, will dominate the performance profile of such a device. Solid progress in this area will require some fundamental understanding of the underlying chemical processes under the operating conditions of electrodes. Very little validated experimental information is available regarding the nature and reactivity of solvated ions in the electric double layer or about their transport and chemical dynamics. It therefore seems premature to derive definitive conclusions on the tex-

Table 3. Some results of nanocarbon and carbon-containing composite materials for supercapacitors. For comparison, the performance of NiO is also listed.

Sample	Capacity [$F g^{-1}$]	System[a]				Ref.
		Voltage [V]	Scan rate	Electrolyte	System	
MSC25	180–250	0–0.7	0.1–60 mA cm^{-2}	2.0 M H_2SO_4	3/PVI	[177]
PICA	80–125	0–2	10 mA cm^{-2}	1.7 M TEAMS in AN	2/PVI	[187]
	60–115			1.0 M TEAMS in PC		
SWCNTs	65–140	0–0.9	1–50 mA cm^{-2}	7.5 M KOH	2/PVI	[169]
SWCNTs	ca. 20	0–2.5	0.05–20 A g^{-1}	1.0 M Et_4NBF_4 in PC	2/PVI	[170]
	ca. 80				3/[b]	
Polypyrrole/Ti	100–500	−0.8–0.8	10–500 mV s^{-1}	1.0 M KCl	3/CV	[154]
Templated carbons	130–200	0–1	1–20 mV s^{-1}	1.0 M H_2SO_4	2/CV	[237]
	50–205			6.0 M KOH		
	95–110	0–2		1.0 M TEABF$_4$ in CH_3CN		
ACA	66–245	−1–0	10–100 mV s^{-1}	30% KOH	3/CV	[183]
Coffee shells	50–156	0–1	1–10 mV	6.0 M KOH	2/CV	[238]
C/MnO_2	20–700	−0.1–0.9	10 mV s^{-1}	0.1 M K_2SO_4	3/CV	[208]
CA/RuO_2	100–270	0–0.8	0.2–20.0 mV s^{-1}	1.0 M H_2SO_4	3/CV	[214]
VGCF/RuO_2	800–1000	0–1	10–1000 mV s^{-1}	1.0 M H_2SO_4	3/CV	[217]
Bi_2O_3/HOMC	150–230	−0.9–0.1	1–100 mV s^{-1}	6.0 M KOH	3/CV	[218]
PANI/HPCM-2	300–380	0–0.7	0.02–0.17 A g^{-1}	1.0 M H_2SO_4	3/PVI	[224]
Me	50–210	−1–0	1 mV s^{-1}	6.0 M KOH	3/CV	[232]
	20–40	−1.5–0.5		1.0 M TEABF$_4$ in PC	3/CV	
TIC-CDC	90–145	0–2.3	5–100 mA cm^{-2}	1.5 M NEt_4BF_4 in CH_3CN	2/PVI	[197]
TIC-CDC	100–160	0–3	5–100 mA cm^{-2}	IL (EMI-TFSI)	2/PVI	[198]
MWNTs/PANI	20–240	−0.2–0.8	0.25–5 A g^{-1}	1 M $NaNO_3$	3/PVI	[239]
PANI/C	780–900	−0.2–0.7	0.5–5 A g^{-1}	1.0 M H_2SO_4	3/PVI	[240]
BMC-1	85–115	0–0.8	2–50 mV s^{-1}	1.0 M H_2SO_4	3/CV	[241]
	110–130			6.0 M KOH		
OMC-UC	90–125	−0.9–0.1	10–300 mV s^{-1}	6.0 M KOH	3/CV	[179]
OMC-IC	135–145					
HPGC	150–270	0–1	0.02–50 A g^{-1}	6.0 M KOH	2/PVI	[180]
FS-P	130–160	0–1.3	5 A g^{-1}	1.0 M H_2SO_4	2/PVI	[241]
SC-P	140–210					
BC-P	160–200					
AC	40–55	0.05–3	3–100 mA cm^{-2}	0.8 M Et_4NBF_4 in PC	2/PVI	[242]
MAC	45–60					
CA	55–105		3–48 mA cm^{-2}			
MCA	75–110					
CMG	100	0–1.0	20 mV s^{-1}	5.5 M KOH	2/CV	[171]
	99	0–2.5		TEABF$_4$ in CH_3CN		
	82	0–2.7		TEABF$_4$ in PC		
AC	124–286	0–0.6	100 mA g^{-1}	6 M KOH	2/PVI	[193]
CNTs	27	−0.4–0.4	5 mV s^{-1}	1 M H_2SO_4	3/CV	[230]
CNTs-RuO_2	295					
Bare NiO	80–120	0–0.9	10–100 mA g^{-1}	2 M KOH	2/PVI	[231]
NiO/CNTs	140–160					

[a] The numbers 2 and 3 refere to two- and three-electrode tests, respectively. [b] No information available.

tural requirements of the electrode. These arguments also neglect the possible chemical reactivity of solvated ions with active sites on the electrode surface. In the case where the chemistry of the electrode is poorly defined a "capacitor" may act as a "fast battery." In the case that ultrasmall pores lead to exceedingly high capacities it may be envisaged that the geometric location of the storage of charge is no longer the surface of the pore walls. In this case porosity would not be the property of relevance but would represent a proxy for the reactivity of the electrode. More rational progress in this area will strongly benefit from in situ analytics observing the electrode in operation and under an electrical potential. Such studies require the adaptation of in situ experiments such as NMR and eventually also the design of novel instruments such as in situ electron spectroscopy.

The authors note a certain tendency towards unidimensional optimizations. The quest for surface area is a typical example. It is not the BET surface area that is relevant but the active surface area (ASA) for the process (electrolyte) intended. It would thus be useful to devise experiments that use the electrolyte as probe adsorbent when steering the development of the material. Another example is the energy capacitance. If one considers the scale of possible applications it is not useful to research on material combinations with prohibitive and nonscaleable costs. Such studies may serve well as pathfinders exploiting the physical limits of the concept of "supercapacitor," however theses studies should be complemented by the intensive search for scaleable alternatives even at the expense of not attaining the maximum capacitance. The definition of a figure of merit for such devices combining the stability, the capacitance and the likely cost (from laboratory supplies of the materials and processing used) would be a practical solution steering the phenomenological research towards more rapid implementation in applications. It is clear, however, that a substantial shortcoming in this area is the lack of fundamental scientific understanding caused by the enormous difficulties of performing meaningful in situ studies on the function of such devices.

4. Concluding Remarks

Building materials for electrical energy storage is a complex challenge that has been taken on by many groups on an empirical basis, starting from fundamental insight into electrochemistry. This science, despite having still unanswered fundamental questions regarding the dynamics and structure of the interface processes, provides numerous possibilities to characterize the performance of an electrode material.

Electrochemical characterization has been used in many studies to reach conclusions on the dominant role of ion transport processes as a limiting factor. A critical issue frequently discussed is the exact nature of the interface between the fluid and the solid phase. The atomic structure and termination of the electrode and the nature of the electric double layer in the fluid facing the electrode are the standard electrochemical issues. In batteries, and eventually also in pseudocapacitors, there is additional chemistry arising from the decomposition processes of the electrolyte and/or the reaction of the electroactive ions with the electrode bulk leading to additional phase formation at the interface where the elementary processes of charge exchange occur. Such a complex situation with an interplay of electron transfer processes and atomic transport is reminiscent of the analysis of heterogeneous catalysis, where exactly the same intertwined multiscale phenomenology precludes any straightforward functional analysis and hence the application of a rational design strategy.[248,249] The cooperation between catalysis and electrochemistry could accelerate the progress in both fields[250,251] and is a desire arising from the present analysis.

The element carbon is a natural and very flexible choice for building electrical energy storage devices. The unique combination of enormous chemical stability with electrical conductivity and an endless variability of texture in multiple scales render carbon a chemical of eminent relevance in energy storage technology.[16] The combination of polymers with inorganic nanostructured carbons probably offers the good way forward to design hierarchical carbon-only systems offering high stability, excellent functionality and moderate cost which are prerequisites for scaleable technologies.[252,253] Interfaces between carbon and oxides or metal alloys with nanostructured textures may, although much more demanding in their design, offer a solution for the critical challenge of finding effective cathode materials for the Li ion technology.

However, after more than 10 years on intensive research in the two domains with hundreds of publications in the literature, the best and most materials used in current industry are still graphite and activated carbons for anodes of lithium-ion batteries and electrodes of capacitors, respectively. What are the reasons?

At first, nanostructured (carbon) electrodes also have systemic shortcomings and disadvantages. An important one is the expected but undesirable electrode–electrolyte reactions arising from their high surface areas. The results could be large irreversible loss in capacity and big voltage crosstalk. A second shortcoming is the low density of nanostructured materials, especially mesoporous carbon, such that any practical use of them is not realistic due to the large effective volume. One solution for these two challenges could be a suitable nanoarchitecture that can synergistically take advantage of the combination of ordered building block units with their excellent electrical transport and stability properties together with a nonperiodic suprastructure providing transport in larger dimensions with shorter characteristic time scale.[17] The rational and scaleable synthesis of organic–inorganic carbon composites, avoiding expensive templates and excessive energy for production, through well-designed building blocks is a major strategy towards achieving a breakthrough in electrical energy storage devices. Achieving this would be an excellent example of the evolution of conventional chemistry into systems chemistry.

Moreover, we believe that in order to fully exploit the possibilities of new carbon or new electrode materials we need to optimize both synthesis and material properties to a much more creative level than has been done so far. The authors note that very little systematic optimization work has been

done on the chemistry and texture of any of the many architectures suggested so far. With respect to the critical role of transport kinetics it seems highly rewarding to optimize every critical parameter alone and for the hierarchical system in a coupled manner. This is only possible with reasonable efforts when reproducible and scaleable synthesis techniques are available. As variable as our toolbox of making carbon is today, we still have much to do in order to optimize each and every synthesis step. The extent of graphitization, the chemical purity, and the surface functionalization of inorganic nanocarbons may serve as examples. Regarding the polymer side, it is critical to develop controllable protocols for pyrolysis and hydrothermal treatment techniques in order to master the defect properties of the resulting solids. Finally, the metrology of functional hierarchical carbon also remains a challenge. The standard tools of organic chemistry and of structure determination are insufficiently sensitive to multiscale nonperiodic structural details of hierarchical nanocarbons. The study of chemical reactivity in situ has hardly been touched, as the density of the solid–fluid interface of metallic conductivity is in itself a great challenge for analytical science. The functional characterization with electroanalytical tools is highly advanced and is ready for application. Many examples of this can be found in the literature discussed herein. The interpretation of the electrokinetic fingerprints, for example with respect to transport and texture, can still be improved by advanced textural analysis using suitable probe systems in addition to the standard nitrogen gas adsorption.

Taking all of this into consideration and acknowledging the enormous creativity seen in the results discussed in the present Review, it is possible to expect a breakthrough improvement of the performance of electrical storage devices. It is not yet a high-priority task to think about the "post-Li" time (which chemically is hard to imagine anyway). It seems more appropriate to work in a systematic manner along the avenues of material developments indicated and sketched above. Moving forward, however, it is critical to make this process more effective as we see it today. To this end the involvement of fundamental understanding, including theory and in situ experimentation, augmenting material synthesis efforts remains the best way. In the materials arena the development of rational and scaleable synthesis procedures have the same high priority as the search for novel building blocks for functional nanocarbon which may even be of biological origin.[254]

Finally, we should not forget that the engineering of electrodes is an important factor which is not fully considered in many academic publications. Nanostructuring materials alone cannot provide batteries/capacitors with high energy/power densities. The present Review has reduced the conceptually necessary systems view on storage devices to a discussion about material problems of the electrodes and challenges in this area. Fundamental issues regarding interface processes and the defect dynamics of electrodes have been systematically investigated. Furthermore, the electrolyte, membranes, current collectors, and packaging issues as well as more practical challenges controlling the overall performance have to be intensively studied.

Acknowledgements

D.S.S. thanks especially the comments of Dingcai Wu, Yong-Sheng Hu, Lin Zou, Chengjun Xu, and Zhenghui Li for the summary of Table 2 and Table 3, and Mengqiang Zhao and Qiang Zhang for technical help with finishing the manuscript. This work was performed within the EnerChem project of the Max Planck Society.

Keywords: batteries · carbon · capacitors · electrodes · lithium

[1] M. Endo, C. Kim, K. Nishimura, T. Fujino, K. Miyahita, *Carbon* **2000**, *38*, 183.
[2] F. Béguin, E. Frackowiak, *Adsorption by Carbons*, Elsevier, **2008**, p. 593.
[3] Y. P. Wu, E. Rahm, R. Holze, *J. Power Sources* **2003**, *114*, 228.
[4] A. G. Pandolfo, A. F. Hollenkamp, *J. Power Sources* **2006**, *157*, 11.
[5] M. Endo, Y. J. Kim, K. Park, *Advanced Battery Applications of Carbons, in Carbons for Electrochemical Energy Storage and Conversion Systems* (Ed.: F. Béguin, E. Frackowiak), Taylor & Francis, London **2009**, p. 469.
[6] N. A. Kaskhedikar, J. Maier, *Adv. Mater.* **2009**, *21*, 2664.
[7] B. Scrosati, *Electrochim. Acta* **2000**, *45*, 2461.
[8] J. M. Tarascon, M. Armand, *Nature* **2001**, *414*, 359.
[9] C. R. Sides, N. Li, C. J. Patrissi, B. Scrosati, C. R. Martin, *MRS Bull.* **2002**, 684.
[10] M. R. Palacín, *Chem. Soc. Rev.* **2009**, *38*, 2565.
[11] C. Jiang, E. Hosono, H. Zhou, *Nano Today* **2006**, *1*, 28.
[12] P. G. Bruce, B. Scrosati, J. M. Tarascon, *Angew. Chem.* **2008**, *120*, 2972; *Angew. Chem. Int. Ed.* **2008**, *47*, 2930.
[13] J. Maier, *Solid State Ionics* **2002**, *154–155*, 291.
[14] J. Maier, *Z. Phys. Chem. (Muenchen Ger.)* **2003**, *217*, 415.
[15] Y. G. Guo, J. S. Hu, L. J. Wan, *Adv. Mater.* **2008**, *20*, 2878.
[16] R. Schlögl, *Handbook of Heterogenous Catalysis* (Eds.: G. Ertl, H. Kniizinger, J. Weitkamp), Wiley-VCH, Weinheim, **2008**, p. 357.
[17] G. Centi, S. Perathoner, *Eur. J. Inorg. Chem.* **2009**, 3851.
[18] M. G. Kim, J. Cho, *Adv. Funct. Mater.* **2009**, *19*, 1497.
[19] F. Cheng, Z. Tao, J. Liang, J. Chen, *Chem. Mater.* **2008**, *20*, 667.
[20] E. Frackowiak, F. Béguin, *Carbon* **2002**, *40*, 1775.
[21] A. S. Aricò, P. Bruce, B. Scrosati, J. M. Tarascon, W. van Schalkwijk, *Nat. Mater.* **2005**, *4*, 366.
[22] P. Simon, Y. Gogotsi, *Nat. Mater.* **2008**, *7*, 845.
[23] E. Raymundo-Pinero, F. Béguin, *Activated Carbon Surface in Environmental Remdiation* (Ed.: T. J. Bandosz), Elsevier, **2006**, p. 293.
[24] E. Frackowiak, F. Béguin, *Recent Advances in Supercapacitors, Transwrold Research Network* (Ed.: V. Gupta), Kerala, **2006**, p. 79.
[25] C. Peng, S. W. Zhang, D. Jewell. G. Z. Chen, *Prog. Nat. Sci.* **2008**, *18*, 777.
[26] DOE reports at http://www.sc.doe.gov/bes/reports/files/EES_rpt.pdf (accessed January 2010.
[27] M. Armand, J. M. Tarascon, *Nature* **2008**, *451*, 652.
[28] T. Zheng, W. Xing, J. R. Dahn, *Carbon* **1996**, *34*, 1501.
[29] O. Yamamoto, M. Wakihara, *Lithium-Ion Batteries*, Wiley-VCH, Weinheim, **1998**.
[30] P. B. Balbuena, Y. Wang, *Lithium Ion Batteries: Solid-Electrolyte Interphase*, World Scientific Books, **2004**.
[31] P. L. Taberna, S. Mitra, P. Poizot, P. Simon, J. M. Tarascon, *Nat. Mater.* **2006**, *5*, 567.
[32] A. Herold, in *Chemical Physics of Intercalation* (Eds.: A. P. Legrand, S. Flandrois), Vol. B172, Plenum, New York, **1987**.
[33] M. S. Dresselhaus, G. Dresselhaus, *Adv. Phys.* **2002**, *51*, 1.
[34] M. Winter, J. O. Besenhard, M. E. Spahr, P. Novak, *Adv. Mater.* **1998**, *10*, 725.
[35] M. Winter, J. O. Besenhard,in *Lithium Ion Battery: Fundamentals and Performance* (Eds.: M. Wahihara, O. Yamamoto), Wiley-VCH, Weinheim, **1998**.
[36] K. Tatsumi, T. Akai, T. Imamura, K. Zaghib, N. Iwashita, S, Higuchi, Y. Sawada, *J. Electrochem. Soc.* **1996**, *143*, 1923.

[37] M. Letellier, F. Chevallier, C. Clinard, E. Frackowiak, J. N. Rouzaud, F. Béguin, M. Morcrette, J. M. Tarascon, *J. Chem. Phys.* **2003**, *118*, 6038.
[38] K. Sato, M. Noguchi, A. Demachi, N. Oki, M. Endo, *Science* **1994**, *264*, 556.
[39] H. Fujimoto, A. Mabuchi, K. Tokumitsu, T. Kasuh, *J. Power Sources* **1995**, *54*, 440.
[40] J. R. Dahn, T. Zheng, Y. Liu, J. S. Xue, *Science* **1995**, *270*, 590.
[41] J. C. Withers, R. O. Loufty, T. P. Lowe, *Fullerene Sci. Technol.* **1997**, *5*, 1.
[42] V. A. Nalimova, D. F. Sklovsky, G. N. Bondarenko, H. Alvergnat-Gaucher, S. Bonnamy, F. Béguin, *Synth. Met.* **1997**, *88*, 89.
[43] F. Leroux, K. Méténier, S. Gautier, E. Frackowiak, S. Bonnamy, F. Béguin, *J. Power Sources* **1999**, *81*, 317.
[44] A. S. Claye, J. E. Fischer, C. B. Huffman, A. G. Rinzler, R. E. Smalley, *J. Electrochem. Soc.* **2000**, *147*, 2845.
[45] W. Lu. , D. D. L. Chung, *Carbon* **2001**, *39*, 493.
[46] B. Gao, A. Kleinhammes, X. P. Tang, C. Bower, L. Fleming, Y. Wu, O. Zhou, *Chem. Phys. Lett.* **1999**, *307*, 153.
[47] J. P. Tessonnier, D. Rosenthal, T. W. Hansen, C. Hess, M. E. Schuster, R. Blume, F. Girgsdies, N. Pfänder, O. Timpe, D. S. Su, R. Schlögl, *Carbon* **2009**, *47*, 1779.
[48] B. Gao, C. Bower, J. D. Lorentzen, L. Fleming, A. Kleinhammens, X. P. Tang, L. E. McNeil, Y. Wu, O. Zhou, *Chem. Phys. Lett.* **2000**, *327*, 69.
[49] E. Frackowiak, S. Gautier, H. Gaucher, S. Bonnamy, F. Béguin, *Carbon* **1999**, *37*, 61.
[50] G. Wu, C. S. Wang, X. B. Zhang, H. S. Yang, Z. Qi, P. He, W. Li, *J. Electrochem. Soc.* **1999**, *146*, 1696.
[51] K. Balasubramanian, M. Burghard, *Small* **2005**, *1*, 180.
[52] A. Hirsch, O. Vostrowsky, *Functionalization of Carbon Nanotubes, in Functional Organic Materials* (Eds.: T. J. J. Müller, U. H. F. Bunz), Wiley-VCH, Weinheim, **2007**.
[53] D. Tasis, N. Tagmatarchis, A. Bianco, M. Prato, *Chem. Rev.* **2006**, *106*, 1105.
[54] A. Hirsch, O. Vostrowsky, *Top. Curr. Chem.* **2005**, *245*, 193.
[55] P. X. Hou, C. Liu, H. M. Cheng, *Carbon* **2008**, *46*, 2003.
[56] P. V. Lakshminarayanan, H. Toghiani, C. U. Pittman Jr. , *Carbon* **2004**, *42*, 2433.
[57] X. L. Chen, W. S. Li, C. L. Tan, W. Li, Y. Z. Wan, *J. Power Sources* **2008**, *184*, 668.
[58] D. Larchera, C. Mudaligeb, M. Gharghouri, J. R. Dahn, *Electrochim. Acta* **1999**, *44*, 4069.
[59] I. Mukhopadhyay, N. Hoshino, S. Kawasaki, F. Okino, W. K. Hsu, H. Touhara, *J. Electrochem. Soc.* **2002**, *149*, A39.
[60] R. T. Lv, L. Zou, X. C. Gui, F. Y. Kang, Y. Q. Zhu, H. W. Zhu, J. Q. Wei, J. L. Gu, K. L. Wang, D. H. Wu, *Chem. Commun.* **2008**, 2046.
[61] Z. Yang, Y. Feng, Z. Li, S. Sang, Y. Zhou, L. Zeng, *J. Electroanal. Chem.* **2005**, *580*, 340.
[62] D. S. Su, X. W. Chen, G. Weinberg, A. K. Hofmann, O. Timpe, S. B. A. Hamid, R. Schlögl, *Angew. Chem.* **2005**, *117*, 5624; *Angew. Chem. Int. Ed.* **2005**, *44*, 5488.
[63] W. Xia, D. S. Su, R. Schlögl, A. Birkner, M. Muhler, *Adv. Mater.* **2005**, *17*, 1677.
[64] W. Xia, D. S. Su, A. Birkner, L. Ruppel, Y. M. Wang, C. Wöll, J. Qian, C. H. Liang, G. Marginean, W. Brandl, M. Muhler, *Chem. Mater.* **2005**, *17*, 5737.
[65] X. Li, F. Kang, W. Shen, *Carbon* **2006**, *44*, 1334.
[66] K. Sheem, Y. H. Lee, H. S. Lim, *J. Power Sources* **2006**, *158*,1425.
[67] C. Sotowa, G. Origi, M. Takeuchi, Y. Nishimura, K. Takeuchi, I. Y. Jang, Y. J. Kim, T. Hayashi, Y. A. Kim, M. Endo, M. S. Dresselhaus, *ChemSusChem* **2008**, *1*, 911.
[68] A. Oberlin, M. Endo, T. Koyama, *J. Cryst. Growth* **1976**, *32*, 335.
[69] M. Endo, *ChemTech* **1988**, *18*, 568.
[70] S. H. Yoon, C. W. Park, H. Yang, Y. Korai, I. Mochida, R. T. K. Baker, N. M. Rodriguez, *Carbon* **2004**, *42*, 21.
[71] M. Endo, C. Him, T. Karaki, Y. Nishimura, J. J. Matthews, S. C. W. Brown, M. S. Dresselhaus, *Carbon* **1999**, *37*, 561–568.
[72] M. Endo, Y. A. Kim, T. Hayashi, K. Nishimuar, T. Matusita, K. Miyashita, M. S. Dresselhaus, *Carbon* **2001**, *39*, 1287.
[73] C. Kim, K. S. Yang, M. Kojima, K. Yohida, Y. J. Kim, Y. A. Kim, *Adv. Funct. Mater.* **2006**, *16*, 2393.
[74] C. Kim, Y. I. Jeong, B. T. N. Ngoc, K. S. Yang, M. Kojima, Y. A. Kim, M. Endo, J. W. Lee, *Small* **2007**, *3*, 91.
[75] L. Ji, X. Zhang, *Nanotechnology* **2009**, *20*, 155705.
[76] J. Zhang, Y. S. Hu, J. P. Tessonnier, G. Weinberg, J. Maier, R. Schlögl, D. S. Su, *Adv. Mater.* **2008**, *20*, 1450.
[77] G. H. Wrodnigg, T. M. Wrodnigg, J. O. Besenhard, M. Winter, *Electrochem. Commun.* **1999**, *1*, 148.
[78] M. Liang, L. Zhi, *J. Mater. Chem.* **2009**, *19*, 5871.
[79] G. Wang, X. Shen, J. Yao, J. Park, *Carbon* **2009**, *47*, 2049.
[80] E. J. Yoo, J. Kim, E. Hosono, H. Zhou, T. Kudo, I. Honma, *Nano Lett.* **2008**, *8*, 2277.
[81] H. S. Zhou, S. M. Zhu, M. Hibino, I. Honma, M. Ichihara, *Adv. Mater.* **2003**, *15*, 2107.
[82] A. Oberlin, *Chemistry and Physics of Carbon 22* (Ed.: P. Thrower), Marcel Dekker, New York, **1989**.
[83] M. D. Levi, D. Aurback, *J. Phys. Chem. B* **1997**, *101*, 4641.
[84] Q. Wang, H. Li, L. Q. Chen, X. J. Hunag, *J. Electrochem. Soc.* **2001**, *148*, A737.
[85] R. Ryoo, S. H. Joo, S. Jun, *J. Phys. Chem. B* **1999**, *103*, 7743.
[86] S. Jun, S. H. Joo, R. Ryoo, M. Kruk, M. Jaroniec, Z. Liu, T. Ohsuna, O. Terasaki, *J. Am. Chem. Soc.* **2000**, *122*, 10712.
[87] Y. S. Hu, P. Adelhelm, B. M. Smarsly, S. Hore, M. Antonietti, J. Maier, *Adv. Funct. Mater.* **2007**, *17*, 1873.
[88] K. Sonnenburg, P. Adelhelm, B. Sarsly, M. Antonietti, R. Nöske, P. Strauch, *Phys. Chem. Chem. Phys.* **2006**, *8*, 3561.
[89] A. Thomas, F. Goettmann, M. Antonietti, *Chem. Mater.* **2008**, *20*, 738.
[90] M. Endo, C. Kim, T. Hayashi, K. Nishimura, T. Matsushita, K. Miyashita, M. S. Dresselhaus, *Carbon* **2001**, *39*, 1287.
[91] M. Winter, J. O. Besenhard, *Chem. Unserer Zeit* **1999**, *33*, 320.
[92] B. Gao, S. Sinha, L. Fleming, O. Zhou, *Adv. Mater.* **2001**, *13*, 816.
[93] M. Winter, J. O. Besenhard, *Electrochim. Acta* **1999**, *45*, 31.
[94] R. A. Huggins, in *Lithium Batteries* (Eds: G. A. Nazri, G. Pistoia), Kluwer Adademic, Boston, **2004**, p. 270.
[95] A. M. Wilson, J. R. Dahn, *J. Electrochem. Soc.* **1995**, *142*, 326.
[96] J. Saint, M. Morcrette, D. Larcher, L. Laffont, S. Beattie, J. P. Pérès, D. Talaga, M. Couzi, J. M. Tarascon, *Adv. Funct. Mater.* **2007**, *17*, 1765.
[97] I. A. Courtney, J. R. Dahn, *J. Electrochem. Soc.* **1997**, *144*, 2943.
[98] L. Y. Beaulieu, J. R. Dahn, *J. Electrochem. Soc.* **2000**, *147*, 3237.
[99] O. Mao, R. A. Dunlap, J. R. Dahn, *J. Electrochem. Soc.* **1999**, *146*, 405.
[100] T. Zhang, L. J. Fu, J. Gao, Y. P. Wu, R. Holze, H. Q. Wu, *J. Power Sources* **2007**, *174*, 770.
[101] D. G. Kim, H. Kim, H. J. Sohn, T. Kang, *J. Power Sources* **2002**, *104*, 221.
[102] N. Li, C. R. Martin, B. Scrosati, *Electrochem. Solid-State Lett.* **2000**, *3*, 316.
[103] C. R. Martin, N. Li, B. Scrosati, *J. Power Sources* **2001**, 97–98, 240.
[104] G. Cui, Y. Hu, L. Zhi, D. Wu, I. Lieberwirth, J. Maier, K. Müllen, *Small* **2007**, *3*, 2066.
[105] Z. W. Zhao, Z. P. Guo, P. Yao, H. K. Liu, *J. Mater. Sci. Technol.* **2008**, *24*, 1245.
[106] J. Hassoun, g. Derrien, S. Panero, B. Scrosati, *Adv. Mater.* **2008**, *20*, 3169.
[107] G. Norman, *J. Polym. Sci.* **1984**, *22*, 71.
[108] K. T. Lee, Y. S. Jung, S. M. Oh, *J. Am. Chem. Soc.* **2003**, *125*, 5652.
[109] W. M. Zhang, J. S. Hu, Y. G. Guo, S. F. Zheng, L. S. Zhong, W. G. Song, L. J. Wan, *Adv. Mater.* **2008**, *20*, 1160.
[110] I. Grigoriants, L. Sominski, H. Li, I. Ifargan, D. Aurbach, A. Gedanken, *Chem. Commun.* **2005**, 921.
[111] Z. Wang, M. A. Fierke, A. Stein, *J. Eelecrochmical Soc.* **2008**, *155*, A658.
[112] T. Prem Kumar, R. Ramesh, Y. Y. Lin, G. Ting-Kuo Fey, *Electrochem. Commun.* **2004**, *6*, 520.
[113] Y. Wang, M. Wu, Z. Jiao, J. Y. Lee, *Chem. Mater.* **2009**, *21*, 3210.
[114] D. Deng, J. Y. Lee, *Angew. Chem.* **2009**, *121*, 1688; *Angew. Chem. Int. Ed.* **2009**, *48*, 1660.
[115] Y. Yan, L. Gu, C. Zhu, P. A. Van Aken, J. Maier, *J. Am. Chem. Soc.* **2009**, *131*, 15984.
[116] Y. Yu, L. Gu, C. Wang, A. Dhanabalan, P. A. Van Aken, J. Maier, *Angew. Chem.* **2009**, *121*, 6607; *Angew. Chem. Int. Ed.* **2009**, *48*, 6485.
[117] Z. P. Guo, D. Z. Jia, L. Yuan, H. K. Liu, *J. Power Sources* **2006**, *159*, 332.
[118] S. H. Ng, J. Wang, D. Wexler, K. Konstantinov, Z. P. Guo, H. K. Liu, *Angew. Chem.* **2006**, *118*, 7050; *Angew. Chem. Int. Ed.* **2006**, *45*, 6896.
[119] Y. S. Hu, R. Demir-Cakan, M. M. Titirici, J. O. Müller, R. Schlögl, M. Antonietti, J. Maier, *Angew. Chem.* **2008**, *120*, 1669; *Angew. Chem. Int. Ed.* **2008**, *47*, 1645.

[120] Y. S. Hu, P. Adelhelm, B. M. Smarsly, J. Maier, *ChemSusChem* **2009**, DOI: 10.1002/cssc.200900191.
[121] H. Kim, J. Cho, *Nano Lett.* **2008**, *8*, 3688.
[122] J. Saint, M. Morcrette, D. Larcher, L. Laffont, S. Beattie, J.-P. Pérès, D. Talaga, M. Couzi, J. M. Tarascon, *Adv. Funct. Mater.* **2007**, *17*, 1765.
[123] J. Graetz, C. C. Ahn, R. Yazami, B. Fultz, *J. Electrochem. Soc.* **2004**, *151*, A698.
[124] G. Cui, L. Gu, L. Zhi, N. Kaskhedikar, P. A. Aken, K. Müllen, J. Maier, *Adv. Mater.* **2008**, *20*, 3079.
[125] P. Poizot, S. Laruelle, S. Grugeon, L. Dupont, J. M. Tarascon, *Nature* **2000**, *407*, 496.
[126] D. Larcher, G. Sudant, J. B. Leriche, Y. Chabre, J. M. Tarascon, *J. Electrochem. Soc.* **2002**, *149*, A234.
[127] K. M. Shaju, F. Jiao, A. Débart, P. G. Bruce, *Phys. Chem. Chem. Phys.* **2007**, *9*, 1837.
[128] S. A. Needham, G. X. Wang, K. Konstantinov, Y. Tournayre, Z. Lao, H. K. Liu, *Electrochem. Solid-State Lett.* **2006**, *9*, A315.
[129] R. Z. Yang, Z. X. Wang, J. Y. Liu, L. Q. Chen, *Electrochem. Solid-State Lett.* **2004**, *7*, A496.
[130] L. J. Zhi, Y. S. Hu, B. El Hamaoui, X. Wang, I. Lieberwirth, U. Kolb, J. Maier, K. Müllen, *Adv. Mater.* **2008**, *20*, 1727.
[131] S. Yang, G. Cui, S. Pang, Q. Cao, U. Kolb, X. Fang, J. Maier, K. Müllen, *ChemSusChem*, DOI: 10.1002/cssc.200900106.
[132] C. H. Jiang, I. Honma, T. Kudo, H. S. Zhou, *Electrochem. Solid-State Lett.* **2007**, *10*, A127.
[133] Y. S. Hu, L. Kienle, Y. G. Guo, J. Maier, *Adv. Mater.* **2006**, *18*, 1421.
[134] Y. G. Guo, Y. S. Hu, W. Sigle, J. Maier, *Adv. Mater.* **2007**, *19*, 2087.
[135] I. Moriguchi, R. Hidaka, H. Yamada, T. Kudo, H. Marakami, H. Nakashima, *Adv. Mater.* **2006**, *18*, 69.
[136] D. Wang, D. Choi, J. Li, Z. Yang, Z. Nie, R. Kou, D. Hu, C. Wang, L. V. Saraf, J. Zhang, I. A. Aksay, J. Liu, *ACS Nano* **2009**, *3*, 907.
[137] Y. S. Hu, X. Liu, J. O. Müller, R. Schlögl, J. Maier, D. S. Su, *Angew. Chem.* **2008**, *120*, 1669; *Angew. Chem. Int. Ed.* **2008**, *47*, 1645.
[138] Z. P. Zhu, D. S. Su, G. Weinberg, R. Jentoft, R. Schlögl, *Small* **2005**, *1*, 107.
[139] A. L. M. Reddy, M. M. Shaijumon, S. R. Gowda, P. M. Ajayan, *Nano Lett.* **2009**, *9*, 1002.
[140] L. Y. Beaulieu, J. R. Dahn, *J. Electrochem. Soc.* **2000**, *147*, 3237.
[141] K. T. Lee, J. C. Lytle, N. S. Ergang, S. M. Oh, A. Stein, *Adv. Funct. Mater.* **2005**, *15*, 547.
[142] W. Zhang, X. Wu, J. Hu, Y. Guo, L. Wan, *Adv. Funct. Mater.* **2008**, *18*, 3941.
[143] Y. J. Kwon, J. Cho, *Chem. Commun.* **2008**, 1109.
[144] R. D. Cakan, M. M. Titirici, M. Antonietti, .G. L. Cui, J. Maier, Y. S. Hu, *Chem. Commun.* **2008**, 3759.
[145] Z. Wen, Q. Wang, Q. Zhang, J. Li, *Adv. Funct. Mater.* **2007**, *17*, 2772.
[146] M. S. Park, S. A. Needham, G. X. Wang, Y. M. Kang, J. S. Park, S. X. Dou, H. K. Liu, *Chem. Mater.* **2007**, *19*, 2406.
[147] G. Chen, Z. O. Wang, D. Xia, *Chem. Mater.* **2008**, *20*, 6951.
[148] J. Bréger, K. Kang, J. Cabana, G. Ceder. C. P. Grey, *J. Mater. Chem.* **2007**, *17*, 3167.
[149] Y. H. Lee, K. H. An, J. Y. Lee, C. H. Lin, in *Encyclopedia of Nanoscience and Nanotechnology* (Ed.: H. S. Nalwa), American Scientific Publishers, **2004**, p. 625.
[150] L. L. Zhang, X. S. Zhao, *Chem. Soc. Rev.* **2009**, *38*, 2520.
[151] R. Miller, S. M. Butler, in *Recent Advances in Supercapacitors, Transwrold Research Network* (Ed.: V. Gupta), Kerala, India, **2006**, p. 1.
[152] F. Béguin, E. Frackowiak, in *Nanomaterials Hanbook* (Ed.: Y. Gogotsi), CRC Press, Boca Raton, **2006**, p. 713.
[153] J. Maier, *Nat. Mater.* **2005**, *4*, 805.
[154] L. Z. Fan, J. Maier, *Electrochem. Commun.* **2006**, *8*, 937.
[155] C. Niu, E. K. Sichel, R. Hoch, D. Moy, H. Tennet, *Appl. Phys. Lett.* **1997**, *70*, 1480.
[156] R. Z. Ma, J. Liang, B. Q. Wei, B. Zhang, C. L. Xu, D. H. Wu, *J. Power Sources* **1999**, *84*, 126.
[157] Ch. Emmenegger, P. Mauron, A. Zuttel, Ch. Nutzenadel, A. Schneuwly, R. Gallay, L. Schlapbach, *Appl. Surf. Sci.* **2000**, *162*, 452.
[158] E. Frackowiak, K. Jurewicz, S. Delpeux, F. Béguin, *J. Power Sources* **2001**, *97*, 822.
[159] C. Niu, E. K. Sichel, R. Hoch, D. Moy, H. Tennet, *Appl. Phys. Lett.* **1997**, *70*, 1480.
[160] E. Frackowiak, F. Béguin, *Carbon* **2001**, *39*, 937.
[161] E. Frackowiak, S. Delpeux, K. Jurewicz, K. Szostak, D. Cazorla-Amoros, F. Béguin, *Chem. Phys. Lett.* **2002**, *361*, 35.
[162] C. Liu, A. J. Bard, F. Wudl, I. Weitz, J. R. Heath, *Electrochem. Solid-State Lett.* **1999**, *2*, 577.
[163] C. Liu, A. J. Bard, F. Wudl, I. Weitz, J. R. Heath, *J. Power Sources* **2001**, *97–98*, 822.
[164] J. N. Barisci, G. G. Wallace, R. H. Baughman, *Electrochim. Acta* **2000**, *46*, 509.
[165] K. A. An, W. S. Kim, Y. S. Park, Y. C. Choi, S. M. Lee, D. C. Chung, D. J. Bae, S. C. Lim, Y. H. Lee, *Adv. Mater.* **2001**, *13*, 497.
[166] S. Shiraishi, H. Kurihara, K. Okabe, D. Hulicova, A. Oya, *Electrochem. Commun.* **2002**, *4*, 593.
[167] E. Frackowiak, K. Jurewicz, K. Szostak, S. Delpeux, F. Béguin, *Fuel Process. Technol.* **2002**, *77/78*, 213.
[168] Y. H. Lee, K. H. An, S. C. Lim, W. S. Kim, J. J. Jeong, C. H. Doh, S. I. Moon, *New Diamond Front. Carbon Technol.* **2002**, *12*, 209.
[169] K. J. An, W. S. Kim, Y. S. Park, Y. C. Choi, S. M. Lee, D. C. Chung, D. J. Bae, S. C. Lim, Y. H. Lee, *Adv. Mater.* **2001**, *13*, 497.
[170] D. N. Futaba, K. Hata, T. Yamada, T. Hiraoka, Y. Haramizu, Y. kakudate, O. Tanaike, H. Hatori, M. Yumura, S. Iijima, *Nat. Mater.* **2006**, *5*, 987.
[171] K. S. Subrahmanyam, S. R. C. Vivekchand, A. Govindaraj, C. N. R. Rao, *J. Mater. Chem.* **2008**, *18*, 1517.
[172] M. D. Stoller, S. Park, Y. Zhu, J. An, R. S. Ruoff, *Nano Lett.* **2008**, *8*, 3498.
[173] X. Zhao, H. Tian, M. Zhu, K. Tian, J. J. Wang, F. Kang, R. A. Outlaw, *J. Power Sources* **2009**, *194*, 1208.
[174] C. Vix-Guterl, S. Saadallah, K. Jurewicz, *Mater. Sci. Eng. B* **2004**, *108*, 148.
[175] S. Han, K. T. Lee, S. M. Oh, T. Hyeon, *Carbon* **2003**, *41*, 1049.
[176] K. Jurewicz, C. Vix-Guterl, E. Frackowiak, S. Saadallah, M. Reda, J. Parmentier, J. Patarin, F. Béguin, *J. Phys. Chem. Solids* **2004**, *65*, 287.
[177] S. Yoon, J. Lee, T. Hyeon, S. M. Oh, *J. Electrochem. Soc.* **2000**, *147*, 2507.
[178] C. Vix-Guterl, E. Frackowiak, K. Jurewicz, S. Saadallah, M. Friebe, J. Parmentier, J. Patarin, F. Béguin, *Carbon* **2005**, *43*, 1293.
[179] Y. Liang, D. C. Wu, R. W. Fu, *Langmuir* **2009**, *25*, 7783.
[180] D. W. Wang, F. Li, M. Liu, G. Q. Lu, H. M. Cheng, *Angew. Chem.* **2008**, *120*, 379; *Angew. Chem. Int. Ed.* **2008**, *47*, 373.
[181] W. Xing, C. C. Huang, S. P. Zhuo, X. Yuan, G. Q. Wang, D. Hulicova-Jurcakova, Z. F. Yan, G. Q. Lu, *Carbon* **2009**, *47*, 1715.
[182] D. Wu, R. Fu, M. S. Dresselhaus, G. Dresselhaus, *Carbon* **2006**, *44*, 675.
[183] J. Wang, X. Yang, D. Wu, R. Fu, M. S. Dresselhaus, G. Dresselhaus, *J. Power Sources* **2008**, *185*, 589.
[184] H. Shi, *Electrochim. Acta* **1996**, *41*, 1633.
[185] D. Qu, H. Shi, *J. Power Sources* **1998**, *74*, 99.
[186] S. Yoon, J. Lee, T. Hyeon, S. M. Oh, *J. Electrochem. Soc.* **2000**, *147*, 2507.
[187] G. Salitra, A. Soffer, L. Eliad, Y. Cohen, D. Aurbach, *J. Electrochem. Soc.* **2000**, *147*, 2486.
[188] J. Gamby, P. L. Taberna, P. Simon, J. F. Fauvarque, M. Chesneau, *J. Power Sources* **2001**, *101*, 109.
[189] S. Shiraishi, in *Carbon Alloy* (Eds.: E. Yasuda, M. Inagaki, K. Kaneko, M. Endo, A. Oya, Y. Tanabe), Elsevier, **2003**, p. 447.
[190] O. Barbieri, et al., *Carbon* **2005**, *43*, 1303.
[191] D. Qu, *J. Power Sources* **2002**, *109*, 403.
[192] Y. J. Kim, et al., *Carbon* **2004**, *42*, 1491.
[193] E. Raymundo-Pinero, K. Kierzek, J. Machnikowski, F. Béguin, *Carbon* **2006**, *44*, 2498.
[194] J. Chmiola, Y. Gogotsi, *Nanotech. Law Business* **2007**, *4*, 577.
[195] G. Yushin, A. Nikitin, Y. Gogotsi, *Nanomaterial Handbook* (Ed.: Y. Gogotsi), CRC Press, Boca Raton, **2006**, p. 237.
[196] Y. Gogotsi, A. Nikitin, H. Ye, W. Zhou, J. E. Fischer, B. Yi, H. C. Foley, M. W. Barsoum, *Nat. Mater.* **2003**, *2*, 591.
[197] R. K. Dash, G. Yushin, Y. Gogotsi, *Microporous Mesoporous Mater.* **2005**, *86*, 50.
[198] J. Chmiola, G. Yushin, Y. Gogotsi, C. Portet, P. Simon, P. L. Taberna, *Science* **2006**, *313*, 1760.
[199] C. Largeot, C. Portet, J. Chmiola, P. L. Taberna, Y. Gogotsi, P. Simon, *J. Am. Chem. Soc.* **2008**, *130*, 2730.
[200] J. Chmiola, C. Largeot, P. L. Taberna, P. Simon, Y. Gogotsi, *Angew. Chem.* **2008**, *120*, 3440; *Angew. Chem. Int. Ed.* **2008**, *47*, 3392.
[201] H. Nishihara, H. Itoi, T. Kogure, P. X. Hou, H. Touhara, F. Okino, T. Kyotani, *Chem. Eur. J.* **2009**, *15*, 5355.

[202] F. Stöeckli, T. A. Centeno, J. B. Donnet, N. Pusset, E. Papirer, *Fuel* **1995**, *11*, 1582.
[203] A. Rudge, I. Raistrick, S. Gottesfeld, J. P. Ferrais, *J. Power Sources* **1994**, *47*, 89.
[204] A. Laforgue, P. Simon, J. F. Fauvarque, *Synth. Met.* **2001**, *123*, 311.
[205] K. Naoi, S. Suematsu, A. Manago, *J. Electrochem. Soc.* **2000**, *147*, 420.
[206] Y. Z. Zheng, H. Y. Ding, M. L. Zhang, *Mater. Res. Bull.* **2009**, *44*, 403.
[207] H. Liu, P. He, Z. Li, Y. Liu, J. Li, *Electrochim. Acta* **2006**, *51*, 1925.
[208] Y. Lei, C. Fournier, J. L. Pascal, F. Favier, *Microporous Mesoporous Mater.* **2008**, *110*, 167.
[209] J. Li, X. Wang, Q. Huang, S. Gamboa, P. J. Sebastian, *J. Power Sources* **2006**, *160*, 1501.
[210] J. Li, E. H. Liu, W. Li, X. Y. Meng, S. T. Tan, *J. Alloys Compd.* **2009**, *478*, 371.
[211] B. E. Conway, *Electrochemical Supercapacitors: Scientic Fundamentals and Technological Applications*, Kluwer, **1999**.
[212] B. E. Conway, *J. Electrochem. Soc.* **1991**, *138*, 1539.
[213] M. Ramani, B. S. Haran, R. E. White, B. N. Popov, *J. Electrochem. Soc.* **2001**, *148*, A374.
[214] J. M. Miller, B. Dunn, *Langmuir* **1999**, *15*, 799.
[215] J. Hong, I. Yoe, W. Paik, *J. Electrochem. Soc.* **2001**, *148*, A156.
[216] G. Cui, L. Zhi, A. Thomas, I. Lieberwirth, U. Kolb, K. Müllen, *ChemPhysChem* **2007**, *8*, 1013.
[217] B. J. Lee, S. R. Sivakkumar, J. M. Ko, J. H. Kim, S. M. Jo, D. Y. Kim, *J. Power Sources* **2007**, *168*, 546.
[218] D. Yuan, J. Zeng, N. Kristian, Y. Wang, X. Wang, *Electrochem. Commun.* **2009**, *11*, 313.
[219] M. Toupin, T. Brousse, D. Belanger, *Chem. Mater.* **2004**, *16*, 3184.
[220] X. Qin, S. Durbach, G. T. Wu, *Carbon* **2004**, *42*, 451.
[221] J. Y, Lee, K. Liang, K. H. An, Y. H. Lee, *Synth. Met.* **2005**, 150, 153.
[222] H. Liang, F. Chen, R. Li, L. Wang, Z. Deng, *Electrochim. Acta* **2004**, *49*, 3463.
[223] J. H. Park, J. M. Ko, O. O. Park, D. W. Kim, *J. Power Sources* **2002**, *105*, 20.
[224] L. Z. Fan, Y. S. Hu, J. Maier, P. Adelhelm, B. Smarsly, M. Antonietti, *Adv. Funct. Mater.* **2007**, *17*, 3083.
[225] V. Khomenko, E. Frackowiak, F. Béguin, *Electrochim. Acta* **2005**, *50*, 2499.
[226] A. Malinauskas, *Polymer* **2001**, *42*, 3957.
[227] H. Li, H. Xi, S. Zhu, Z. Wen, R. Wang, *Microporous Mesoporous Mater.* **2006**, *96*, 357.
[228] H. A. Andreas, B. E. Conway, *Electrochim. Acta* **2006**, *51*, 6510.
[229] M. A. Montes-Morán, D. Suarez, J. A. Menendez, A. E. Fuente, *Carbon* **2004**, *42*, 1219.
[230] D. Qu, *J. Power Sources* **2002**, *109*, 403.
[231] C. T. Hsieh, H. Teng, *Carbon* **2002**, *40*, 667.
[232] D. Hulicova, J. Yamashita, Y. Soneda, H. Hatori, M. Kodama, *Chem. Mater.* **2005**, *17*, 1241.
[233] F. Béguin, K. Szostak, G. Lota, E. Frackowiak, *Adv. Mater.* **2005**, *17*, 2380.
[234] D. Hulicova, M. Kodama, H. Hatori, *Chem. Mater.* **2006**, *18*, 2318.
[235] Y. J. Kim, Y. Abe, T. Yanagiura, K. C. Park, M. Shimizu, T. Iwazaki, S. Nakagawa, M. Endo, M. S. Dresselhaus, *Carbon* **2007**, *45*, 2116.
[236] W. Li, D. Chen, Z. Li, Y. Shi, Y. Wan, G. Wang, Z. Jiang, D. Zhao, *Carbon* **2007**, *45*, 1757.
[237] A. B. Fuertes, G. Lota, T. A. Centeno, E. Frackowiak, *Electrochim. Acta* **2005**, *50*, 2799.
[238] M. R. Jisha, Y. J. Hwang, J. S. Shin, K. S. Nahm, T. P. Kumar, K. Karthikeyan, N. Dhanikaivelu, D. Kalpana, N. G. Renganathan, A. M. Stephan, *Mater. Chem. Phys.* **2009**, *115*, 33.
[239] L. B. Kong, J. Zhang, J. J. An, Y. C. Luo, L. Kang, *J. Mater. Sci.* **2008**, *43*, 3664.
[240] Y. G. Wang, H. Q. Li, Y. Y. Xia, *Adv. Mater.* **2006**, *18*, 2619.
[241] D. W. Wang, F. Li, Z. G. Chen, G. Q. Lu, H. M. Cheng, *Chem. Mater.* **2008**, *20*, 7195.
[242] C. Portet, Z. Yang, Y. Korenblit, Y. Gogotsi, R. Mokaya, G. Yushin, *J. Electrochem. Soc.* **2009**, *156*, A1.
[243] L. E. Jones, P. A. Thrower, *J. Chem. Phys.* **1987**, *84*, 1431.
[244] *Oxidation protection of carbon materials*D. W. McKee, *Chemistry and physics of carbon* (Eds.: P. A. Thrower, M. Dekker), **1991**, 23, p. 173.
[245] J. Zhang, X. Liu, R. Blume, A. Zhang, R. Schlögl, D. S. Su, *Science* **2008**, *322*, 73.
[246] D. Hulicova-Jurcakova, A. M Puziy, O. I. Poddubnaya, F. Suárez-García, J. M. D. Tascón, M. Lu, *J. Am. Chem. Soc.* **2009**, *131*, 5026.
[247] B. Fang, Y. Z. Wei, K. Suziki, M. Kumagai, *Electrochim. Acta* **2005**, *50*, 3616.
[248] R. Schlögl, *Angew. Chem.* **2003**, *115*, 2050; *Angew. Chem. Int. Ed.* **2003**, *42*, 2004.
[249] R. Schlögl, *Angew. Chem.* **1998**, *110*, 2467; *Angew. Chem. Int. Ed.* **1998**, *37*, 2333.
[250] G. Centi, S. Perathoner, G. Wine, M. Gangeri, *Green Chem.* **2007**, *9*, 671.
[251] M. Gangeri, S. Perathoner, S. Caudo, G. Centi, J. Amadou, D. Bégin, C. Pham-Huu, M. J. Ledoux, J. P. Tessonier, D. S. Su, R. Schlögl, *Catal. Today* **2009**, *143*, 57.
[252] L. Zhi, K. Müllen, *J. Mater. Chem.* **2008**, *18*, 1472.
[253] A. Thomas, F. Goettmann, M. Antonietti, *Chem. Mater.* **2008**, *20*, 738.
[254] R. Schlögl, *Nat. Mater.* **2008**, *7*, 772.
[255] C. Liu, F. Li, L.-P. Ma, H.-M. Cheng, *Adv. Mater.* **2010**, *22*, E1.

Received: July 29, 2009
Revised: November 29, 2009

EXHIBIT B

Available online at www.sciencedirect.com
ScienceDirect
Carbon 45 (2007) 2229–2234
CARBON
www.elsevier.com/locate/carbon

A mechanism for carbon nanosheet formation

Mingyao Zhu [a,b,*], Jianjun Wang [b], Brian C. Holloway [b,c], R.A. Outlaw [b], Xin Zhao [b], Kun Hou [b], V. Shutthanandan [d], Dennis M. Manos [a,b]

[a] Physics Department, College of William and Mary, Williamsburg, VA 23187-8795, United States
[b] Applied Science Department, College of William and Mary, Williamsburg, VA 23187-8795, United States
[c] Luna nanoWorks Division, Luna Innovations, 521 Bridge Street, Danville, VA 24543, United States
[d] Environmental Molecular Sciences Laboratory, Pacific Northwest National Lab, Richland, WA 99352, United States

Received 16 November 2006; accepted 19 June 2007
Available online 27 June 2007

Abstract

The growth, structure and properties of a two-dimensional carbon nanostructure–carbon nanosheet produced by radio frequency plasma enhanced chemical vapor deposition have been investigated. The effects of deposition parameters on the structure and properties of carbon nanosheets were also investigated. A growth model has been described proposing that atomically thin graphene sheets result from a balance between deposition through surface diffusion and etching by atomic hydrogen, and that the observed vertical orientation of these sheets results from the interaction of the plasma electric field with their anisotropic polarizability.

1. Introduction

Graphite and related materials are attractive because of their unique properties, the variety of the behavior under different conditions, and the potential to provide challenges in both experimental and fundamental sciences [1]. Since their discovery, "zero-dimensional" (0-D) fullerenes [2] and "one-dimensional" (1-D) carbon nanotubes (CNT) [3] have been the basis for both fundamental studies of the growth and properties as well as serving as components in new technical applications [4–6]. Here we report a study of the mechanism of growth for a two-dimensional (2-D) allotrope of the carbon family consisting of self-aligned graphene sheets, which we have called carbon nanosheet (CNS) [7,8], for the first time filling in the gap between low dimensional (0-D and 1-D) and bulk (3-D) carbon structures by providing an ideal 2-D model for fundamental studies and unique opportunities in industrial and technological applications [9]. Unlike graphite intercalated compounds and sources of graphene such as exfoliated graphite, carbon nanosheets are metallic impurity free, atomically thin, and free-standing.

2. Experimental and discussion

The radio frequency (RF) plasma enhanced chemical vapor deposition (PECVD) system used for synthesis of all nanosheets in this study has been previously described in detail [7,8]. In brief, 13.56 MHz RF power was coupled through a quartz window into a vacuum chamber by a 3-turn planar antenna. A resistive heater (sample stage) was located ~5 cm beneath the quartz window. Nanosheets were deposited on a variety of substrates in an inductively coupled plasma (ICP) from CH_4 diluted at various concentrations (5–100%) [8] in H_2, at total gas pressures from 20 to 400 mTorr [10], substrate temperatures of 600–950 °C [8], and RF input powers of 400–1200 W [10].

Scanning electron microscope (SEM) and high resolution transmission electron microscope (HR-TEM) observations [7,8] indicate that typical nanosheets (deposited at 40% CH_4 in H_2, 100 mTorr, 680 °C, and 900 W RF power) are "free-standing" (the vertical walls ascend from the base layers on the substrate without lateral support). The sheets also self-assemble into atomically thin structures, consisting of from 1 or 2 up to 7 parallel layers of graphene sheets. Fig. 1a shows an SEM (Hitachi S-5500) image of typical nanosheets directly grown on a Ni TEM grid.

* Corresponding author. Address: Physics Department, College of William and Mary, Williamsburg, VA 23187-8795, United States. Fax: +1 757 221 3540.
E-mail address: mxzhux@wm.edu (M. Zhu).

0008-6223/$ - see front matter © 2007 Elsevier Ltd. All rights reserved.
doi:10.1016/j.carbon.2007.06.017

CNS have a flat surface morphology roughly vertical to the substrate surface, as shown at the curved surface of the grid wire. Fig. 1b is a higher magnification SEM image showing that the edge of a typical nanosheet is less than 1 nm thick. The HR-TEM (Jeol JEM 2010 F) micrograph of a typical nanosheet, Fig. 1c, shows two parallel fringes with a distance of ~0.34 nm at the edge where the nanosheet folds back, indicating a two atom-layer thick sheet with approximately the (002) spacing of graphite (0.335 nm). Although a single graphene layer of macroscopic size is not thought to be thermodynamically stable [11], modeling suggests that stable double-layered graphene structures are possible [12]. Many of the nanosheets we observe by HR-TEM have edges that are only 1–2 graphene layers thick. Given the layered morphology observed by SEM imaging, further evidence supporting an effective average thickness less than three atomic layers comes from measurements of the specific surface area by the Brunauer–Emmett–Teller (BET) method (Clear Science Inc.). We observed ~1000 m^2/g, which lies between the theoretical maximum value of double layered (1315 m^2/g) and triple layered (877 m^2/g) ideal graphene sheets. From the standpoint of gas storage and uptake, the observed values are comparable to that of the best activated charcoals [13]. Both Raman spectroscopy [7,8] and X-ray diffraction (XRD) [14] also confirm that the CNS are graphitic structures containing defects. Parametric studies show that the order of the nanosheets decreases with increasing substrate temperature, increasing CH_4 concentration [8,14], decreasing input RF power, or decreasing total gas pressure [10].

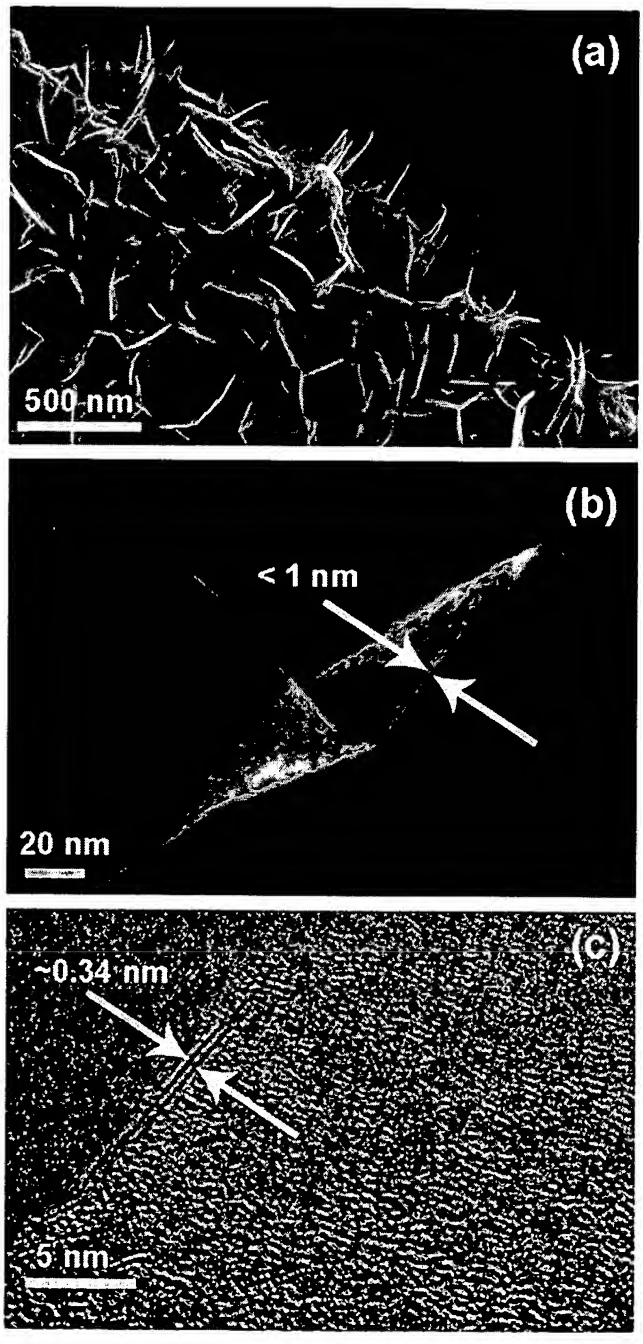

Fig. 1. (a) SEM image of carbon nanosheets directly grown on the curved surface of a Ni wire of a TEM grid shows that the nanosheets have a flat surface morphology and are free-standing roughly vertical to the substrate surface. (b) SEM of an enlarged nanosheets edge with a thickness less than 1 nm. (c) HR-TEM micrographic of a single nanosheet with two graphene layers, as indicated by the two parallel fringes.

In contrast to chemical vapor deposition (CVD) CNT synthesis, CNS deposition in our RF PECVD system does not require a catalyst to predetermine the structure and/or location. In addition, the absence of a catalyst leads to a high purity. Both Auger electron spectroscopy (AES) and X-ray photoelectron spectroscopy (XPS) [10] of CNS detected only carbon, except for a very small amounts of oxygen associated with adsorption of adventitious water, or possibly carbon oxides from sample transfer in air. Particle induced X-ray emission (PIXE) spectra were collected, as shown in Fig. 2. PIXE is a very sensitive technique to detect elements with $Z > 11$ at ppm levels. These spectra show that for CNS grown on an intrinsic Si substrate, Si is the only element detected. Thus, PIXE confirms that there are no detectable metallic impurities (<10's of ppm) in the nanosheet layers. However, thermal desorption spectroscopy (TDS) results [15] indicate high hydrogen concentration (up to 1H atom per 4.5C atom [15]) in nanosheet samples.

A series of short duration depositions, varying from 30 s to 8 min, under typical nanosheet deposition conditions, were performed to elucidate the nature of the early stage of nucleation of the nanosheet layers [16]. These studies indicate that there is a 2–4 min induction-time in the planar nucleation and growth before the onset of vertical nanosheet growth, as indicated by the SEM images in Fig. 3a–c. The base layers are flat and parallel to the substrate surface, therefore difficult to see on as-deposited samples. However, they become observable when the sample

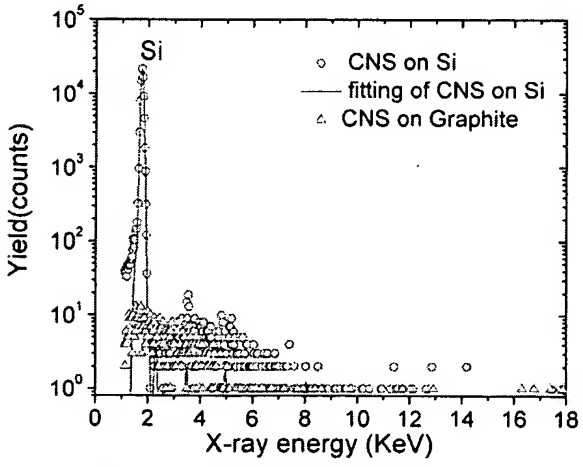

Fig. 2. PIXE spectra of carbon nanosheets on graphite and intrinsic Si substrates show that no elements were detected for nanosheets on graphite, and only Si is detected for nanosheets on Si substrate, so reveal that nanosheets are impurities free. The PIXE experiments were carried out using the +30° beam line (H^+, 2.5 MeV) in the Microbeam End Station of Ion Beam Materials Analysis Laboratory at WR Wiley Environmental Molecular Sciences Laboratory (Richland, WA).

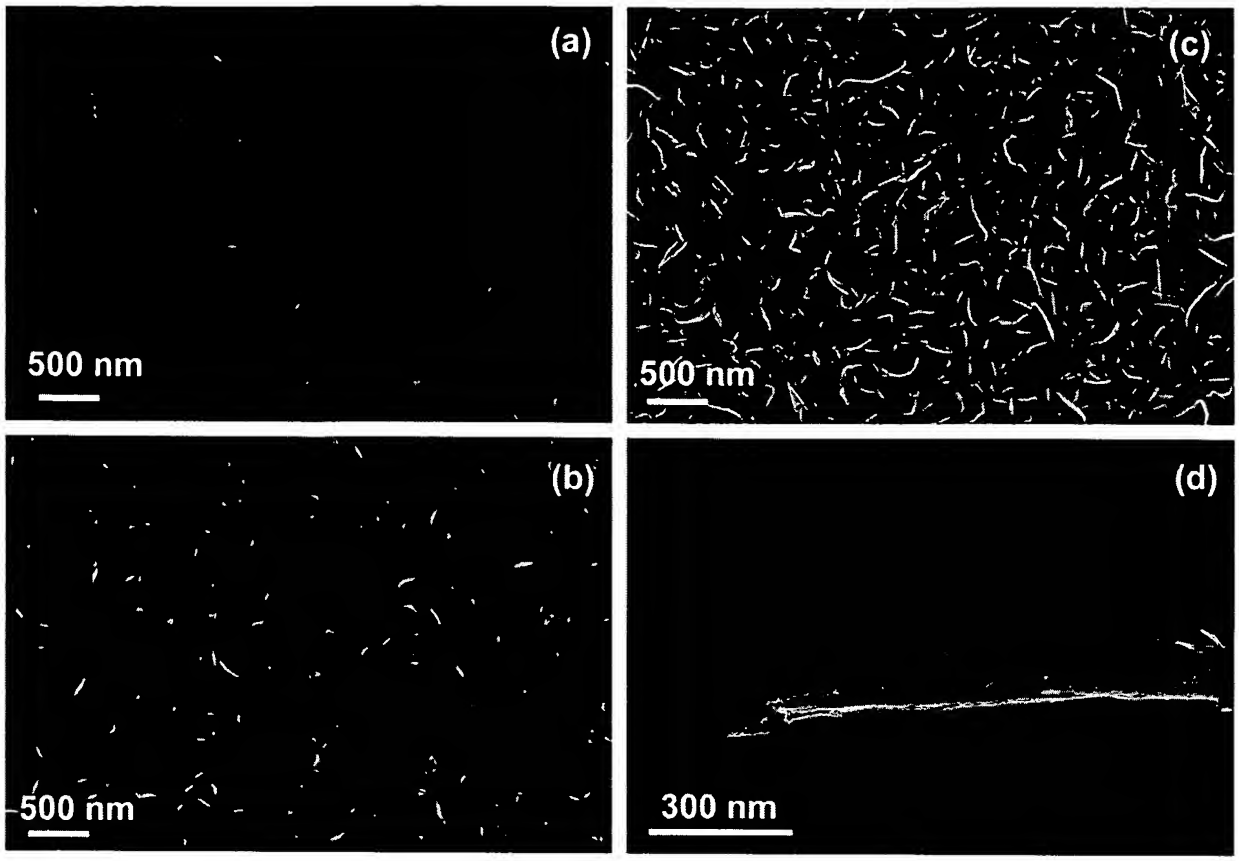

Fig. 3. Top-view SEM images of CNS deposited on Si substrates for (a) 1.5 min; (b) 4 min; and (c) 8 min under typical growth conditions (40% CH_4 in H_2, 100 mTorr, 680 °C, and 900 W RF power). The vertically oriented edges started to form after deposition durations of 1.5–4 min, however, were not observed from samples deposited for 30 s and 1 min (not shown). After 8 min deposition, full coverage is achieved. The base layer parallel to the substrates can be observed by scratching the sample with a sharp metal tip (d) a suspended nanosheets fragment from sample (c) shows the base layer (pointed by the arrow) underneath the vertically oriented sheets is about 10–15 nm thick.

surface is scratched with a sharp metal tip and in imaging at the peeled fragments, as shown in Fig. 3d. Detailed SEM analysis indicates that there is a 1–15 nm thick layer of graphitic sheets that grows parallel to the substrate surface before the onset of vertical growth. It thus appears that during the first few minutes of growth, graphene layers grow parallel to the substrate surface until a sufficient level of force develops at the grain boundaries to curl the leading edge of the top layers upward.

After the top layers curl up being vertical to the substrate surface, which is along the plasma sheath caused electric field direction, the very high surface mobility of incoming carbon-bearing species, and the induced polarization (of the graphitic layers) associated with the local electric field in the sheath layer, combine to cause the nanosheets to grow higher rather than thicker. Precise identity of the mobile species has not yet been determined, but carbon atoms, carbon poly-atomic molecules, or small hydrocarbon molecules are likely to have sufficiently high surface diffusion rates to provide edge growth of the vertical planes. For a C atom on an ideal graphite surface, the surface diffusion energy, E_d, is 0.13 eV [17] while the surface adsorption energy, E_a, is ~1.8 eV [18]. The surface diffusion length [19] (the average distance a particle can migrate along a surface before being re-evaporated) is $\lambda_d = 2a_0\exp[(E_a - E_d)/2kT_s] = 3.7$ μm for typical nanosheet growth conditions ($a_0 = 0.1$ nm, $T_s = 1000$ K, and $k = 1.381 \times 10^{-23}$ J/K or 8.62×10^{-5} eV/K). In the absence of a high flux of energetic H atoms, which might etch the accreting layers or remove adatoms, carbon-bearing species landing on the surface of a growing nanosheet would rapidly move along the sheet surface, reach the edge of the nanosheet, and covalently bond to the edge atoms before being re-evaporated. Carbon-bearing species diffusing toward the substrate instead of toward the growing edges can be re-evaporated because of the weak van der Waals force attaching the species to the substrates. This mechanism accounts for the observation that rather than forming a thick layer of graphite oriented parallel to the substrate, we observe self-assembly of multiple sets of graphene planes that are oriented vertically.

In the above model, the electric field in the plasma both promotes the growth at the nanosheet edges and induces an orientation of the growing planes that is perpendicular to the substrate. An electric-field dependent orientation has been observed by others during the growth of carbon nanotubes [20] and carbon nanowalls [21]. Electric fields have also been used to orient isolated nanotubes for device applications and for purification purposes [22,23]. Alignment of nanosheets in our apparatus is therefore to be expected since prior calculations and measurements yield a three-fold difference between in plane and perpendicular (*c*-axis) polarizability for ideal graphene layers [24]. The relatively higher in-plane mobility of basal-plane electrons allows a field-induced force to align the dipole moments of the nanosheets.

An electric field always exists in the vicinity of a solid object immersed in a plasma. A detailed analysis of this sheath electric field is beyond the scope of this paper. The mechanisms for the formation of the sheath field depend on the details of the geometry, the composition of the plasma, the pressure, the time-dependent energy source of the ionization (DC, inductive, capacitive, high or low frequency electric fields, laser, incoherent photon, or particle beam driven), and the details of the solid material at the boundary and its electrical connection to an external circuit [25]. In our deposition system, the ionization source operates with a pressure-dependent combination of an inductive source and a capacitive source, both coupling at 13.56 MHz. The capacitive contribution comes from the fact that the antenna above the quartz window has peak RF voltages exceeding

1000 V. The resulting potential oscillations in the plasma are rectified at the conducting boundary of the substrate [25] to provide a strong DC field oriented vertically downward toward the substrate [26].

To test one feature of the effects of the magnitude of the local electric field, we grew nanosheets near a grounded conducting metallic cylinder that was placed with its long axis perpendicular to the grounded substrate surface. Such an electrode, in contrast to a floating object, can conduct a substantial current to ground and thus the sheath formation is approximately described by a Langmuir–Child mechanism [25,26]. The local electric field along the central length of this electrode in the vicinity of the substrate is predominantly radially oriented with respect to the cylinder axis. Fig. 4 shows that well-aligned parallel arrays of nanosheets aligned radially in the local electric field direction were formed at the surface of a conductive substrate.

We interpret this experimental observation to be positive evidence of the importance of the local electric field to the overall growth mechanism. The electric field also may play a significant role in overcoming the activation energy barrier (ΔE) associated with the distortion of sp^2 bonded network in the graphene layers that is necessary to bend the nucleating layer. Calculations of the size of this barrier for 100 atom graphene layers [27] estimate it to be of the order of 10 eV. Some of this barrier may possibly be reduced by the introduction and admixture of sp^3 bonding, or lattice distortions from vacancy defects, but the interaction of the field with the induced dipole certainly must be in play to account for the above observation of radial growth.

After nucleation of nanosheets, the activation energy barrier and the electric field forces hold the nanosheets in their two-dimensional configuration, even though enclosed structures, such as fullerenes and nanotubes, have a lower total energy due to elimination of dangling bonds at the edges. However, for a bent nanosheet, the probability for the edges to bond with each other and form a seamless structure is small, so the nanosheets intend to keep their two-dimensional shape.

Our previous parametric studies [28] have shown that inductively coupled plasmas favor nanosheet growth. In contrast to lower power capacitive plasmas, an inductive discharge using a lower neutral gas pressure and higher input powers results in a plasma density ~10 times higher than a similar capacitive plasma because the fractional ionization rate of the inductively coupled plasma can be up to 100 times higher [26]. So capacitive coupling in our system favors CNT deposition, while inductive coupling yields a very high atomic hydrogen to growth species ratio [10,28], which is critical for CNS growth. The atomic hydrogen in the plasma acts as an etchant to rapidly remove amorphous carbon defects promoting a crystalline graphitic structure in the growing layers, to prevent the formation of secondary nuclei which might interfere with their growth, and to remove cross-linking at the free edges of growing sheets, thus, preventing edge thickening which helps to keep them atomically thin. The proposed growth model of CNS is schematically summarized in Fig. 5.

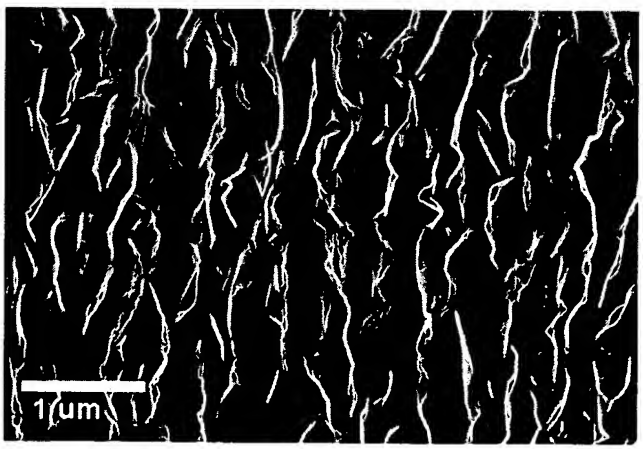

Fig. 4. SEM image of aligned carbon nanosheets on Si substrate formed around a grounded metal electrode. The direction of the nanosheet alignment is along the radial direction of the round electrode.

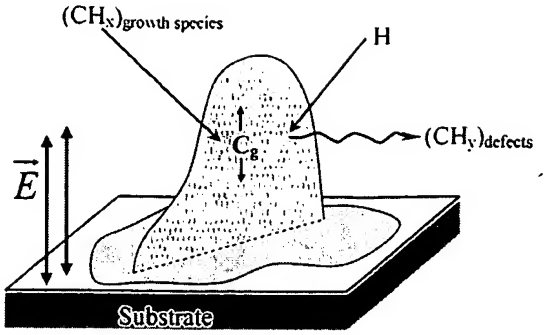

Fig. 5. A schematic explanation of CNS growth model. $\vec{E}$: direction of the electric field near a substrate surface; CH_x: carbon-bearing growth species impinging from gas phase; C_g: growth species diffuse along CNS surface; H: atomic hydrogen impinging from gas phase; CH_y: defects removed from CNS by atomic hydrogen etching effects.

Increasing substrate temperature [8] causes both the growth rate and disorder of nanosheets to increase. We interpret this in terms of surface diffusion and growth from adsorbed carbon-bearing species. The details depend quite heavily on the exact state of carbon and hydrogen and on the band-structure and surface states of the substrate [29,30]. In the model above, we have assumed that the primary traps associated with atom-to-atom excursions, as the growth species surface diffuse along the planar graphene layer, have depths (E_d) ~ 1–2 eV, but that the traps associated with reaching the dangling bonds at the edge of the growing layer lead to covalent bonding with very deep wells (~4–5 eV). The mean time for surface hopping of an adsorbate on the surface is $\tau_d = \nu_1^{-1} \exp[E_d/(kT_s)]$, where ν_1 is the lattice vibrational rate constant ($2kT/h$, $\sim 3 \times 10^{13}$ Hz for $T = 1000$ K [19]), and T_s is the substrate temperature. In this calculation, a higher substrate temperature results in much faster surface diffusion and therefore much faster growth. The growth rate also increases linearly with the impingement rate of growth species. The impingement rate is determined by $R = \sqrt{1/(2\pi mkT_g)} \cdot P_{gs}$, where m, T_g, and P_{gs} are the mass, the gas phase temperature, and the partial pressure of the growth species, respectively. The rate is roughly proportional to the CH_4 concentration [8]; however we observe that the level of disorder also increases, as measured by Raman spectroscopy and XRD [8,14]. A faster growth rate results in an increased number of defects in the nanosheets and a smaller coherent-layer size (the average scale of periodically arranged atoms in crystalline structures).

At the typical RF input power, the observed increase in growth rate with CH_4 concentration, along with an increase in layer disorder, argues against complete dissociation of CH_4 to carbon and hydrogen atoms in the plasma, since complete dissociation would lead to a greater relative increase in hydrogen atom etching that removes defects [28]. We have also examined the effects of varying input RF power at fixed substrate temperature, CH_4 dilution ratio, and total pressure. Fig. 6 shows SEM images of CNS deposited using RF powers varying from 500 to 1200 W. At high RF power, the CNS have smooth surface morphologies, notwithstanding that the change is not obvious. Detailed studies [16] also indicated that increasing RF power caused an increase in CNS growth rate; however, the degree of order also increased as the RF power increased. Our optical emission spectroscopic observation revealed that the atomic hydrogen to growth species ratio also increases with increasing RF power. Therefore, effects of hydrogen etching are stronger at higher RF power, which consequently results in the removal of defects in the CNS.

The effect of variation of the total gas pressure, p, is more complicated. In the range studied (20–400 mTorr), the dissociation rate in our system is inversely proportional to total pressure, thus one naively expects the result of lower total pressure to be similar to raising RF power. The observation, however, is that at lower total pressure we achieve the expected faster growth rate, but the sheets contain relatively more defects rather than

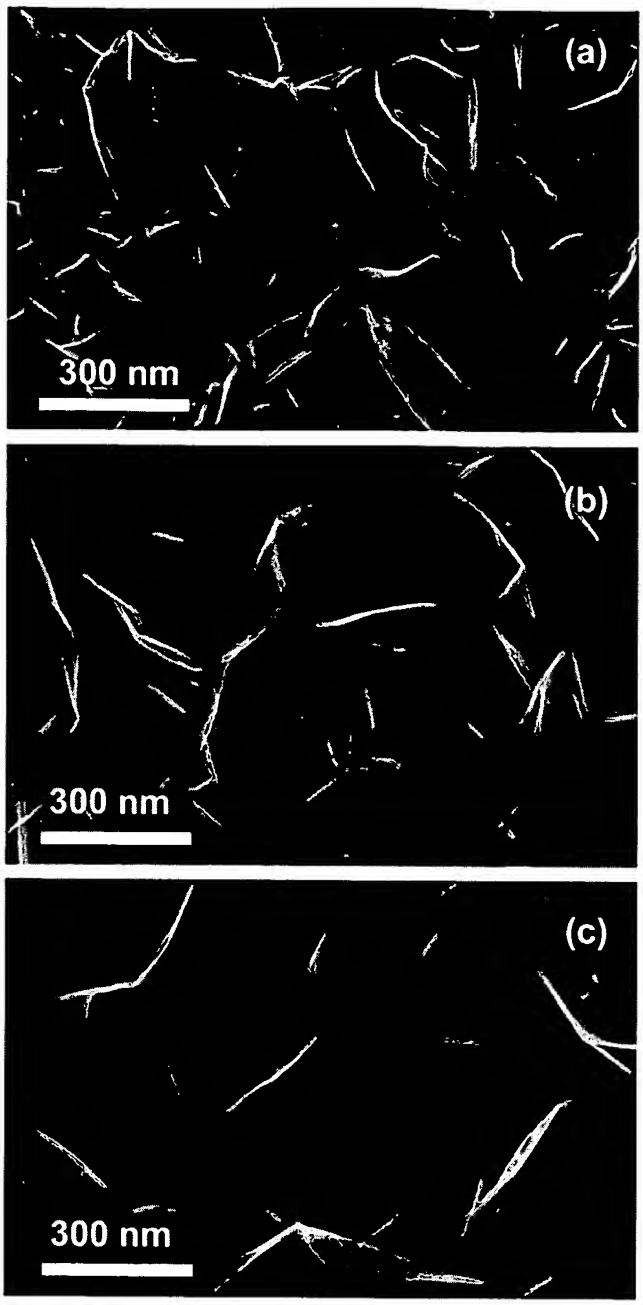

Fig. 6. SEM image of CNS deposited on Si substrates at (a) 500 W; (b) 800 W; and (c) 1200 W RF powers. Other conditions were 40% CH_4 in H_2, 100 mTorr, and 680 °C. The carbon nanosheets have somewhat smoother surface morphologies at higher RF power, although the change is subtle.

fewer defects. To account for this, we suggest that collisions can occur between the ions accelerating through the sheath electric field and neutral atoms in the background gas. Details of the aforementioned arguments can be found in the references [25,26]. Using Langmuir probe methods [25], a plasma potential $V_p \sim 70$ eV was measured in the plasma for nanosheet growth, so for singly ionized ions in the absence of collisions, this upper bound for the energy of an incident ion is well above the binding energy of a carbon atom in a graphene sheet (~7.4 eV) [31]. However, when elastic and charge-exchange collisions with the background gas are taken into account [32], the actual distribution of ions will be well approximated by a decaying exponential with a mean energy that falls as $p^{-1/2}$, yielding numerical values of mean energy far lower than the collisionless sheath voltage [33].

The essence of this analysis comes from considering the primary length parameters that dictate the number of collision in the sheath, n, leading to slowing the energy distribution. These are the sheath thickness, which in such plasmas is proportional [34] to $p^{-1/2}$ and the mean free path for elastic collisions, which is proportional to p^{-1}. These combine to yield n proportional to $p^{1/2}$, and thus a mean energy per ion that is proportional to $p^{-1/2}$. For the experimental conditions for nanosheet deposition, the particle energy is ~2–8 eV over the total pressure range of 400–20 mTorr. At lower pressure, this energy range includes the sp^2 hybridized C–C bonding energy (7.4 eV) in graphene layers, but recall that the detailed distribution has a high energy tail that falls off roughly exponentially. Therefore, the more energetic particle bombardment at lower pressure can produce defect production in crystalline carbon structures. Such damage production is similar to that accounting for ion-enhanced etching during carbon nanofiber synthesis reported by Wei et al. [35].

3. Conclusion

In this work, we have described the details of self-assembled synthesis of vertically-oriented atomically thin, two-dimensional carbon nanosheets. The facile synthesis of such structures fills the gap between 0-D, 1-D and macroscopic (bulk) carbon materials and provides an avenue for important engineering applications including electron devices, gas uptake and storage, catalysis, and more. This paper has presented a qualitative mechanism for oriented nanosheet formation directly from a one-step RF PECVD process. The mechanism is consistent with dominance by surface diffusion processes in the presence of energetic ion bombardment. We conclude that the formation of atomically thin, free-standing carbon nanosheets is strongly favored over the formation of nanotubes for the plasma parameters associated with our inductively coupled plasma. The resulting atomically thin edges require the presence of simultaneous etching by atomic hydrogen coupled to a vertical electrical field near the substrate surface. We have demonstrated that the electric field induces the anisotropic dipoles of the graphene sheets help to provide the observed self-aligned vertical orientation. The qualitative growth model developed and presented in this paper is consistent with, and accounts for, our previously reported parametric studies of nanosheet growth. This model forms the basis for forthcoming computational numerical studies of the nucleation and growth of this form of carbon.

Acknowledgements

Some characterization was performed partly at the Environmental Molecular Sciences Laboratory, a national scientific user facility operated by Pacific Northwest National Laboratory for the Department of Energy's Office of Biological and Environmental Research. The authors thank Ms. Kerry Siebein for her assistance with HRTEM at University of Florida, and the Office of Naval Research (Grant No. N00014-02-1-0711) for funding.

References

[1] Dresselhaus MS. Future directions in carbon science. Ann Rev Mater Sci 1997;27(1):1–34.

[2] Kroto HW, Heath JR, O'Brien SC, Curl RF, Smalley RE. C60: buckminsterfullerene. Nature (London, United Kingdom) 1985;318(6042):162–3.

[3] Iijima S. Helical microtubules of graphitic carbon. Nature (London, United Kingdom) 1991;354(6348):56–8.

[4] Teo KBK, Minoux E, Hudanski L, Peauger F, Schnell J-P, Gangloff L, et al. Microwave devices: carbon nanotubes as cold cathodes. Nature (London, United Kingdom) 2005;437(7061):968.

[5] Arico AS, Bruce P, Scrosati B, Tarascon J-M, Van Schalkwijk W. Nanostructured materials for advanced energy conversion and storage devices. Nat Mater 2005;4(5):366–77.

[6] Javey A, Guo J, Wang Q, Lundstrom M, Dai H. Ballistic carbon nanotube field-effect transistors. Nature (London, United Kingdom) 2003;424(6949):654–7.

[7] Wang JJ, Zhu MY, Outlaw RA, Zhao X, Manos DM, Holloway BC, et al. Free-standing subnanometer graphite sheets. Appl Phys Lett 2004;85(7):1265–7.

[8] Wang JJ, Zhu MY, Outlaw RA, Zhao X, Manos DM, Holloway BC. Synthesis of carbon nanosheets by inductively coupled radio-frequency plasma enhanced chemical vapor deposition. Carbon 2004;42(14):2867–72.

[9] Novoselov KS, Geim AK, Morozov SV, Jiang D, Zhang Y, Dubonos SV, et al. Electric field effect in atomically thin carbon films. Science 2004;306(5296):666–9.

[10] Wang JJ, Zhu MY, Tian H, Zhao X, Outlaw RA, Manos DM, et al. Effect of radio frequency plasma conditions on carbon nanosheet deposition. J Vac Sci Technol B, in preparation.

[11] Sawada S, Hamada N. Energetics of carbon nano-tubes. Solid State Commun 1992;83(11):917–9.

[12] Bourgeois LN, Bursill LA. Single- to multiple-layer transitions of flat and curved graphite sheets. Int J Mod Phys B 1996;10(5):563–77.

[13] Stoeckli F, Centeno TA. On the determination of surface areas in activated carbons. Carbon 2005;43(6):1184–90.

[14] French BL, Wang JJ, Zhu MY, Holloway BC. Structural characterization of carbon nanosheets via X-ray scattering. J Appl Phys 2005;97(11):114317/1–8.

[15] Zhao X, Outlaw RA, Wang JJ, Zhu MY, Smith GD, Holloway BC. Thermal desorption of hydrogen from carbon nanosheets. J Chem Phys 2006;124:194704/1–6.

[16] Zhu M, Carbon nanosheets and carbon nanotubes by RF PECVD. Williamsburg, The College of William and Mary, PhD dissertation, 2006.

[17] Lee YH, Kim SG, Tomanek D. Catalytic growth of single-wall carbon nanotubes: an ab initio study. Phys Rev Lett 1997;78(12): 2393–6.

[18] Louchev OA, Sato Y, Kanda H. Growth mechanism of carbon nanotube forests by chemical vapor deposition. Appl Phys Lett 2002;80(15):2752–4.

[19] Lewis B, Anderson JC. Nucleation and growth of thin films. Academic Press Inc.; 1979. p. 51.

[20] Ural A, Li YM, Dai HJ. Electric-field-aligned growth of single-walled carbon nanotubes on surfaces. Appl Phys Lett 2002;81(18):3464–6.

[21] Wu Y, Yang B. Effects of localized electric field on the growth of carbon nanowalls. Nano Lett 2002;2(4):355–9.

[22] Senthil Kumar M, Kim TH, Lee SH, Song SM, Yang JW, Nahm KS, et al. Influence of electric field type on the assembly of single walled carbon nanotubes. Chem Phys Lett 2004;383(3-4):235–9.

[23] Smith BW, Benes Z, Luzzi DE, Fischer JE, Walters DA, Casavant MJ, et al. Structural anisotropy of magnetically aligned single wall carbon nanotube films. Appl Phys Lett 2000;77(5):663–5.

[24] Nicholson D. Graphite polarizability. Surf Sci Lett 1987;181(3):L189–92.

[25] Manos DM, Flamm DL. Plasma etching, an introduction. Academic Press Inc.; 1989.

[26] Lieberman MA, Lichtenberg AJ. Principles of plasma discharges and materials processing. John Wiley & Sons, Inc.; 1994.

[27] Louchev OA, Hester JR. Kinetic pathways of carbon nanotube nucleation from graphitic nanofragments. J Appl Phys 2003;94(3):2002–10.

[28] Zhu M, Wang J, Outlaw RA, Hou K, Manos DM, Holloway BC. Synthesis of carbon nanosheets and carbon nanotubes by radio frequency plasma enhanced chemical vapor deposition. Diam Relat Mater 2007(16):196–201.

[29] Somorjai GA. Introduction to surface chemistry and catalysis. New York: Wiley; 1994. p. 271–314.

[30] Masel RI. Principles of adsorption and reaction on solid surface. New York: Wiley; 1996.

[31] Dresselhaus MS, Dresselhaus G, Eklund PC. Science of fullerenes and carbon nanotubes. San Diego: Academic Press; 1996. p. 17.

[32] Mason EA, Vanderslice JT. Scattering cross sections and interaction energies of low-velocity He^+ ions in helium. Phys Rev 1957;108(2):293–4.

[33] Davis WD, Vanderslice TA. Ion energies at the cathode of a glow discharge. Phys Rev 1963;131(1):219–28.

[34] Mutsukura N, Kobayashi K, Machi Y. Plasma sheath thickness in radio-frequency discharges. J Appl Phys 1990;68(6):2657–60.

[35] Wei HW, Leou KC, Wei MT, Lin YY, Tsai CH. Effect of high-voltage sheath electric field and ion-enhanced etching on growth of carbon nanofibers in high-density plasma chemical-vapor deposition. J Appl Phys 2005;98(4):044313.